LANGLEY RESEARCH CENTER
3 1176 00504 3287

NASA -CR-167896

NASA CR-167896
PWA-5772-23

NASA-CR-167896
19820017381

FRACTURE MECHANICS CRITERIA FOR TURBINE ENGINE HOT SECTION COMPONENTS
FINAL REPORT

BY

G. J. Meyers

May 1982

UNITED TECHNOLOGIES CORPORATION
Pratt & Whitney Aircraft Group
Commercial Products Division

LIBRARY COPY
JUN 14 1982
LANGLEY RESEARCH CENTER
LIBRARY, NASA
HAMPTON, VIRGINIA

Prepared for

NATIONAL AERONAUTICS AND SPACE ADMINISTRATION
NASA-Lewis Reseach Center
21000 Brookpark Road, Cleveland, Ohio 44135
Contract NAS3-22550

NF02696

1. REPORT NO.	2. GOVERNMENT AGENCY	3. RECIPIENT'S CATALOG NO.
CR-167896		

4. TITLE AND SUBTITLE	5. REPORT DATE
FRACTURE MECHANICS CRITERIA FOR TURBINE ENGINE HOT SECTION COMPONENTS, FINAL REPORT	MAY 1982
	6. PERFORMING ORG. CODE
7. AUTHOR(S)	8. PERFORMING ORG. REPT. NO.
G. J. Meyers, Program Manager	PWA-5772-23
9. PERFORMING ORG. NAME AND ADDRESS	10. WORK UNIT NO.
UNITED TECHNOLOGIES CORPORATION Pratt & Whitney Aircraft Group Commercial Products Division	11. CONTRACT OR GRANT NO. NAS3-22550
12. SPONSORING AGENCY NAME AND ADDRESS	13. TYPE REPT./PERIOD COVERED
National Aeronautics and Space Administration Lewis Research Center 21000 Brookpark Road, Cleveland, Ohio 44135	Final Report 14. SPONSORING AGENCY CODE

15. SUPPLEMENTARY NOTES

NASA Project Manager, T. W. Orange, NASA - Lewis Research Center
Cleveland, OH 44135

16. ABSTRACT

The application of several fracture mechanics data correlation parameters to predicting the crack propagation life of turbine engine hot section components was evaluated. An engine survey was conducted to determine the locations where conventional fracture mechanics approaches may not be adequate to characterize cracking behavior. Both linear and nonlinear fracture mechanics analyses of a cracked annular combustor liner configuration were performed. Isothermal and variable temperature crack propagation tests were performed on Hastelloy X combustor liner material. The crack growth data was reduced using the stress intensity factor, the strain intensity factor, the J-Integral, Crack Opening Displacement (COD), and Tomkins' model. The parameter which showed the most effectiveness in correlating high temperature and variable temperature Hastelloy X crack growth data was Crack Opening Displacement (COD).

17. KEY WORDS (SUGGESTED BY AUTHOR(S))	18. DISTRIBUTION STATEMENT
Crack Propagation, Fracture Mechanics Thermal-Mechanical Fatigue Life Prediction, J-Integral Crack Opening Displacement	

19. SECURITY CLASS THIS (REPT)	20. SECURITY CLASS THIS (PAGE)	21. NO. PGS	22. PRICE *
Unclassified	Unclassified	123	

* For sale by the National Technical Information Service, Springfield, VA 22161

N82-25257#

This Page Intentionally Left Blank

FOREWORD

The work described in this report was performed by Pratt & Whitney Aircraft Group, Commercial Products Division, for the National Aeronautics and Space Administration, under Contract NAS3-22550. The Principal Investigator was Mr. G. J. Meyers, with technical assistance provided by Dr. E. H. Jordon of the University of Connecticut, Dr. A. D. Fine, and Mr. A. E. Gemma. The specimen testing was conducted by Mr. R. M. Masci. The NASA Technical Project Manager was Mr. T. W. Orange. Mr. G. T. Smith was the Project Manager in the initial stages of the contract.

This Page Intentionally Left Blank

TABLE OF CONTENTS

SECTION	TITLE	PAGE
1.0	SUMMARY	1
2.0	INTRODUCTION	3
3.0	TASK I - DEFINITION OF CRACK PROPAGATION CONDITIONS	5
	3.1 Introduction	5
	3.2 Survey Data	6
	3.2.1 Combustor Liners	6
	3.2.2 Turbine Vanes and Blades	12
	3.2.3 Turbine Disks, Seals, Spacers, and Cases	17
4.0	TASK II - DEFINITION OF DATA AND TEST REQUIREMENTS	19
	4.1 General Comments	19
	4.2 Testing Capability Requirements	19
	4.3 Specimen Testing Conditions	20
5.0	TASK III - ANALYSIS OF CRACKED ENGINE COMPONENTS AND TEST SPECIMENS	23
	5.1 Introduction	23
	5.2 Strain Intensity Factor Analyses	23
	5.2.1 Specimen Analysis	23
	5.2.2 Component Analyses	24
	5.2.2.1 Combustor Liner Analysis	24
	5.2.2.2 Turbine Blade and Vane Analyses	26
	5.2.3 Specimen-Component Analysis Comparisons	27
	5.3 J-Integral Analyses	29
	5.3.1 Specimen Analysis	29
	5.3.1.1 Preliminary Test and Analysis	29
	5.3.1.2 Cyclic Analysis for Hastelloy X	32
	5.3.2 Combustor Liner Component Analysis	36
	5.3.2.1 Finite Element Analysis Procedures	36
	5.3.2.2 Analysis Technique Verification Studies	38
	5.3.2.3 Cyclic Component Analysis	44
	5.3.3 Specimen-Component Analysis Comparisons	47
6.0	TASK IV - DEVELOPMENT OF CRACK PROPAGATION DATA	49
	6.1 Purpose of Specimen Testing	49
	6.2 Specimen Testing Program	49
	6.2.1 Specimen Material	49
	6.2.2 Types of Tests	50
	6.2.3 Specimen Geometry	50
	6.2.4 Component Conditions	50
	6.2.5 Specimen Loading	52
	6.2.6 Crack Length Measurements and Data Reduction	56

TABLE OF CONTENTS

SECTION	TITLE	PAGE
7.0	TASK V- DATA CORRELATION AND GENERALIZATION	57
	7.1 Definition of Correlation Parameters	57
	7.2 Strain Intensity Factor	61
	7.3 Stress Intensity Factor	64
	7.4 J-Integral	67
	7.5 Crack Opening Displacement	67
	7.6 Tomkins' Model	72
	7.7 TMF Data Prediction	75
	7.8 Metallurgical Examination	83
	7.9 Conclusions on Data Correlation Parameters	86
8.0	SUMMARY OF RESULTS	91
REFERENCES		93
APPENDICIES		97
	Appendix A Strain Intensity Factor Data Reduction	97
	Appendix B Stress Intensity Factor Data Reduction	105
	Appendix C J - Integral Data Reduction	111
DISTRIBUTION LIST		117

LIST OF ILLUSTRATIONS

Number	Title	Page
1	Typical Combustor Liner Louvered Construction.	6
2	Extensive Damage on Low Time, Low Cycle Combustor Outer Liner.	7
3	Extensive Damage on High Time, High Cycle Combustor Outer Liner.	7
4	Localized Damage on Medium Time, High Cycle Combustor Outer Liner.	8
5	Localized Damage on High Time, Medium Cycle Combustor Outer Liner.	8
6	Close-Up View of Dilution-Air Hole Cracking on Low Time, Low Cycle Combustor Inner Liner.	9
7	Aft End Circumferential and Axial Cracking on Medium Time, Medium Cycle Combustor Inner Liner.	9
8	Typical Combustor Outer Liner Axial Crack Showing Close-Up View and Fracture Surface.	11
9	Examples of Typical Crack Propagation in High-Pressure Turbine First-Stage Vanes.	13
10	Examples of Typical Spanwise Crack Propagation in High-Pressure Turbine First-Stage Blades (Blade Coating Has Been Removed).	14
11	Geometry of Cracked Tubular Specimen.	24
12	Finite Element Mesh for Axisymmetric Analysis of Combustor Liner.	25
13	Strain-Temperature Response at Several Locations Along Combustor Liner Louver.	25
14	Spanwise Turbine Vane Crack.	27
15	Comparison of Combustor Liner Component and Tubular Test Specimens using Strain Intensity Factor.	28

LIST OF ILLUSTRATIONS (Continued)

Number	Title	Page
16	Comparison of Turbine Vane and Blade Components and Tubular Test Specimens using Strain Intensity Factor.	29
17	Smoothed Load-Displacement Curves from Preliminary Tests of B-1900 Tubular Specimens.	30
18	J-Integral Solutions from Preliminary Specimen Tests.	31
19	J-Integral Calculation Procedure using Compliance Approach.	32
20	Area Under Load-Displacement Curves for 871°C(1600°F), 0.4 percent Strain Range Test.	33
21	Crack Growth Data Reduction using Compliance Approach for J Calculation.	34
22	Comparison of Alternate J-Integral Solutions for 871°C(1600°F) Test.	35
23	Contour used in J-Integral Definition.	36
24	Coarse Grid Finite Element Mesh for J-Integral Test Cases.	38
25	Effect of Elastic Modulus Variation on J-Integral Calculation using Coarse Grid.	39
26	Effect of Linear Temperature Gradient on J-Integral Calculation Using Coarse Grid.	40
27	Refined Grid Finite Element Mesh for J-Integral Test Cases.	41
28	Effect of Elastic Modulus Variation on J-Integral Calculation using Refined Grid.	42
29	Finite Element Mesh for Combustor Liner J-Integral Calculation.	43
30	Schematic of Load - Displacement Information Obtained from Finite Element Analysis.	43

LIST OF ILLUSTRATIONS (Continued)

Number	Title	Page
31	Hastelloy X Stress - Strain Representation for MARC Combustor Liner Analysis.	45
32	J-Integral Solutions from Combustor Liner Structural Analysis.	46
33	Comparison of Combustor Liner Component and Tubular Test Specimens using J-Integral.	47
34	Tubular Strain-Controlled Crack Propagation Specimens.	51
35	Strain-Temperature Cycles used in Thermomechanical Fatigue Testing.	54
36	982°C(1800°F) Crack Growth Rates Based on Elastic Strain Intensity Factor Range.	62
37	426°C(800°F) to 926°C(1700°F) Cycle I Crack Growth Rates Based on Elastic Strain Intensity Factor Range.	62
38	Cycle I, 0.25 Percent Strain Range Crack Growth Rates Based on Elastic Strain Intensity Factor Range.	63
39	Spread in Low- to High-Temperature Crack Growth Rates Based on Elastic Strain Intensity Factor Range.	63
40	982°C(1800°F) Crack Growth Rates Based on Elastic Stress Intensity Factor Range.	65
41	426°C(800°F) to 926°C(1700°F) Cycle I Crack Growth Rates Based on Elastic Stress Intensity Factor Range.	65
42	Cycle I, 0.25 Percent Strain Range Crack Growth Rates Based on Elastic Stress Intensity Factor Range.	66
43	Spread in 0.4 Percent Strain Range Low- to High-Temperature Crack Growth Rates Based on Elastic Stress Intensity Factor Range.	66

LIST OF ILLUSTRATIONS (Continued)

Number	Title	Page
44	982°C(1800°F) Crack Growth Rates Based on J-Integral Range.	68
45	426°C(800°F) to 926°C(1700°F) Cycle I Crack Growth Rates Based on J-Integral Range.	68
46	Cycle I, 0.25 Percent Strain Range Crack Growth Rates Based on J-Integral Range.	69
47	Spread in 0.4 Percent Strain Range Low- to High-Temperature Crack Growth Rates Based on J-Integral Range.	69
48	Spread in 0.4 Percent Strain Range Low- to High-Temperature Crack Growth Rates Based on Simplified COD Model.	71
49	Spread in 0.4 Percent Strain Range Low- to High-Temperature Crack Growth Rates Based on COD Solutions by Shih.	71
50	Spread in 0.4 Percent Strain Range Low- to High-Temperature Crack Growth Rates Based on COD Solutions by McMeeking.	72
51	982°C(1800°F) Actual versus Predicted Crack Growth Rates Based on Tomkins' Model.	74
52	871°C(1600°F) Actual versus Predicted Crack Growth Rates Based on Tomkins' Model.	74
53	426°C(800°F) Actual versus Predicted Crack Growth Rates Based on Tomkins' Model.	75
54	Prediction of 426°C(800°F) to 926°C(1700°F) Cycle I Crack Growth Data Using Elastic Strain Intensity Factor.	79

LIST OF ILLUSTRATIONS (Continued)

Number	Title	Page
55	Prediction of 426°C(800°F) to 926°C(1700°F) Cycle II and Faithful Cycle Crack Growth Data Using Elastic Strain Intensity Factor.	79
56	Prediction of 426°C(800°F) to 871°C(1600°F) Cycle I Crack Growth Data Using Elastic Strain Intensity Factor.	80
57	Prediction of 426°C(800°F) to 926°C(1700°F) Cycle I and Faithful Cycle Crack Growth Data Using Simplified COD Model.	82
58	Prediction of 426°C(800°F) to 871°C(1600°F) Cycle I Crack Growth Data Using Simplified COD Model.	82
59	Degree of Nonplanar Crack Growth for Low-Temperature, High-Temperature, and TMF Specimen Tests.	86
60	Extent of Surface Roughness for Low-Temperature, High- Temperature, and TMF Specimen Tests.	87
61	Spread of Crack Growth Rates for Fracture Mechanics Data Correlation Parameters.	89

This Page Intentionally Left Blank

SECTION 1.0

SUMMARY

This document describes a 14-month program conducted by Pratt & Whitney Aircraft (P&WA) to assess the use of several fracture mechanics criteria in the prediction of crack propagation in engine hot section components. The ability to predict accurately the initiation and propagation of cracks within hot section components is expected to have a substantial return in the form of longer service lives.

The program is arranged into five technical tasks. Under Task I, important crack propagation conditions in the engine hot section were defined by conducting an engine survey and assessing the usefulness of conventional fracture mechanics methods. The second task defined the data, test facilities, and test specimens needed to establish the effectiveness of data correlation parameters for the components identified in Task I. Under Task III, fracture mechanics analyses were conducted on both the components and specimens identified in Tasks I and II and the results of each were compared. A crack propagation test program was defined and conducted under Task IV; crack propagation tests were conducted under conditions which related to a typical Hastelloy-X combustor liner design. The fifth task correlated and generalized the Task IV data for isothermal and variable temperature conditions so that several crack propagation parameters could be compared and evaluated.

This Page Intentionally Left Blank

SECTION 2.0

INTRODUCTION

The objective of this program is to develop and evaluate improved crack growth prediction methods for hot section components of aircraft turbine engines. This effort is in support of the National Aeronautics and Space Administration's (NASA) objective of increasing the durability and maintainability of engine hot section components.

In many turbine engine components, particularly those comprising the hot section of the engine, the stress and temperature conditions may be sufficiently severe as to require evaluation of the effect of inelastic material behavior. The development of crack growth prediction methods, the generation of experimental data, and the reliable application of the data to the engine components are difficult because of the severe engine operating conditions. The requirement to accurately identify and experimentally duplicate the salient features of the high-temperature, high-stress crack-propagation process presents a difficult experimental challenge, and the accompanying requirement for developing effective correlation and generalization parameters presents similar, strenuous analytical requirements.

Present linear elastic fracture mechanics methods are limited in their ability to provide accurate crack growth predictions for the severe stress and temperature conditions encountered in aircraft turbine engine hot section components. This program identifies and defines the problems that limit present prediction methods, and aims toward providing partial solutions to these problems.

The major objectives of the program are as follows:

- Determine those components in the engine hot section for which the conventional approaches to crack propagation may not be adequate.
- Establish the types of specimen testing required to adequately characterize the crack propagation behavior of the hot section components.
- Calculate the values of elastic and inelastic data correlation parameters for the combustor liner and other hot section components by performing fracture mechanics analyses.
- Determine the applicability of several elastic and inelastic data correlation parameters in characterizing high temperature and variable temperature crack growth in Hastelloy X material.
- Perform a prediction of variable temperature crack growth by using the results of isothermal crack propagation testing.

Details of the work conducted under this program are given in Sections 3 through 7, and a summary of the results is presented in Section 8.

This Page Intentionally Left Blank

SECTION 3.0

TASK I - DEFINITION OF CRACK PROPAGATION CONDITIONS

3.1 INTRODUCTION

In this section, a survey of engine hot section component cracking problems is described to identify significant cracking conditions. The major purpose of this section is to identify locations where currently available crack propagation theory (specifically, linear elastic fracture mechanics using isothermal crack growth data) may be deficient in characterizing crack propagation rates in engine hardware.

In conducting the engine survey, the following procedure was followed. First, the engine components were surveyed to determine those areas which experience stress and temperature levels which are severe enough to cause a significant amount of cyclic nonlinear material behavior and thermal-mechanical cycling. Second, for those parts identified in step 1, the conditions likely to affect the crack propagation rate were characterized. These conditions include identification of material, temperature, and stress and/or strain obtained from currently available heat transfer and stress analysis results. Third, the significance of the cracking for the various parts were identified, based on detrimental effect to the operator. Maintenance material costs and risk of secondary damage are examples of the failure consequences that were qualitatively examined. Fourth, an assessment of current crack propagation theory in addressing the cracking behavior in the engine components was made. This assessment is preliminary in nature; in Section 4, testing programs which would permit a better assessment were defined.

The engine survey covered the service experience of Pratt & Whitney Aircraft's most advanced turbofan engine in commercial service, the JT9D, including its various models. The reasons the JT9D was chosen are as follows:

- The JT9D is a mature fleet, with millions of hours of operational service.
- Component cracking information is well documented.
- Hot section cracking is proportionally a more important engine maintenance problem in the advanced high bypass ratio turbofans than in earlier engines.

In this section, the components surveyed included combustor liners, turbine blades, turbine vanes, turbine spacers, turbine seals, turbine cases, and turbine disks. The results of the survey for these components are presented in the following sections. The combustor liner service experience is given in the greatest amount of detail, since for this component the largest amount of documented service experience was readily available.

3.2 SURVEY DATA

3.2.1 Combustor Liners

As shown in Figure 1, current combustor liner construction consists of a series of sheet-metal louvered shell structures, seam-welded together. The results of combustor liner damage surveys and estimates of liner life are presented below. Typical combustor outer liner distress is illustrated in Figures 2 through 5, and typical combustor inner liner distress is shown in Figures 6 and 7. Pertinent information on each of these pictured liners is presented in Table I, including the number of hours and cycles presented as percentages of the calculated B-50 removal lives. (The B-50 life is defined as the median service life.)

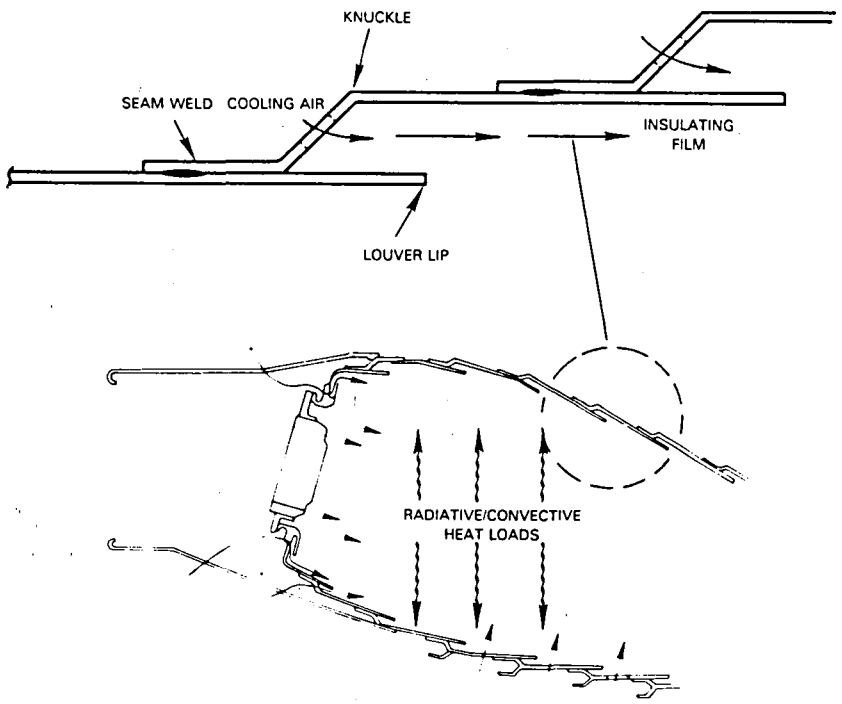

Figure 1 Typical Combustor Liner Louvered Construction.

A number of significant points should be be made concerning combustor liner damage. First, over the range of time and cycles shown, the damage is similar, that is, there is no apparent effect of block time (average mission length, which is equal to time divided by cycles) (see Figures 4 and 5). Second, there may be a large liner-to-liner variation in damage for combustors with similar numbers of service hours (see Figures 3 and 5). Third, the damage generally is not circumferentially uniform around the liner. Fourth, although the temperatures and strains are calculated for a new liner, deterioration in engine performance, fuel nozzles, and the liner itself (louver lip distortion and buckling) may cause the actual temperatures to run hotter (well over 1800°F), particularly in the badly streaked and burned regions. Fifth, although the statistical removal life of outer and inner liners are nearly identical, there are significant differences in damage progression (see Table I).

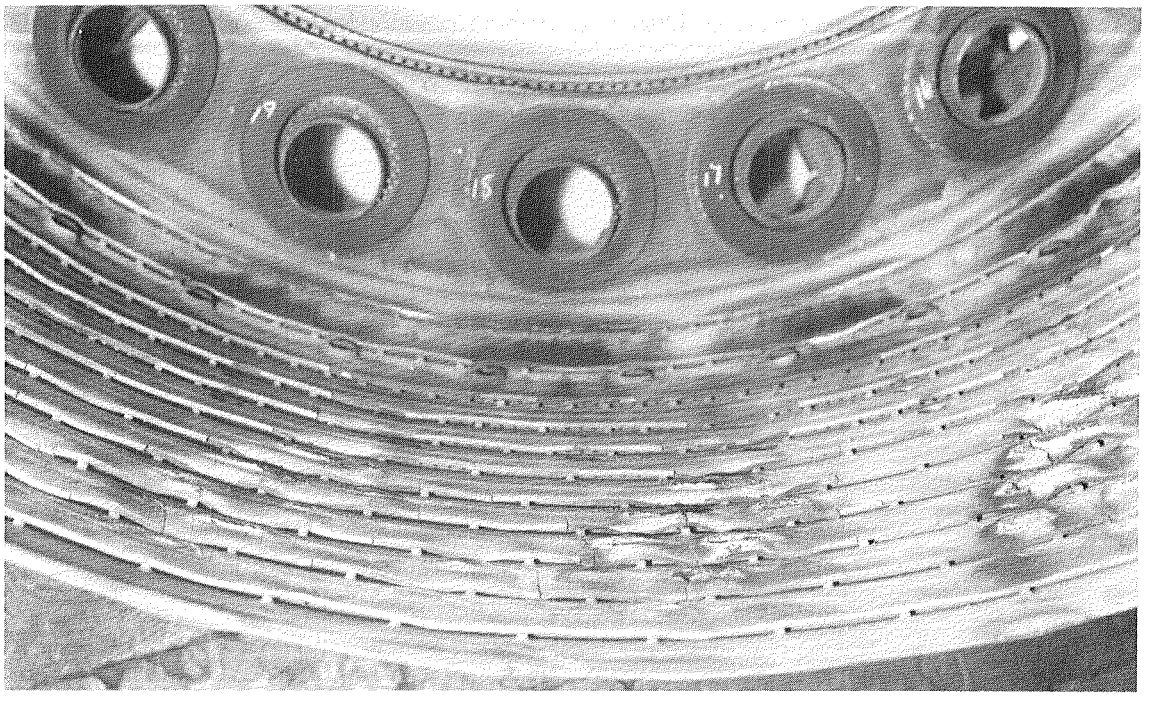

Figure 2 Extensive Damage on Low Time, Low Cycle Combustor Outer Liner.

Figure 3 Extensive Damage on High Time, High Cycle Combustor Outer Liner.

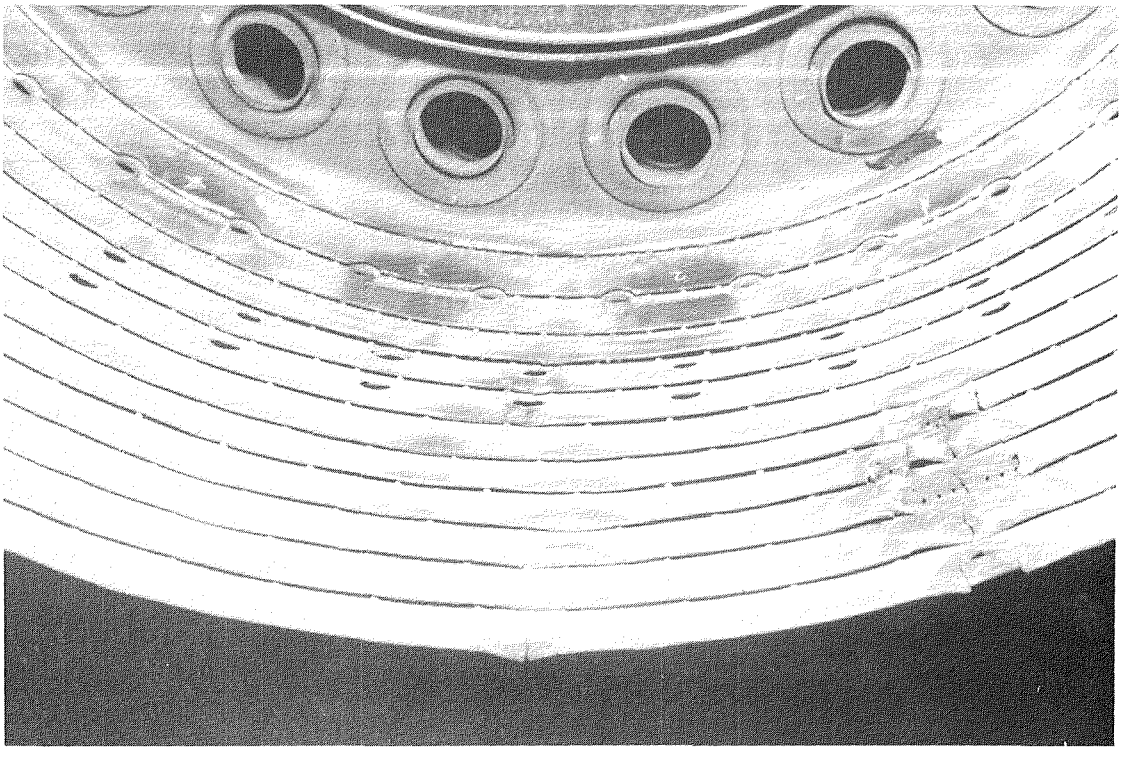

Figure 4 Localized Damage on Medium Time, High Cycle Combustor Outer Liner.

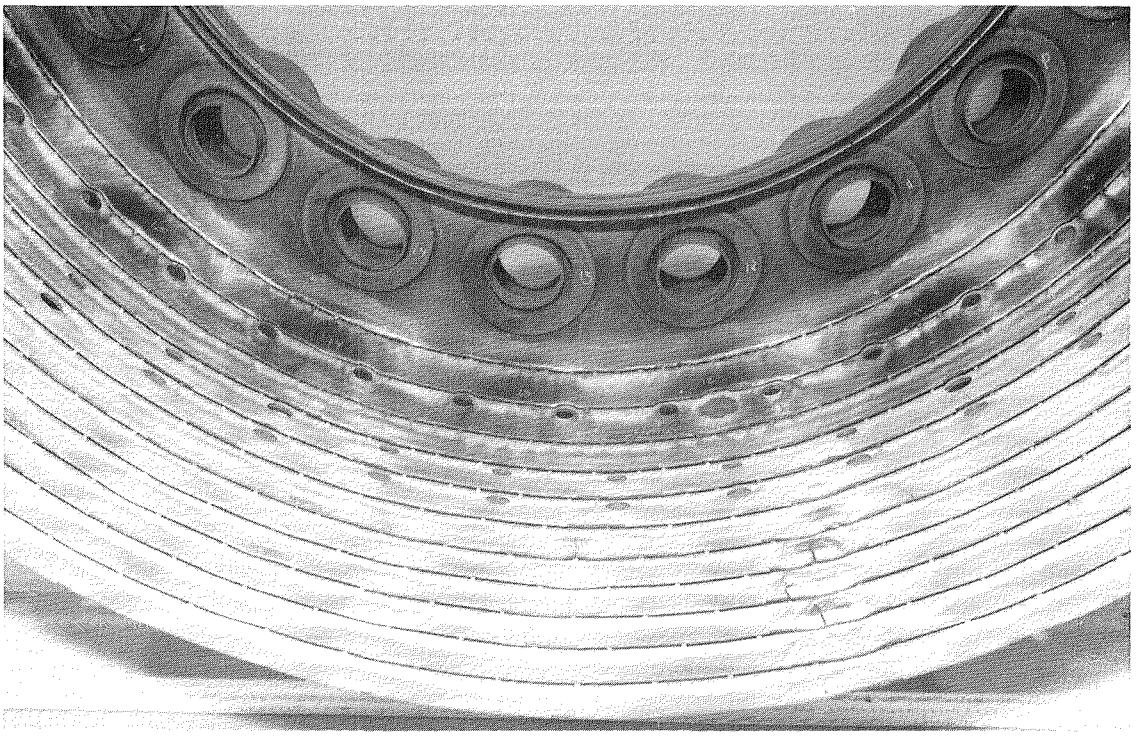

Figure 5 Localized Damage on High Time, Medium Cycle Combustor Outer Liner.

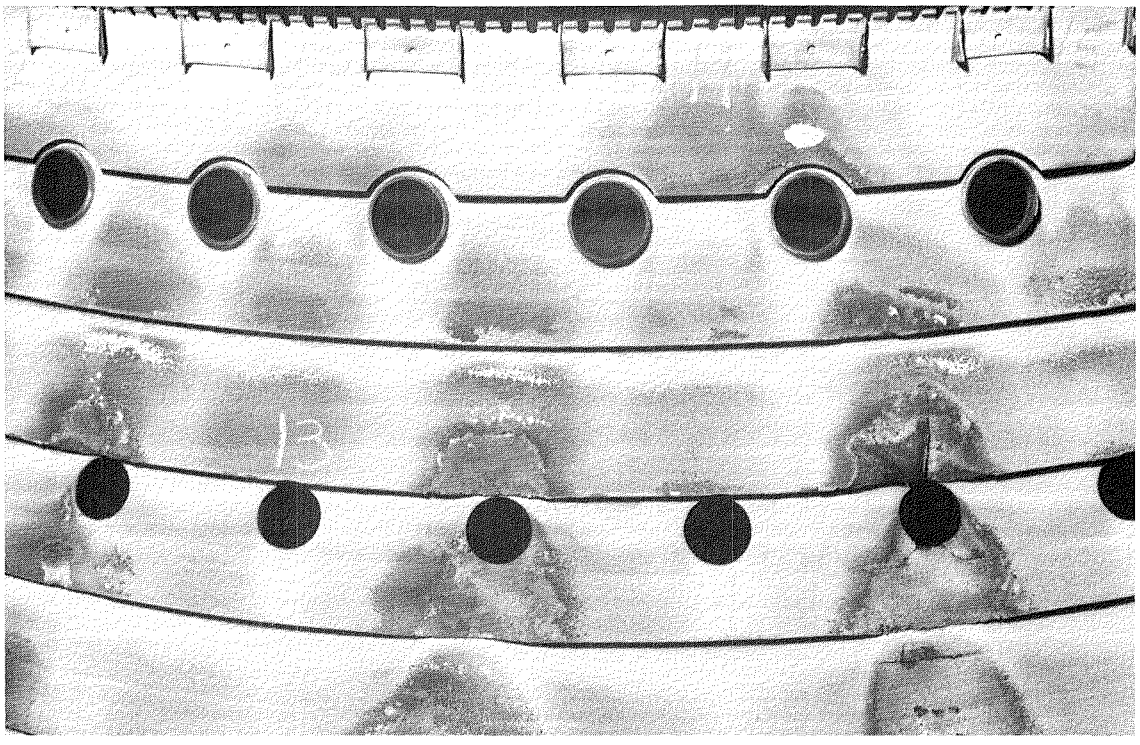

Figure 6 Close-Up View of Dilution-Air Hole Cracking on Low Time, Low Cycle Combustor Inner Liner.

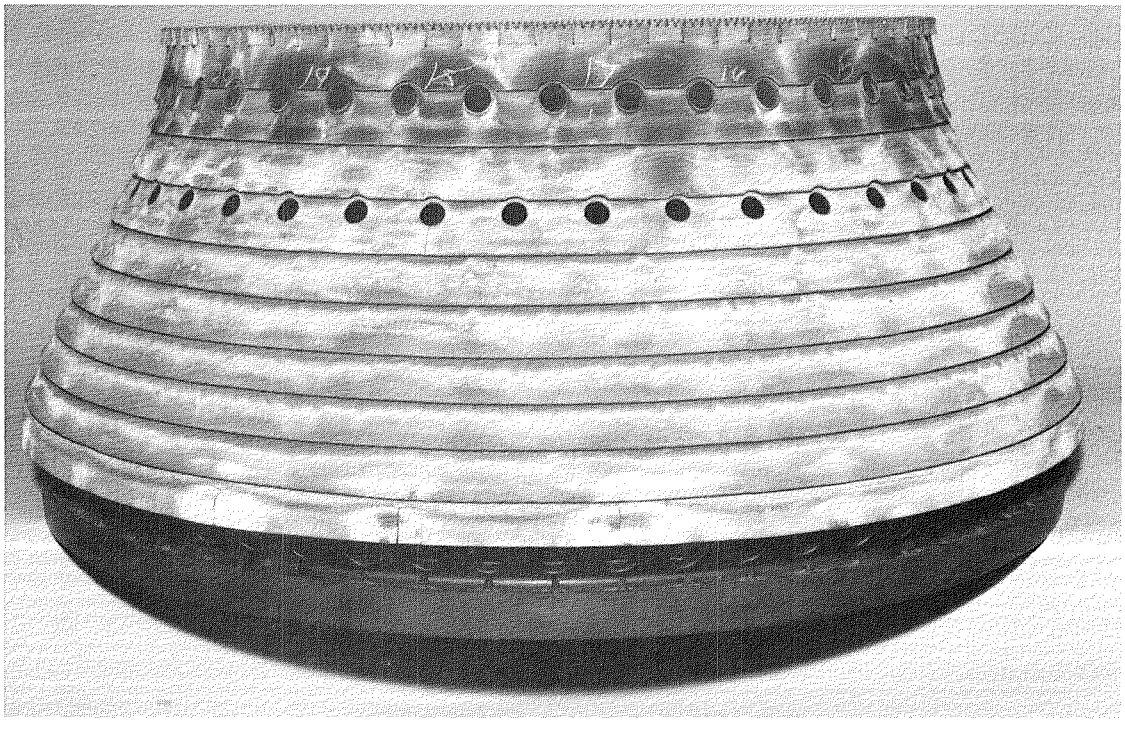

Figure 7 Aft End Circumferential and Axial Cracking on Medium Time, Medium Cycle Combustor Inner Liner.

TABLE I

DOCUMENTATION OF DAMAGE RESULTS IN JT9D COMBUSTOR LINERS
(Outer and Inner)

Figure Number	Time (% of Calculated B-50)	Cycles (% of Calculated B-50)	Calculated Temperature C (°F)	Calculated Strain Range (%)	Nature of Damage
			COMBUSTOR OUTER LINERS		
2	38	20	971(1780)	0.45	o Lip Collapse o Coating Spallation o Burning o Extensive Cracking
3	84	85	987(1810)	0.45	o Cracking and Burning (Similar to Figure 2)
4	51	88	971(1780)	0.45	o Extensive Cracking o Localized Distress
5	81	51	971(1780)	0.45	o Extensive Cracking (One Severe Crack)
			COMBUSTOR INNER LINERS		
6	27	10	943(1730)	0.25	o Erosion and Burning o Axial and Circumferential Cracking o Dilution Air Hole Cracking
7	53	34	943(1730)	0.37	o Mild Dilution Air Hole Cracking o Cracking in Aft End

NOTES:

Cooling Type; Film Cooled Material; Hastelloy-X Coating; Metallic-Ceramic Thermal Barrier

Crack Initiation Location: Outer Liner; End of louver lip
Inner Liner; End of louver lip and circumferential seam weld

Liners must be weld-repaired or eventually replaced.

B-50 is calculated median service life.

FAILURE CONSEQUENCES:

Outer Liner: Axial cracks link together, resulting in liner deformation. This deformation may affect combustor exit temperature distribution with an ultimate effect on turbine performance and durability.

Inner Liner: Intersection of large axial and circumferential cracks can result in liberation of pieces of the liner, causing secondary damage to turbine blades and vanes.

Figure 8 shows a close-up view of a typical cracked area of a combustor outer liner, as well as a cross-section of the cracked area. This example, which does not have the extensive amount of burning seen in Figures 2 through 5, is considered to be representative of early to intermediate stages of crack growth. Crack propagation occurs axially from the end of the louver lip to the double thickness resistance weld region. This is the type of cracking which was extensively tested and analyzed during this program, and the results are described in Sections 5 through 7 of this document.

CLOSE-UP VIEW

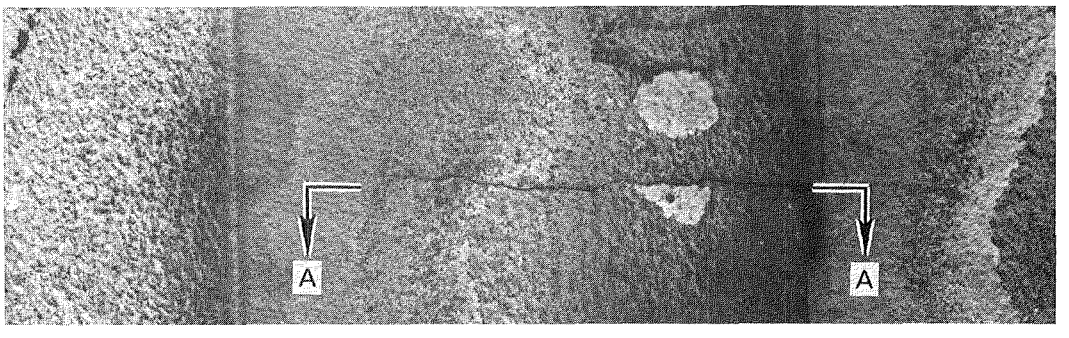

CROSS-SECTION A-A

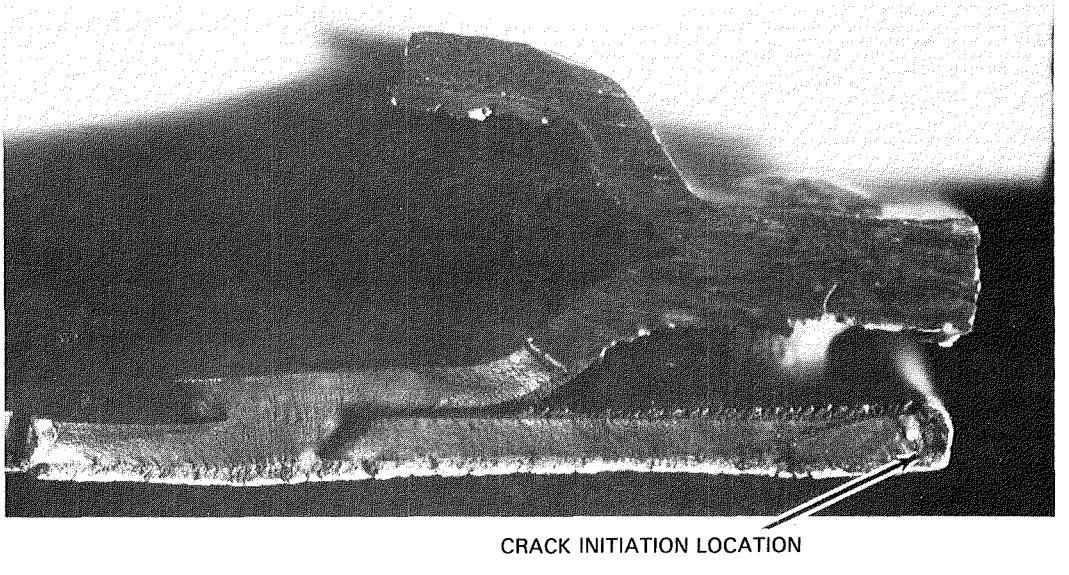

Figure 8 Typical Combustor Outer Liner Axial Crack Showing Close-Up View and Fracture Surface.

Current prediction models for combustor liner life provide crack initiation data which are calibrated with in-house and field experience. While the ultimate removal life is related to the predicted crack initiation life, experience has shown that the time (or cycles) involved in propagating cracks similar to those seen in Figures 2 through 7 is often a factor of two to four

times the predicted crack initiation life. Since liners are rarely removed because of short cracks (less than 2.5 cm(1-in) length), and since the relationships between crack propagation rate and strain, temperature, hold time, etc. are different than for crack initiation, it is apparent that an improved prediction capability is warranted. The crack propagation testing and data correlation performed during this program effort are essential ingredients in the nonlinear fracture mechanics life prediction capability required for combustor liners.

3.2.2 Turbine Vanes and Blades

The turbine airfoil portion of the survey is presented in this section. Table II lists the damage mechanisms for all airfoils which are considered to have the greatest significance in terms of engine maintenance costs. The most significant propagation conditions in the turbine airfoils have been found to be located in the high-pressure turbine first-stage vanes and first-stage blades. The important locations in the first-stage vanes are the leading edge, the pressure-side wall, and the trailing edge fillet (Figure 9). In the first-stage blades, radial cracking is a significant damage mechanism (Figure 10).

TABLE II

IMPORTANT DAMAGE MECHANISMS FOR
JT9D HIGH-PRESSURE TURBINE AIRFOILS

Airfoil	Damage Mechanisms
First-Stage Turbine Vane	o Cracking (oxidation-assisted) of leading edge and pressure-side wall. o Burning around leading edge cooling holes.
Second-Stage Turbine Vane	o Leading edge cracking (early models). o Coating oxidation and impact damage (later models).
First-Stage Turbine Blade	o Radial cracking of pressure- and suction-side walls. o Blade tip oxidation. o Stress rupture. o Impact damage.
Second-Stage Turbine Blade	o Impact damage. o Stress rupture (early models).

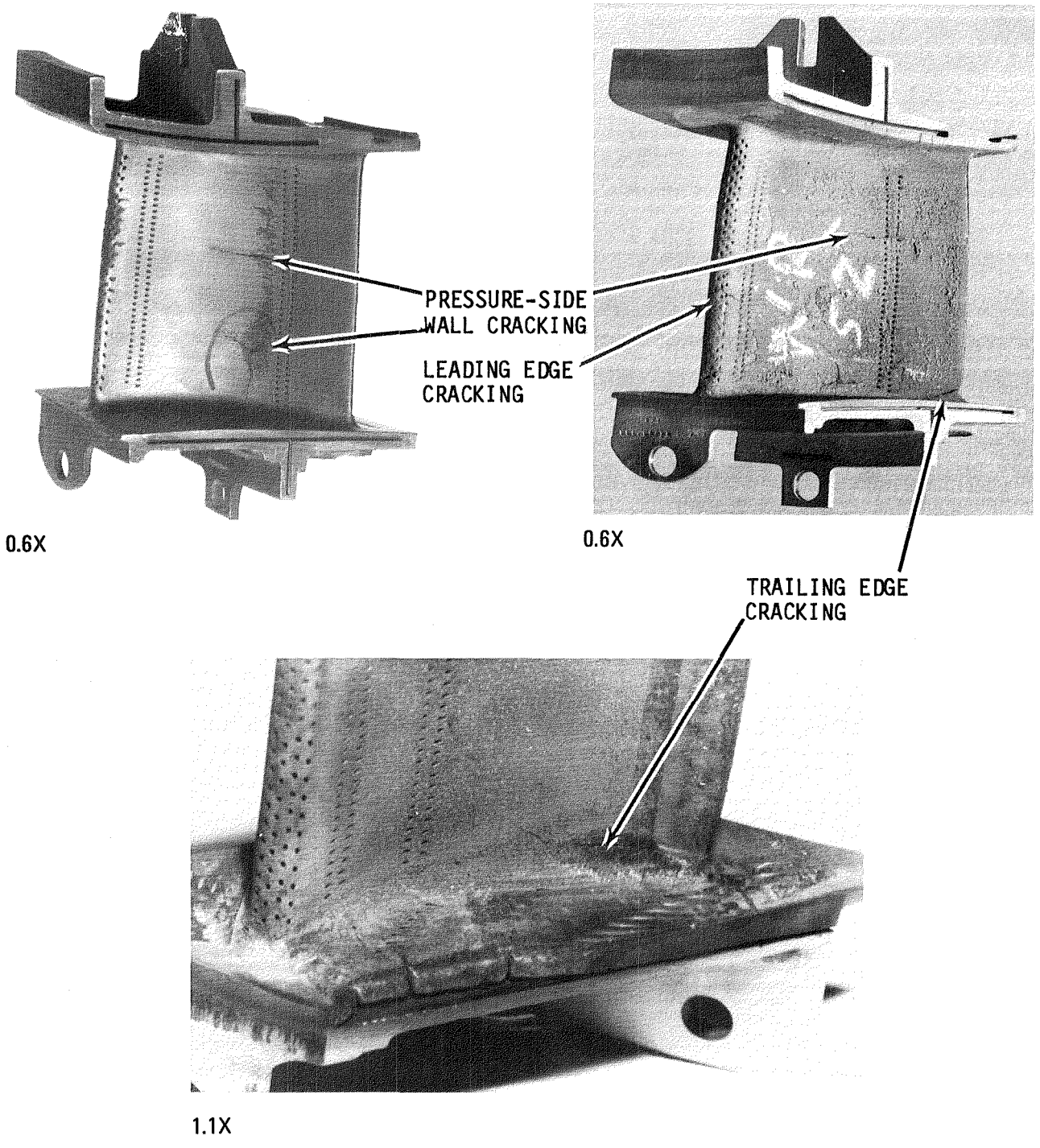

Figure 9 Examples of Typical Crack Propagation in High-Pressure Turbine First-Stage Vanes.

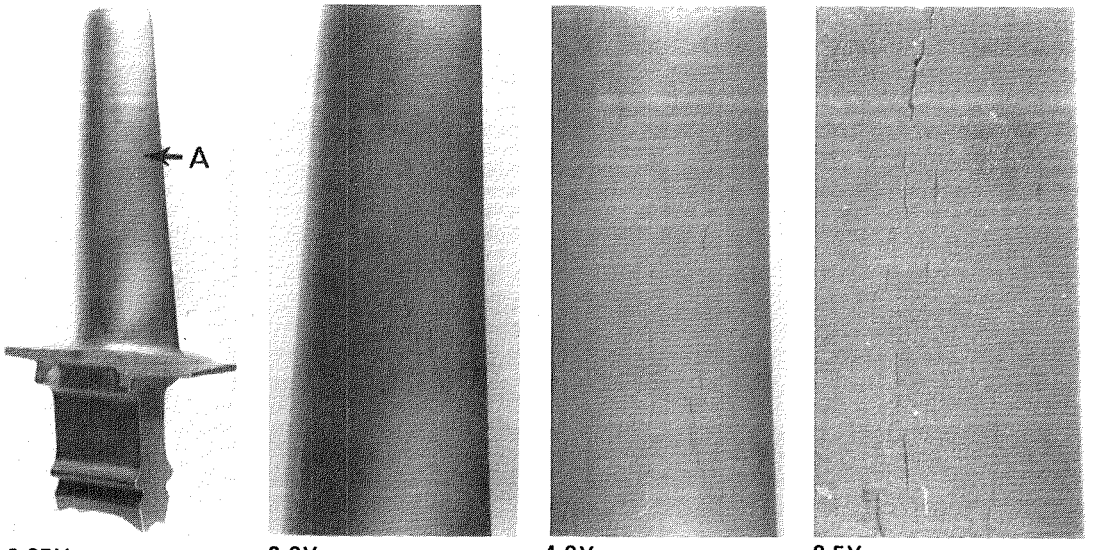

0.65X 2.6X 4.6X 6.5X

SUCTION-SIDE WALL CRACKING (ARROW A)

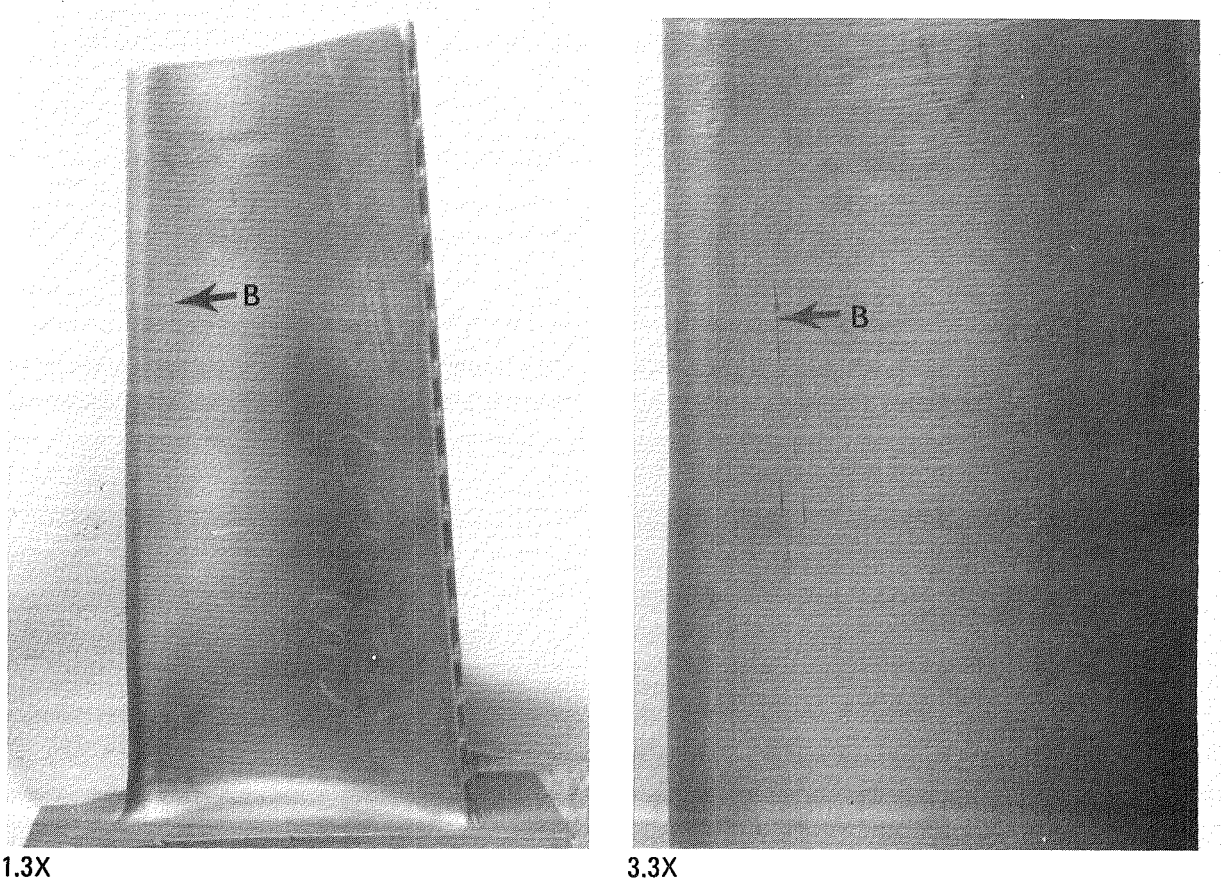

1.3X 3.3X

PRESSURE-SIDE WALL CRACKING (ARROWS B)

Figure 10 Examples of Typical Spanwise Crack Propagation in High-Pressure Turbine First-Stage Blades (Blade Coating Has Been Removed).

Turbine vanes are complex structures exposed to a wide range of gas temperature levels and gradients which are dependent on combustor exit gas temperature distribution. As a result, metal temperatures and strains can be predicted by conventional analysis methods only near the vane midspan. The results of these analyses are presented in Table III. Platform and fillet temperature and strain predictions would require more complex three-dimensional analyses which were not performed for the vanes surveyed in this program. Such analyses currently are costly and time-consuming and would be undertaken only for investigating serious safety concerns.

TABLE III

JT9D FIRST-STAGE TURBINE VANES

TYPICAL PREDICTED TEMPERATURES AND STRAINS:

Crack Initiation Location	Steady-State Temperature C (°F)	Strain Range (%)
Leading Edge Midspan	926 (1700)	0.36
Pressure-Side Wall	982 (1800)	0.37

NOTES:

Cooling Type; Film Cooled
Material; MAR-M 509
Coating; Diffusion Aluminide

FAILURE CONSEQUENCES:

- o Loss of performance due to burning and cracking.
- o Loss of pieces of vane causing downstream impact damage.
- o Blade vibration due to aerodynamic excitation stemming from loss of vane (some early model engines).

When a vane leading edge crack is initiated in the vicinity of the cooling holes, the cooling air distribution is affected. This influence usually results in a local increase in temperature, which has the following two effects: 1) the local strain distribution is changed, the extent of which is difficult to analytically predict; and 2) severe burning of the vane leading edge can occur as a result of relatively short cracks. The burning then becomes the life-limiting damage mechanism in the vane leading edge. For the above reasons, detailed crack propagation studies of the turbine vane leading edges are currently considered to be of limited value in obtaining a more accurate life prediction for service hardware.

It is useful to observe that body cracking in the first-stage vanes shares many features with distress in the combustor liners, as described in Section 3.2.1. First, cracking is generally not considered to be a safety factor, but it is a major factor in engine maintenance costs. Secondly, vanes and combustors must be inspected for crack size on a regular schedule. This inspection is a factor in the maintenance cost, as well as the cost of actual repair or replacement of the hardware. Third, relatively long cracks can be tolerated, resulting in a significant portion of the service life being spent in crack propagation. Fourth, current prediction systems are based on crack initiation with a correction factor, based on engine experience, added to account for crack propagation.

Information concerning radial (spanwise) cracking in the first-stage turbine blades is provided in Table IV. For these blades, cracks generally are initiated in the coating and propagated into the base-metal substrate. Blade life is considered to be exhausted when the crack has grown completely through the airfoil wall. Thus, the maximum depth to which the crack can be allowed to grow is relatively short, less than about 0.125 cm(0.050 in). This situation contrasts sharply with that for the turbine vane, where cracks on the order of centimeters (inches) can be tolerated.

TABLE IV

JT9D FIRST-STAGE TURBINE BLADES

TYPICAL PREDICTED TEMPERATURES AND STRAINS:

Crack Initiation Location	Steady-State Temperature (°F)	Strain Range (%)
Pressure-Side Wall Spanwise Crack	926 (1700)	0.32

NOTES:

Cooling Type;	Impingement-Cooled
Material;	Directionally-Solidified MAR-M 200 + Hafnium
Coating;	NiCoCrAly

FAILURE CONSEQUENCES:

- o Crack can propagate through airfoil wall, leading to vibration or stress rupture.
- o Loss of cooling, causing blade failure.
- o Performance deterioration arising from excessive degradation of smooth airfoil surfaces.

Inherent defects in the base metal are not considered to be significant crack initiation sites for either vanes or blades included in the survey.

3.2.3 Turbine Disks, Seals, Spacers, and Cases

In the turbine disks, seals, spacers, and cases, significant amounts of cyclic nonlinear material behavior are not generally found to occur. Very high strength materials, such as nickel base superalloys, are typically used in these applications. The components are designed for high service lives, with stress levels well below the material yield strength, even in the high temperature environment. Components operating to design conditions are subjected to linear elastic material behavior. There are locations in regions of stress concentrations, such as in turbine-disk bolt holes and fir-tree slots, where material yielding occurs on the first engine cycle, but subsequent cyclic behavior is linear elastic. Only in unusual, atypical circumstances do the component stresses significantly exceed the yield stress. An example of this high stress condition occurs during severe local over-temperature due to rigorous operator practices or an inefficient design.

This linear elastic behavior in the turbine contrasts with the combustor liner, in which substantial cyclic nonlinear material behavior occurs under normal operating conditions. In turbine disks, turbine seals, turbine spacers, and turbine cases, the tools of linear elastic fracture mechanics are considered to be suitable for design purposes.

This Page Intentionally Left Blank

SECTION 4.0

TASK II - DEFINITION OF DATA AND TEST REQUIREMENTS

4.1 GENERAL COMMENTS

Testing capability requirements and testing conditions were defined for the significant hot section cracking locations identified in Task I. These locations include three in the first-stage turbine vanes, one in the first-stage turbine blades, and one in the combustor liner.

Cracking in the hot section vanes and blades share many features in common with cracking in current annular combustor liners. These common features include:

- o Relatively high temperatures (typical peak temperature in the range of 982°C(1800°F) but can exeed 1093°C(2000°F)),
- o Time-dependent nonlinear material behavior,
- o Variable cyclic strains and temperatures leading to Thermo-mechanical Fatigue (TMF) conditions, and
- o Predominantly thermal loading, leading to a strain-controlled, rather than load-controlled, situation.

The similar cracking characteristics between combustors, vanes, and blades listed above imply that testing capability requirements and testing programs for the vanes and blades closely parallel those for the combustor liner. These requirements are discussed in the following paragraphs. A more detailed description of the test program specifically related to the combustor liner testing performed in this effort is given in Section 6.

4.2 TESTING CAPABILITY REQUIREMENTS

The requirements for testing facilities and test specimens for crack propagation testing of turbine vanes, turbine blades, and combustor liners are:

- o Strain control - to simulate the thermal loading of the component. The mechanical strain (total strain minus thermal strain) must be controlled.
- o Strain hold time - to simulate steady state conditions, allowing the material to undergo creep/relaxation behavior.
- o Compressive load-carrying capability of the specimen - to sustain compressive stresses.
- o High temperature furnace - to simulate component thermal conditions.
- o Transient heating and cooling - to duplicate component strain/-temperature phase relationship.

Table V presents a particular choice of specimen geometry, heating and cooling techniques, and other related information that is applicable to turbine vane, turbine blade, and combustor liner crack propagation testing.

TABLE V

DESCRIPTION OF CRACK PROPAGATION TESTS

	Isothermal Test	Variable Temperature (TMF) Test
Specimen Type	External Ridge	Internal Ridge
Heating Technique	Electric Furnace	Low Frequency (10 kHz) Induction Heating
Cooling Technique	Lower Furnace Temperature	Forced Air Convective Cooling
Temperature Measurements	Thermocouples Tack-Welded to Specimen	Optical Pyrometer
Strain Measurements	ASTM Class B-1 Extensometer	LVDT* and Quartz Internal Extensometer
Crack Length Measurements	50X Telescope Equipped with Calibrated Micrometer Graduated to 0.0012 cm(0.0005 in). Measurements Taken at no Greater Than 0.050 cm (0.020 in) Intervals and at Maximum Tensile Load	
Accuracy	Temperature, ±2.2°C(4°F); Strain Range, ±1%; Crack Length, 0.002 to 0.012 cm (0.001 to 0.005 in) (Depends on Crack Tip Clarity)	

* LVDT = Linear Variable Differential Transformer.

4.3 SPECIMEN TESTING CONDITIONS

Crack propagation specimen testing for the locations cited above should include testing of the base metal (substrate) only since this type of cracking is readily studied by a fracture mechanics approach. The amount of component life spent in starting a crack in the coating and growing into the base metal may be addressed in terms of crack initiation techniques. Testing should include both isothermal tests in the temperature range from 426 to 1093°C(800 to 2000°F) and TMF tests with a minimum temperature of 426°C (800°F) and a maximum temperature ranging from 760 to 1093°C (1400 to 2000°F). The TMF tests should include several strain-temperature relationships, concentrating on Cycle I. (Cycle I is defined as having a linear relationship between strain

and temperature. The peak temperature in the cycle occurs at the point of maximum compressive strain.) The following variables should also be included in the testing plan:

- o Strain range, 0.15 to 0.70 percent;
- o Mean strain, -0.3 to +0.3 percent;
- o High temperature, compressive strain hold time, 1 to 5 minutes;
- o Crystal orientation, for directionally-solidified first-stage turbine blades.

It is recommended that the specific testing procedures and conditions for turbine vanes and blades parallel those for combustor liner specimen testing. Detailed information concerning the combustor liner related test program carried out in this effort is provided in Section 6.

SECTION 5.0

ANALYSIS OF CRACKED ENGINE COMPONENTS AND TEST SPECIMENS

5.1 INTRODUCTION

Fracture mechanics analyses were performed for each component and specimen identified in Sections 3 and 4. The purpose of the analyses was to compare the value of the correlation parameter calculated for the component with that obtained for the specimen. This comparison gives an indication of the value of the specimen testing for performing crack propagation life predictions for the component.

Analyses related to the combustor liner were given the most emphasis, for the following reasons. First, a major portion of the contract effort involved specimen testing of combustor material, as described in Sections 6 and 7. Crack growth data reduction required calculation of the correlation parameter for the specimen. Second, both linear and nonlinear analyses of the combustor liner specimen and component were necessary for data reduction. However, cyclic nonlinear fracture mechanics finite element analyses are very costly and time consuming. Therefore, the only nonlinear analysis was performed for the combustor liner. Third, it is not certain, a priori, whether nonlinear parameters are necessarily required for any of the hot section components other than the combustor liner. Only specimen testing would establish the requirement for nonlinear correlation parameters.

In summary, elastic strain intensity factor analyses were performed for combustors, turbine vanes, and turbine blades, and are described in Section 5.2. The nonlinear "J-Integral" analyses performed for the combustor liner is described in Section 5.3.

5.2 STRAIN INTENSITY FACTOR ANALYSES

5.2.1 Specimen Analysis

The specimen used in the testing is a uniaxial, strain controlled, thin walled tube. A schematic of the specimen is shown in Figure 11. The equation used for data reduction purposes is given by (1)*:

$$\Delta K_{\varepsilon} = \Delta\varepsilon \sqrt{\pi a} \; f(a^2/Rt)\, g(a/R)$$

where:

$\Delta\epsilon$ is the nominal strain range

$f(a^2/Rt)$ is the curvature correction factor for a circumferential crack in a cylinder of radius, R, and wall thickness, t, obtained from a curve-fit of solutions contained in (2)

$g(a/R)$ is a geometric correction to convert projected length to arc length

* Numbers in ( ) are references; see list at end of document.

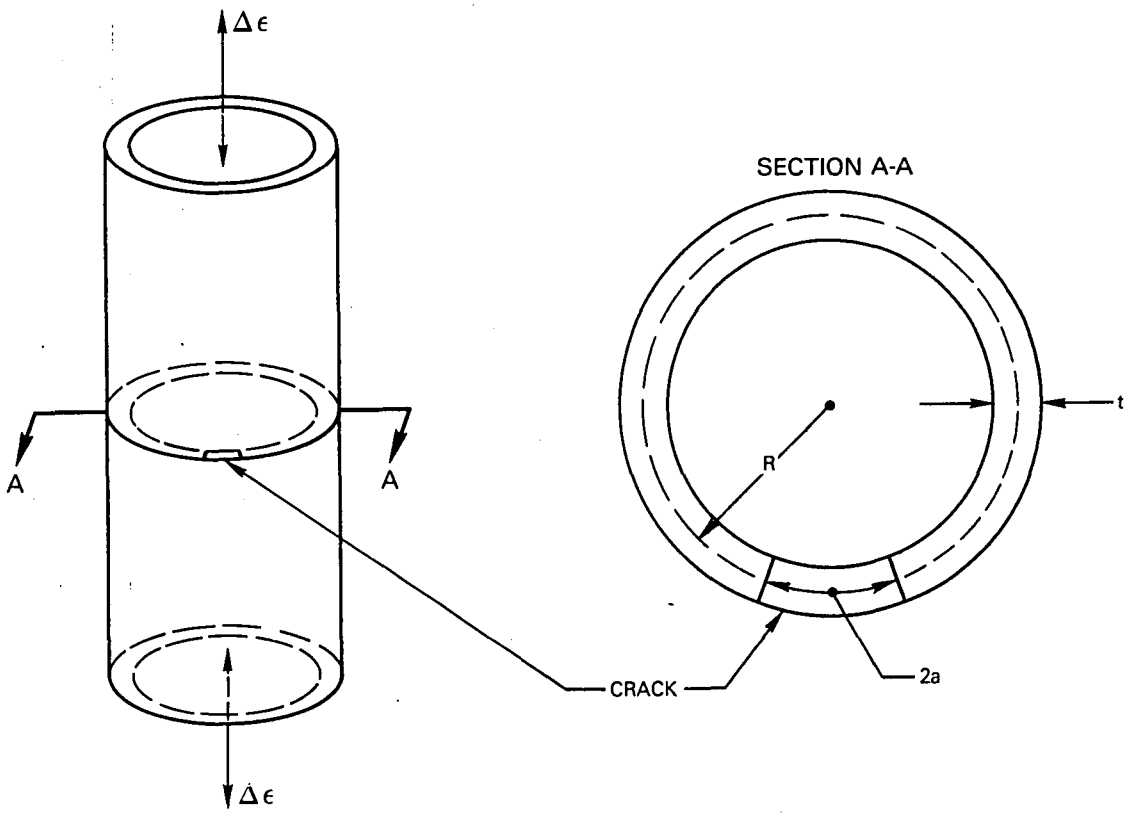

Figure 11 Geometry of Cracked Tubular Specimen.

A graph of the strain intensity factor as a function of crack length is given in Section 5.2.3, and the crack propagation data obtained in this contract are shown as a function of strain intensity factor in Section 7.

5.2.2 Component Analyses

5.2.2.1 Combustor Liner Analysis

A cross-section of a typical combustion liner louver is shown in Figure 8. The louver had been analyzed previous to this contract using the mesh shown in Figure 12.

A finite element analysis was performed using axisymmetric continuum elements. A transient nonlinear analysis was performed. The loading consisted of temperature distributions obtained from a heat transfer analysis. The temperature differences among various points in the structure result in strains which vary both geometrically and as a function of time. The type of cracking of interest is an axial crack starting at the edge and progressing through the louver lip. This type of crack is driven by hoop "mechanical" strains - total minus thermal. The second cycle strain-temperature plots for several locations along the louver obtained from the analysis are given in Figure 13.

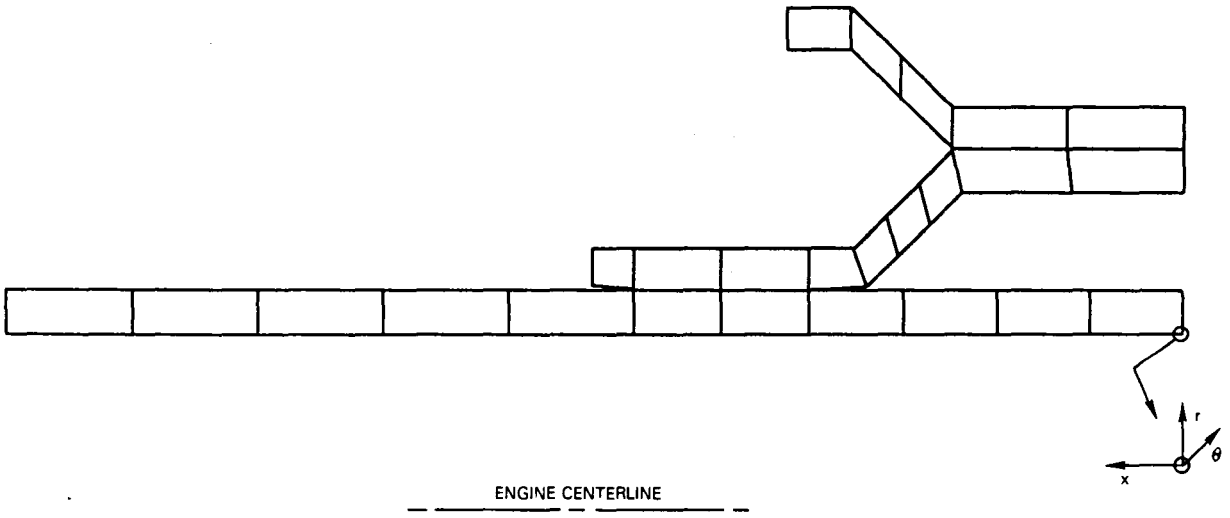

Figure 12 Finite Element Mesh for Axisymmetric Analysis of Combustor Liner.

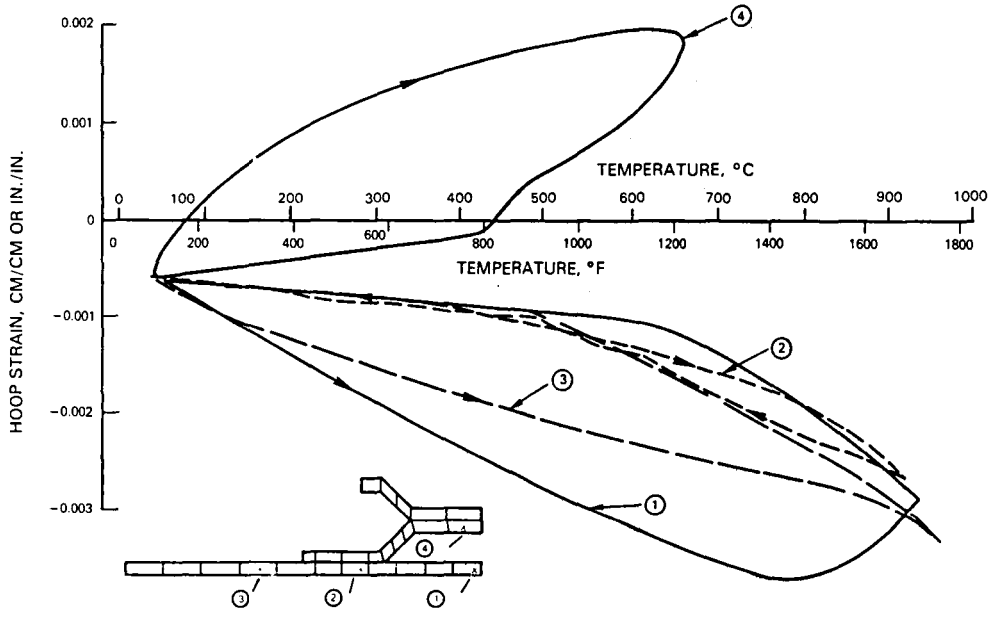

Figure 13 Strain-Temperature Response at Several Locations Along Combustor Liner Louver.

The fracture mechanics analysis modeled the axial crack in the combustor liner as an edge cracked sheet. A handbook solution is available for this situation; however, here there is the complicating feature of strain distributions changing with location. This distribution was accounted for using the "influence function" approach (3). This technique requires knowledge only of the stress (or strain) distribution of the uncracked structure. The strain intensity factor (ΔK_ϵ) is obtained from a numerical solution to the equation

$$\Delta K_\varepsilon(a) = \frac{2\sqrt{\pi a}}{\pi} \int_o^a \frac{\Delta\varepsilon(x)}{\sqrt{a^2 - x^2}} f \, dx$$

where a = crack length, f = a function of geometry (taken to be a constant 1.12 for the edge cracked louver), and $\epsilon(x)$ = hoop strain range. The strain range distribution is computed from the analysis of the uncracked combustor as shown in Figure 13.

This approach is valid as long as the crack is relatively small compared to overall structural dimensions. For this reason values of strain intensity factor were obtained only for the louver lip portion of the structure. The analysis results are given in Section 5.2.3.

5.2.2.2 Turbine Vane and Blade Analyses

The analyses performed for turbine vanes and blades were for those locations identified in Section 3 where further investigation of crack propagation behavior is warranted and where reasonable strain range predictions can be made. The two locations which fit both of these criteria are chordwise cracking on the pressure-side wall of the first-stage turbine vane and spanwise cracking on the pressure-side wall of the first-stage turbine blade. The fracture mechanics analyses for both locations consisted of obtaining estimates of the elastic strain intensity factor as a function of crack length. The values obtained are compared to those for the tubular strain-controlled specimen in Section 5.2.3.

The most accurate strain intensity factor solutions for the chordwise turbine vane crack would be obtained from a full three-dimensional fracture mechanics analysis of the vane, including explicit modeling of several through-thickness cracks of various lengths. This type of analysis is best since the long cracks in the vane affect the overall compliance of the structure. In the absence of such a complex detailed analysis, strain intensity factor values were obtained from a handbook solution for a center-cracked plate. The spanwise strain range was taken from Section 3, assuming a uniform value of 0.37 percent.

The spanwise turbine blade crack was analyzed as an edge-cracked panel with the width of the panel being equal to the thickness of the blade wall. An initial crack depth equal to a typical coating thickness of about 0.012 cm (0.005 in) was assumed for the analysis. The chordwise strain driving the crack was resolved into a bending and a membrane component. The bending

component of the strain is the result of a temperature difference through the thickness of the wall of about 204°C (400°F). The membrane portion of the strain is then obtained by subtracting the bending strain from the total strain of 0.32 percent reported in Section 3. Thus, the strain intensity factor range was obtained from

$$\Delta K = \Delta K_M + \Delta K_B$$

$$\Delta K = \Delta\varepsilon_M\sqrt{\pi a}\ \ F_M(a/h) + \Delta\varepsilon_B\sqrt{\pi a}\ \ F_B(a/h)$$

$$\Delta\epsilon_M = 0.2 \text{ percent}; \qquad \Delta\epsilon_B = 0.12 \text{ percent}$$

where the subscripts M and B refer to membrane and bending components, respectively.

F_M and F_B are the geometry correction factors for an edge-cracked plate under pure membrane and pure bending strain loading, respectively. A schematic of the geometry is shown in Figure 14.

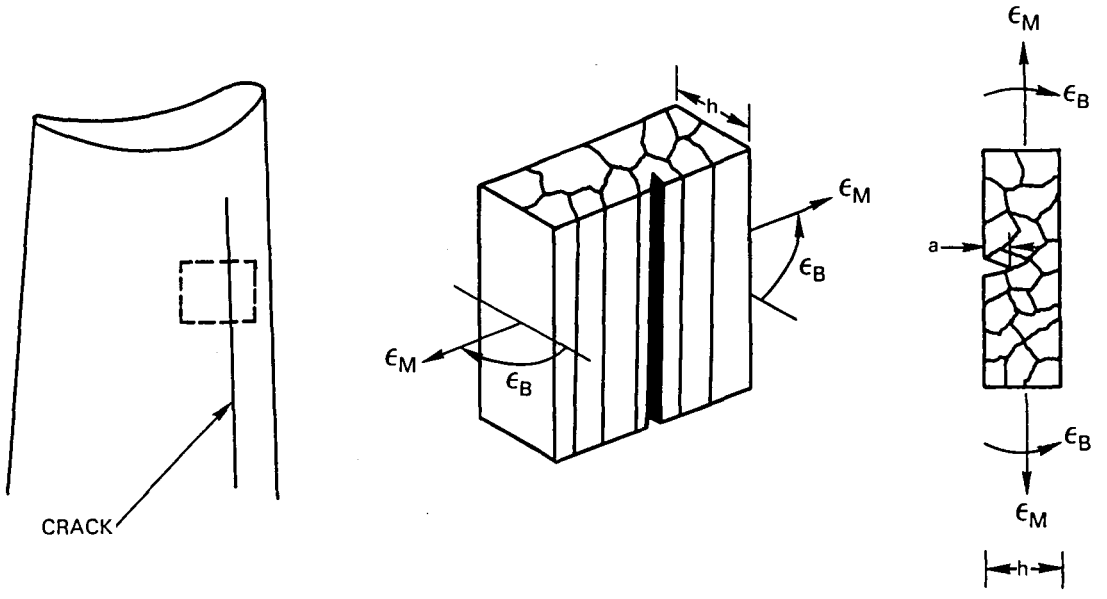

Figure 14 Spanwise Turbine Vane Crack.

The strain intensity factor solutions for the vane and blade crack are given in Section 5.2.3.

5.2.3 Specimen-Component Analysis Comparisons

The comparison of the strain intensity factor solutions for the specimens given in Section 5.2.1 and the components given in Section 5.2.2 are presented here. The result of the combustor liner analyses and the tubular specimen results are superimposed in Figure 15. It is clear that the range of ΔK_ϵ

values obtained during specimen testing ($6.4 \times 10^{-4} \leq K_\epsilon \leq 6.4 \times 10^{-3} \sqrt{cm}$. ($4.0 \times 10^{-4} \leq K_\epsilon \leq 4.0 \times 10^{-3} \sqrt{in.}$)) is large enough to include the range of values for the combustor liner. Therefore, a combustor liner crack propagation analysis using the strain intensity factor could be performed using the specimen crack growth data without need for data extrapolation.

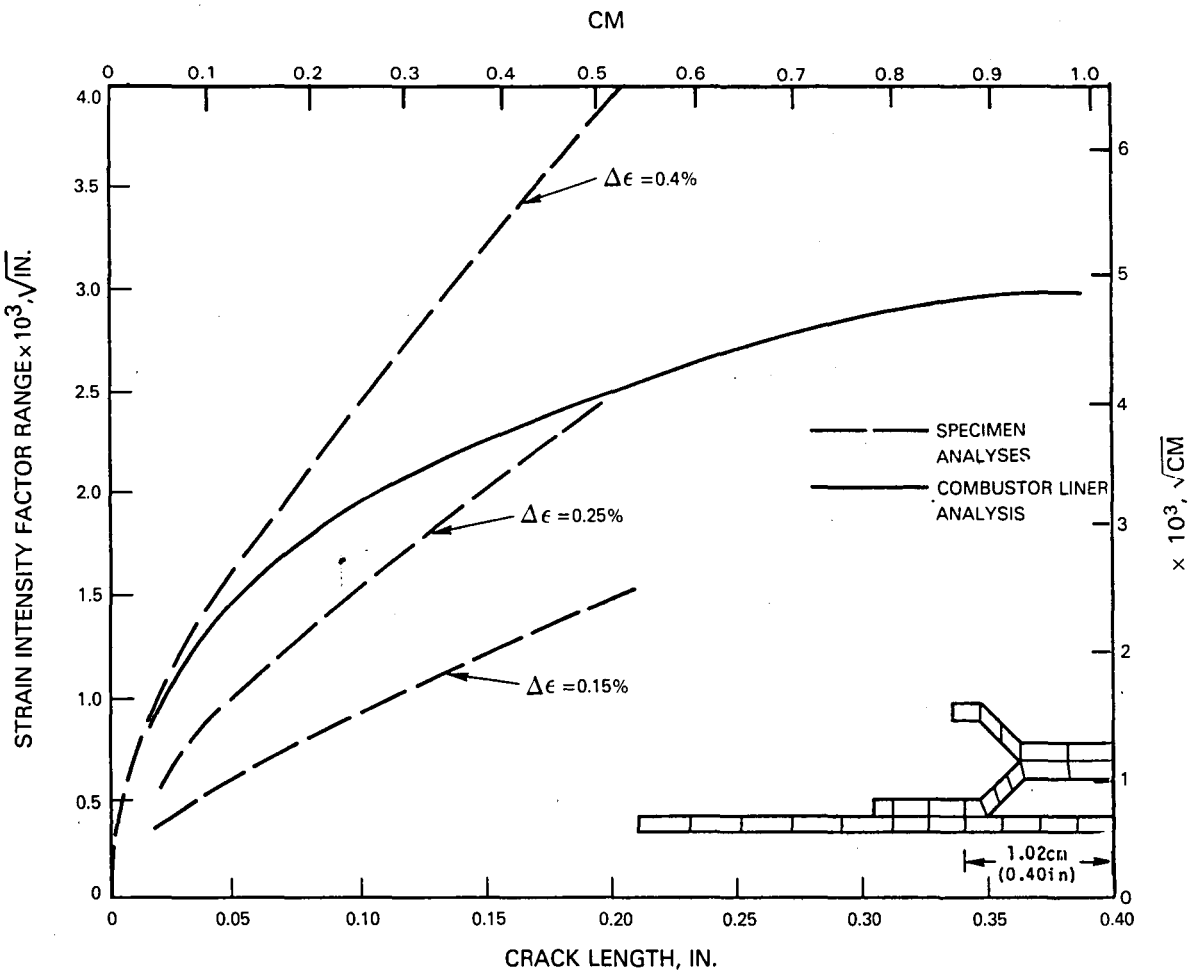

Figure 15 Comparison of Combustor Liner Component and Tubular Test Specimens using Strain Intensity Factor.

The results of the turbine vane, blade, and specimen fracture mechanics analyses are shown in Figure 16. It is noted that the typical crack length values for the vane and blade are radically different, and are also different for the range of crack length values in the tubular specimens. However, the range of values for the strain intensity factor is about the same for the vane, blade, and specimen. Thus, testing of the tubular specimens will provide

crack growth data which are directly applicable to the component, so long as the following assumption is made. This assumption is that crack growth rates are uniquely determined by the value of the correlation parameter, independent of the crack length. Specimen testing described in Section 4 will determine if this assumption is correct for turbine vane and blade materials.

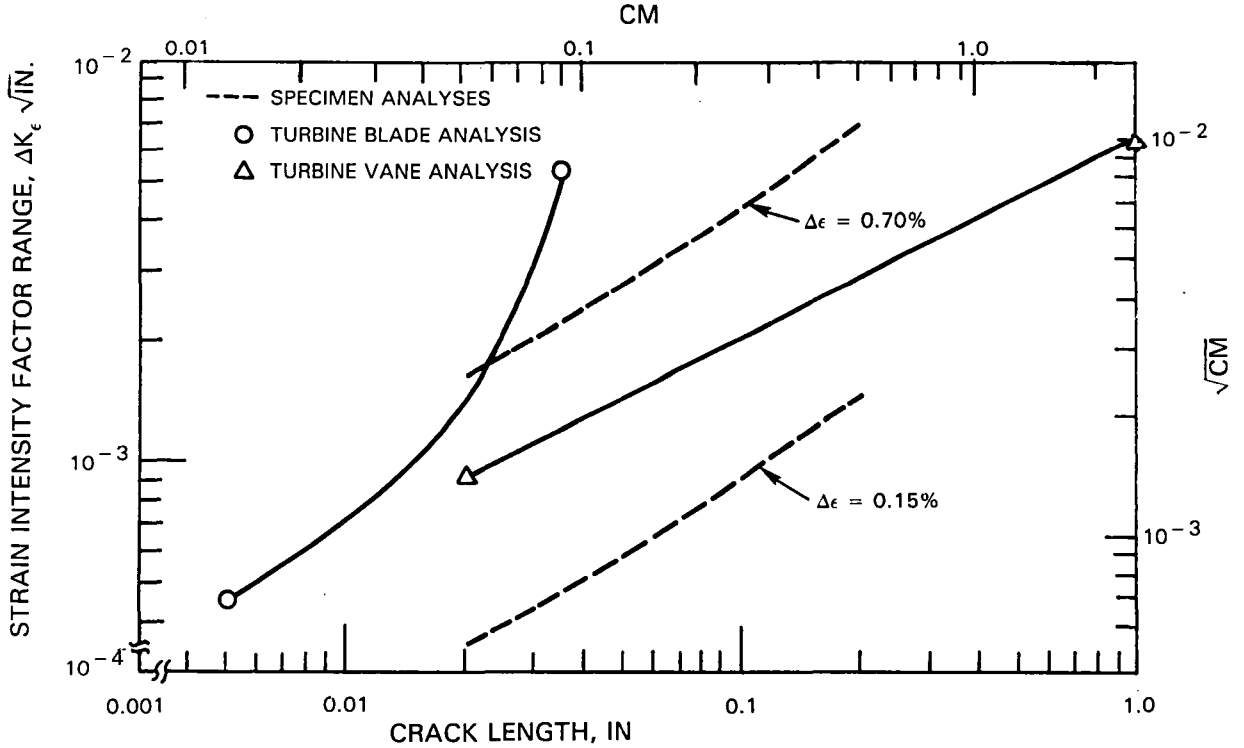

Figure 16 Comparison of Turbine Vane and Blade Components and Tubular Test Specimens using Strain Intensity Factor.

5.3 J-INTEGRAL ANALYSES

5.3.1 Specimen Analysis

5.3.1.1 Preliminary Test and Analysis

To perform the crack propagation data reduction described in Section 7, it was necessary to determine the value of the J-Integral for the tubular specimen. To investigate techniques for its calculation, a preliminary test program was conducted. The procedure used load-deflection (compliance) curves of several tubular specimens containing various crack lengths which span those expected in the crack propagation testing. The material tested was B-1900, a nickel-base superalloy used in turbine blade applications. This material was used since specimens were readily available from a previous test program and could be supplied at no cost.

The specimens were the ones shown previously in Figure 11. Circumferential slots were machined into three specimens using an EDM (Electrical Discharge Machining) technique. The slots had lengths of 0.680 cm (0.268 in), 0.972 cm

(0.383 in), and 1.066 cm (0.420 in), compared to a total specimen circumference of about 3.8 cm (1.5 in). A fourth specimen was unslotted to obtain nominal stress-strain behavior. The specimens had a nominal wall thickness of about 0.10 cm (0.04 in).

The load-deflection data from the test specimens were smoothed to give the curves shown in Figure 17. A value for J was then calculated based on:

$$J = \int_{o}^{\Delta} \left(\frac{\partial P}{\partial a}\right)_{\Delta} d\Delta$$

where: Δ = load point displacement
P = load (force per unit length of crack front)
a = 2 x crack length x thickness

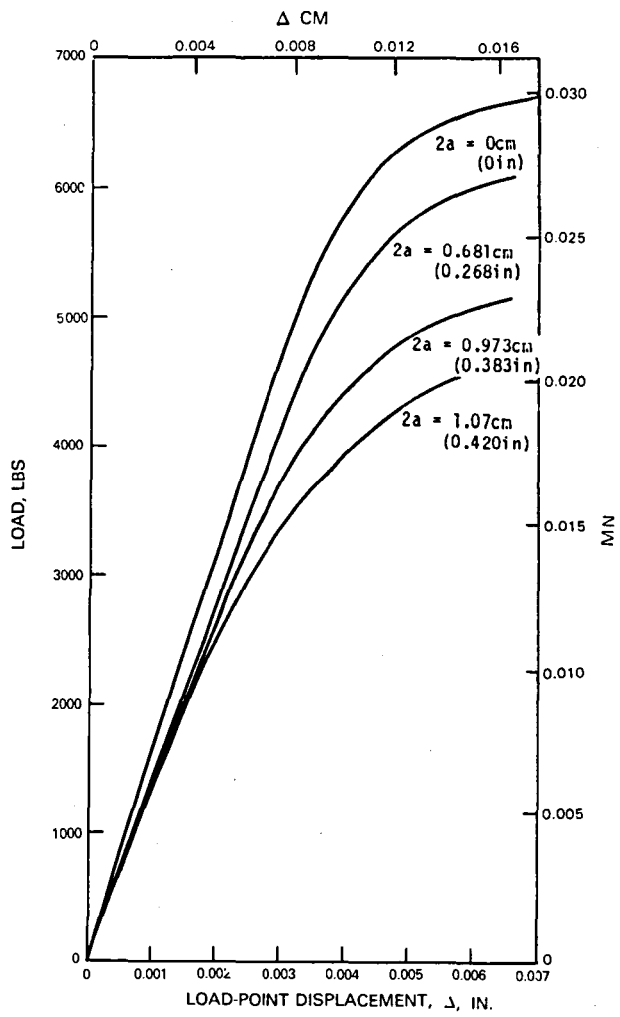

Figure 17 Smoothed Load-Displacement Curves from Preliminary Tests of B-1900 Tubular Specimens.

The above form is used in the standard Begley-Landes data reduction scheme (4). The value of J calculated by this method is shown in Figure 18. The procedure used is similar to that shown in Figure 19, with the following exception. Rather than using a curve fit to the three crack lengths as shown in Step 2, straight line segments were drawn between the work, crack-length pairs. The slope of the resulting line is then used to calculate J, which is then applicable to crack lengths between those actually tested. In the elastic range, it was found that the experimental value of the stress intensity factor computed from $K_\sigma = \sqrt{EJ}$, and the theoretical value, computed from $K_\sigma = \sigma\sqrt{\pi a}\ f$ (geometry) (see Section 7.1), agreed to within 5 percent.

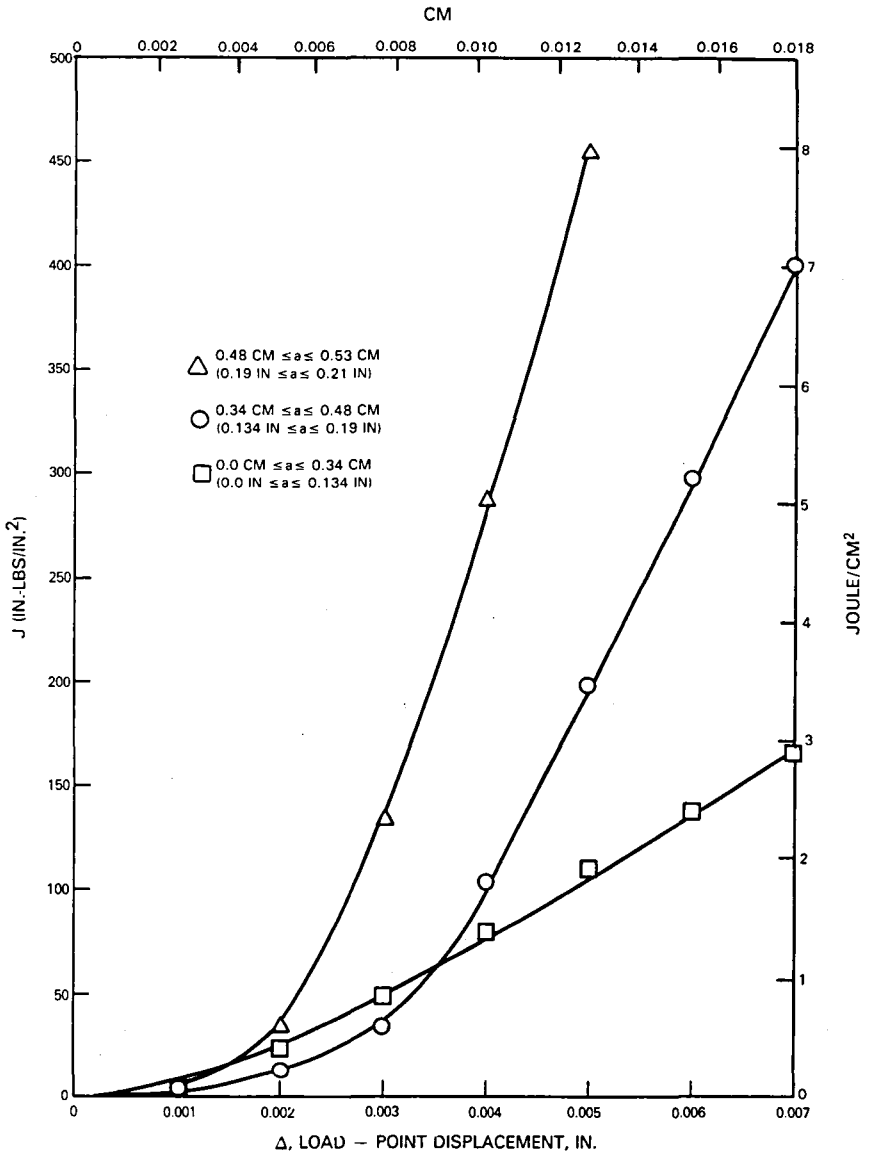

Figure 18 J-Integral Solutions from Preliminary Specimen Tests.

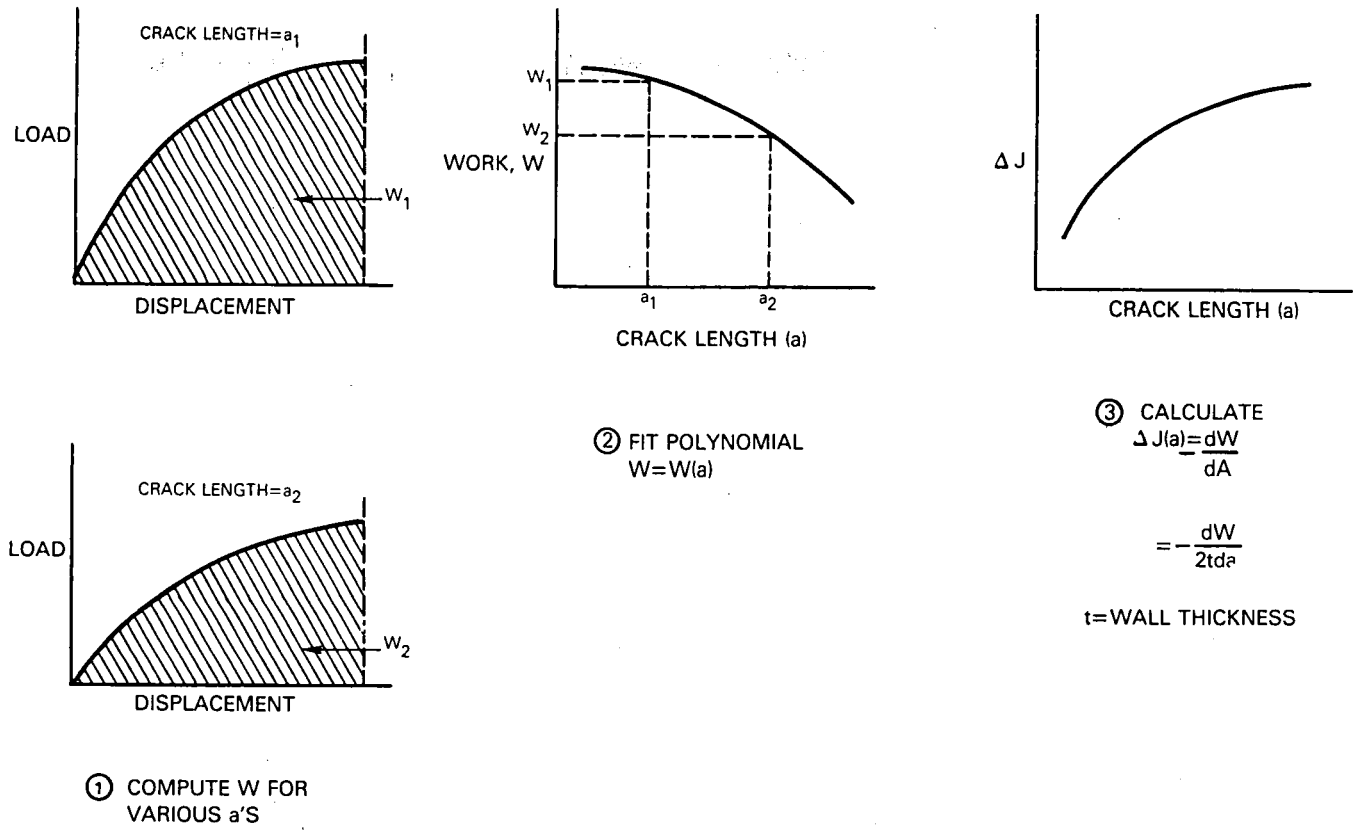

Figure 19 J-Integral Calculation Procedure using Compliance Approach.

The data from the preliminary test program served two major purposes. First, it demonstrated that changes in specimen compliance as a function of crack length were large enough to allow J-Integral calculations to be made for the tubular specimen using experimental load-displacement data, at least for the case of non-cyclic (i.e., monotonic) loading. Second, the elastic J calculation described above provided a check for the formulas used in the stress and strain intensity factors given in Section 7.1. The analysis procedure actually used for the Hastelloy X specimens is given below.

5.3.1.2 Cyclic Analysis for Hastelloy X

The procedure described above was extended to the case of the Hastelloy X cyclic loading described in Section 7 by the following procedure.

1. A number of load-displacement records are obtained for each specimen in the course of conducting the crack propagation test. The area under the up-loading portion of each load-displacement curve is measured with a planimeter.

2. The area (work) is plotted as a function of crack length. A polynomial is fitted to this curve.

3. The polynomial is analytically differentiated with respect to crack area to give J as a function of crack length: $\Delta J(a) = -dW(a)/dA$, where W = work (area under load-displacement curve) and A = crack area (2 x thickness x crack length).

A schematic of this procedure is given in Figure 19. The technique was used to obtain J-values for one of the isothermal Hastelloy X crack propagation tests (Test I-16, 871°C (1600°F), 0.4-percent strain range). The work as a function of crack length is shown in Figure 20. The curve is nearly linear for longer crack lengths. Differentiation of the curve gives a nearly constant value of J for these crack lengths. This result is unacceptable since plotting crack growth rates versus J from the testing described in Section 7 (Figure 21) shows the crack growth rates increasing while J is constant. The implication is that this method of J calculation is very sensitive to the exact shape of the work vs. crack length curve for cyclic loading; an alternate technique is required.

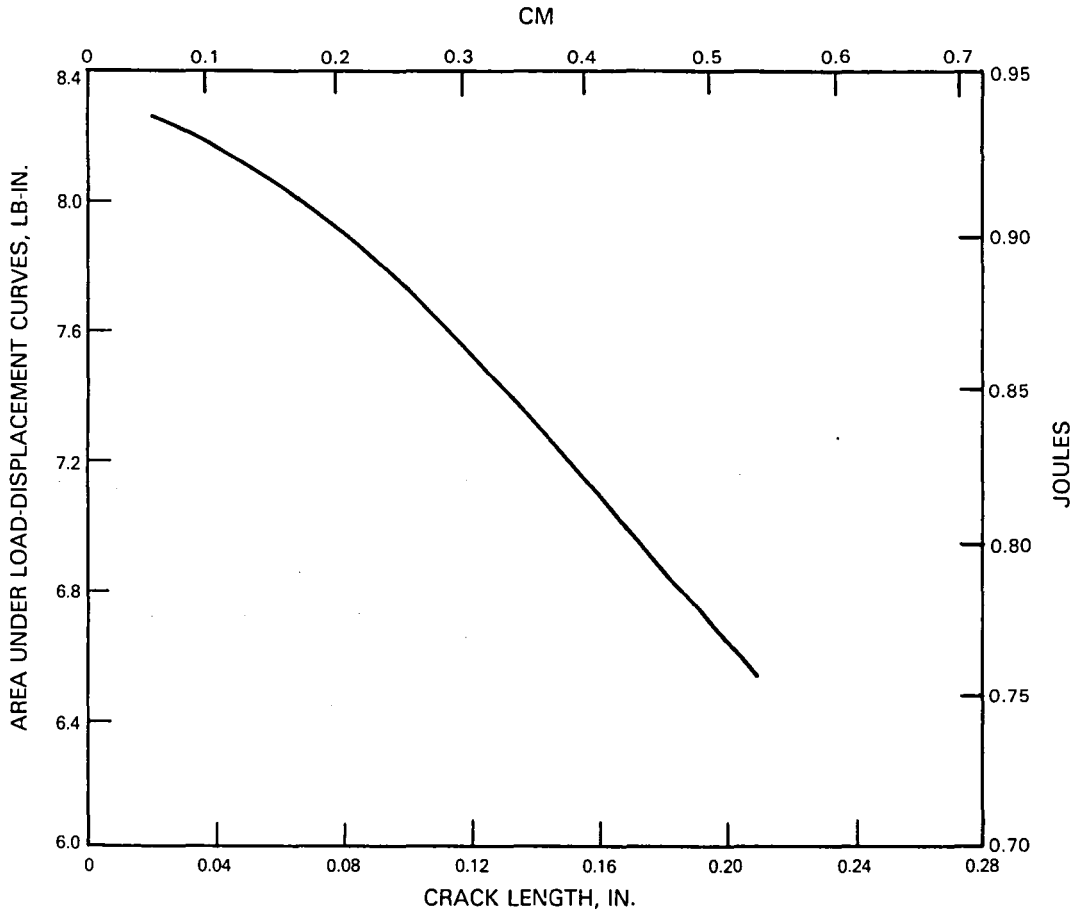

Figure 20 Area Under Load-Displacement Curves for 871°C(1600°F), 0.4 percent Strain Range Test.

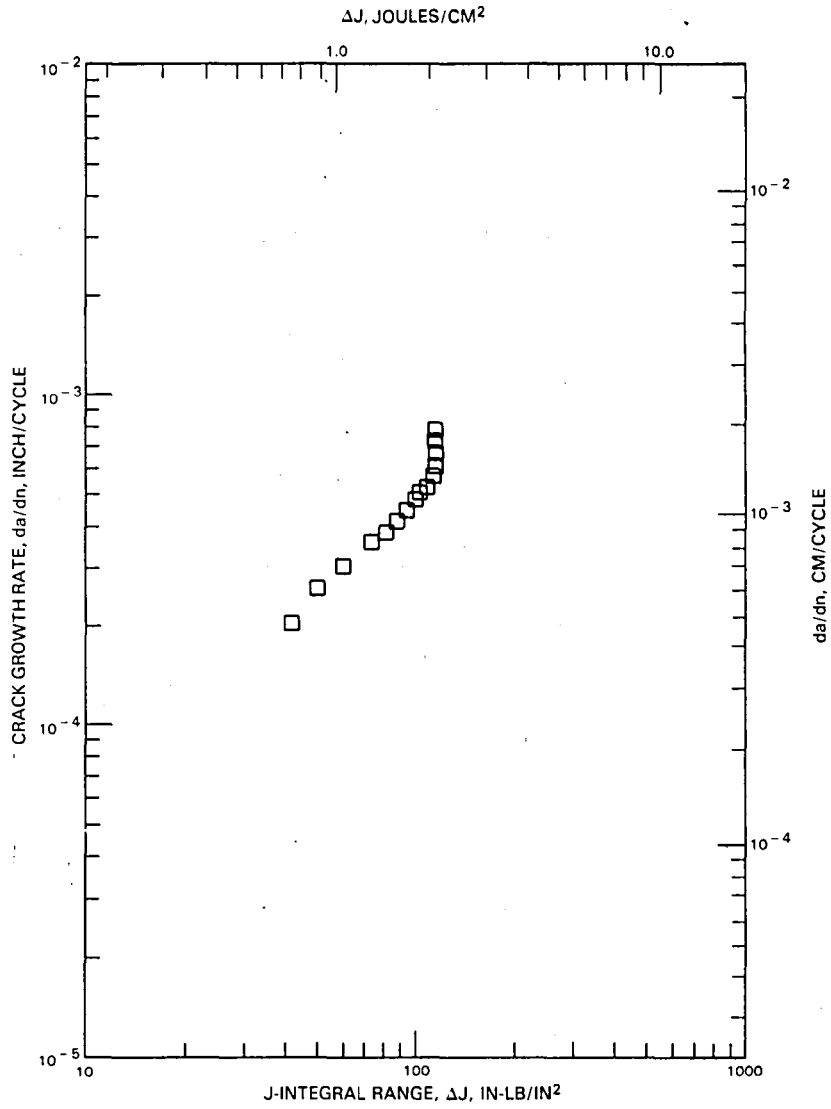

Figure 21 Crack Growth Data Reduction using Compliance Approach for J Calculation.

The procedure actually employed in the data reduction was to calculate J by adding together the elastic and plastic values, using load-deflection data obtained during the testing to calculate elastic work and plastic work quantities. The equations used in this calculation procedure, based on an approach suggested by Shih and Hutchinson (5), are as follows:

$$\Delta J_{Total} = \Delta J_{Elastic} + \Delta J_{Plastic}$$

$$\Delta J_E = 2\pi \Delta W_E \, a \, F_1(\text{geometry})$$

$$\text{where } \Delta W_E = (\Delta \sigma)^2/2E$$

$$\Delta Jp = \pi \Delta Wp\ a\ (1 + \lambda)\ F_2(\text{geometry})$$

where $\Delta Wp = (\Delta \sigma \Delta \epsilon_p)/(1 + \lambda)$

is obtained from the cyclic stress-strain curve where:

$$(\Delta \sigma/2) = K(\Delta \epsilon p/2)^{\lambda}$$

F_1 = the elastic geometry correction factor for the tube specimens, given in Section 5.2.1.

F_2 = the approximate plastic geometry correction factor for the tube.

$F_2 = F_1 \times C(\lambda)$, where $C(\lambda)$ = the plastic magnification term, taken from small crack length J-Integral solutions for a flat plate obtained in (5).

A comparison of the J values obtained using the compliance technique and using the sum of the elastic and plastic values is given in Figure 22. Further J calculation results are given in Section 5.3.3.

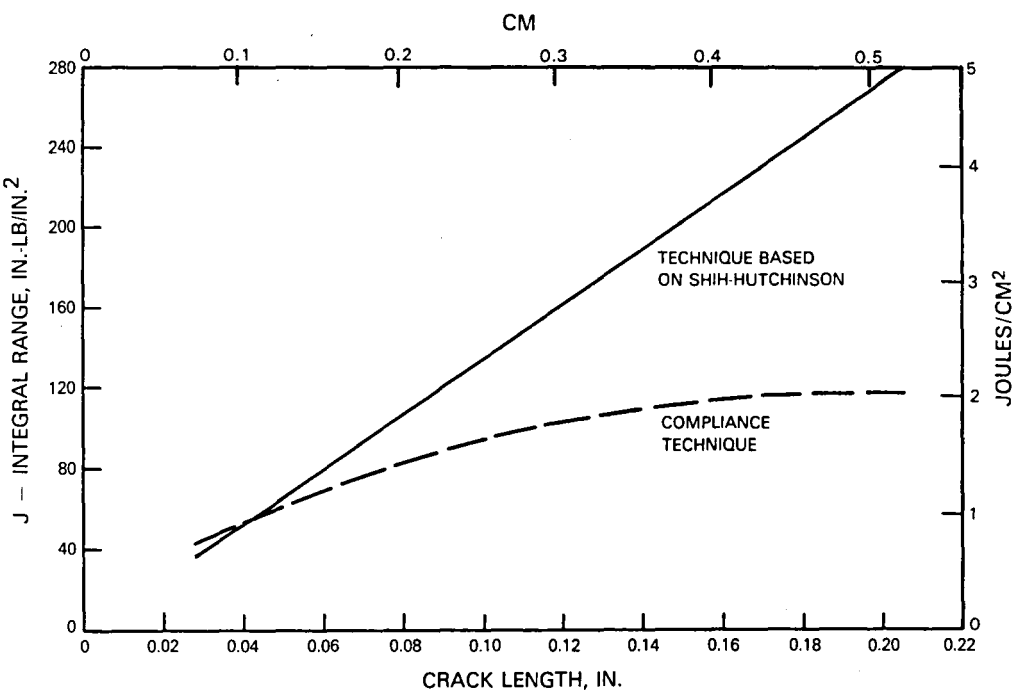

Figure 22 Comparison of Alternate J-Integral Solutions for 871°C(1600°F) Test.

5.3.2 Combustor Liner Component Analysis

5.3.2.1 Finite Element Analysis Procedure

The J-Integral concept, first introduced by Rice (6), has gained some acceptance in recent years as a parameter to use for non-elastic materials in predicting crack growth life. Rice showed the important path-independence characteristic of the J-Integral definition for a two-dimensional, isotropic, isothermal, homogeneous non-linear elastic material. For this case, he defined the strain energy density W as

$$W = \int_0^{\varepsilon_{ij}} \bar{\sigma}_{ij} \, d\bar{\varepsilon}_{ij}$$

where σ_{ij} and ϵ_{ij} are the stress and strain components respectively.

Then,

$$\sigma_{ij} = \frac{\partial W}{\partial \varepsilon_{ij}}$$

Looking at the neighborhood of a crack tip, Figure 23, the J-Integral can be written as

$$J = \int_\Gamma (W \, dx_2 - \sigma_{ij} n_j \frac{\partial u_i}{\partial x_1} \, ds)$$

where Γ is any path starting at the bottom crack surface and moving in a counterclockwise direction around the crack tip to the top crack surface and u_i is the displacement vector. Path independence for J can then be proven in a straightforward manner (7).

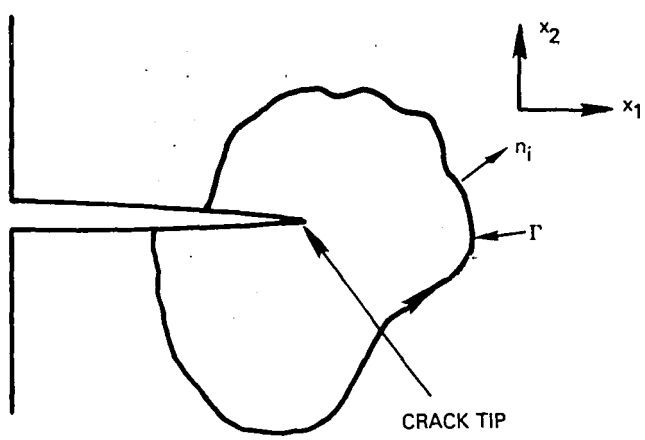

Figure 23 Contour used in J-Integral Definition.

If the crack in the body under consideration is described by the length parameter, a, then the potential energy of the body, $\Pi(a)$, can be written as:

$$\Pi(a) = \int_A W d\bar{A} - \int_{\Gamma_T} \sigma_{ij} n_j u_i ds$$

where A is the area of the body containing the crack and Γ_T is the portion of the boundary curve about area A on which tractions (that is, loads) are specified. It can then be proven (7) that J is related to $\Pi(a)$ simply as

$$J = \frac{-d\Pi(a)}{da}$$

This last relationship of J to potential energy provides a technique for calculating J both analytically and experimentally.

For our specific needs, the MARC (8) nonlinear finite element structural analysis computer program was utilized for calculating cyclic stress-strain displacement response of a burner liner configuration. The program contains an internal calculation for J on a contour specified by the user. The internal calculation is based on the relationship obtained above. In a finite element formulation, the potential energy $\Pi(a)$ can be written as

$$\Pi(a) = \{u\}^T[K]\{u\} - \{u\}^T\{F\}$$

where $\{u\}$ is the vector of total nodal displacements, [K] is the symmetric stiffness matrix, and $\{F\}$ is the vector of equivalent nodal loads.

An expression for $d\Pi(a)/da$ can then be obtained, with the aid of the equilibrium equation, $[K]\{u\} = \{F\}$, as follows (9):

$$\frac{d\Pi(a)}{da} = \{u\}^T \frac{d[K]}{da} \{u\}$$

where the crack surface is assumed to be traction free. The MARC program calculates numerically the change in stiffness, Δ [K], for a given contour moving an amount Δa in the crack direction, with all other points remaining fixed. Thus, $d[K]/da$ is approximated by $\Delta[K]/\Delta a$, where Δa is typically at least one order of magnitude smaller than a.

The comments presented above are fully applicable for an isotropic, isothermal homogeneous, nonlinear elastic body and have been documented extensively in the literature. The combustor liner situation, however, involves two major complicating factors: nonuniform temperatures and material inhomogeneity (since material properties vary with temperature). When these two features are present, the path independent characteristic of the J-Integral defined by Rice no longer is valid (10). In such a situation, a modified type of J-Integral, such as J* defined by Blackburn (11), may be usable:

$$J^* = \lim_{\Gamma \to 0} \int_{\Gamma} \left[\frac{1}{2}\sigma_{ij}\frac{\partial u_i}{\partial x_j} dx_2 - \sigma_{ij}n_j \frac{\partial u_i}{\partial x_1} ds\right]$$

The internal calculation for J provided by MARC thus is suspect for nonuniform temperatures and material properties. Consequently, an evaluation was carried out of the internal J-Integral calculation in MARC, with specific interest to its usability on a practical basis for the combustor liner. The results of this evaluation are discussed below.

5.3.2.2 Analysis Technique Verification Studies

The first series of cases were run on the geometry provided by the MARC User's Manual (6) for their sample elastic J-Integral calculation, Figure 24. The Barsoum (12) special crack tip element technology was used for all elements containing the crack tip node. The results for pure opening mode mechanical loading were in excellent agreement with those given in the Manual. In addition, solutions for several two-dimensional elastic plane stress situations with uniform opening mode traction loadings were obtained and compared to handbook values as shown below:

Problem Type	K(Handbook)/K(MARC)
Center Cracked Panel	0.987
Single Edge Notch Panel	1.003
Double Edge Notch Panel	0.976

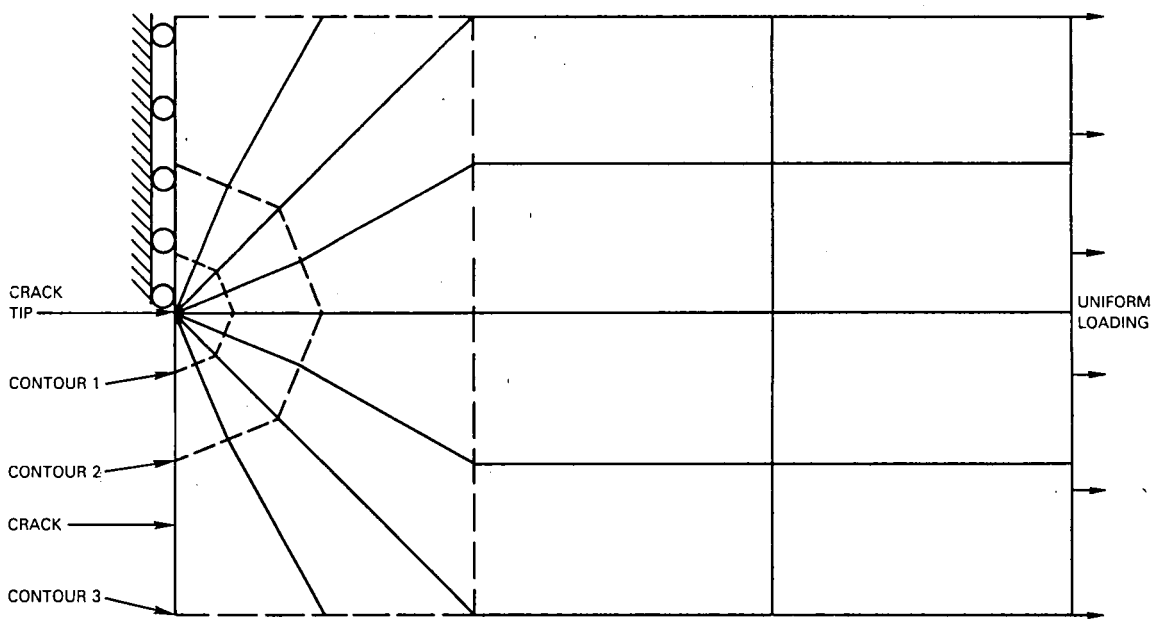

Figure 24 Coarse Grid Finite Element Mesh for J-Integral Test Cases.

Here K is the opening mode stress intensity factor and is related to J for the elastic plane stress case by

$$K = \sqrt{EJ}$$

where E is the elastic modulus.

The next series of cases run on this geometry evaluated directly the effect on the elastic J-Integral calculation of nonuniform temperatures and nonhomogeneous material properties. The applied boundary conditions simulated an edge crack specimen with uniform opening mode tractions. The elastic modulus E

varied spatially in a linear manner in the crack direction, with E_{AVG} = 1/2 (E_{MAX} + E_{MIN}) being the same value for all cases at the crack tip and Δ E = 1/2 (E_{MAX} - E_{MIN}) being a measure of the variation in modulus in the crack direction; all temperature effects were zeroed out. The MARC program allows J to be internally calculated along several different contours in the same analysis. The results shown in Figure 25 indicate that a varying elastic modulus leads to calculated values of J that are dependent on the contour chosen. The variation in J from one contour to another becomes greater as the variation in elastic modulus ($\Delta E/E_{AVG}$) increases. It is clear, therefore, that for a nonhomogeneous material, the J-Integral values calculated by MARC are no longer path independent but can vary by significant amounts (greater than 25 percent) depending upon the path chosen.

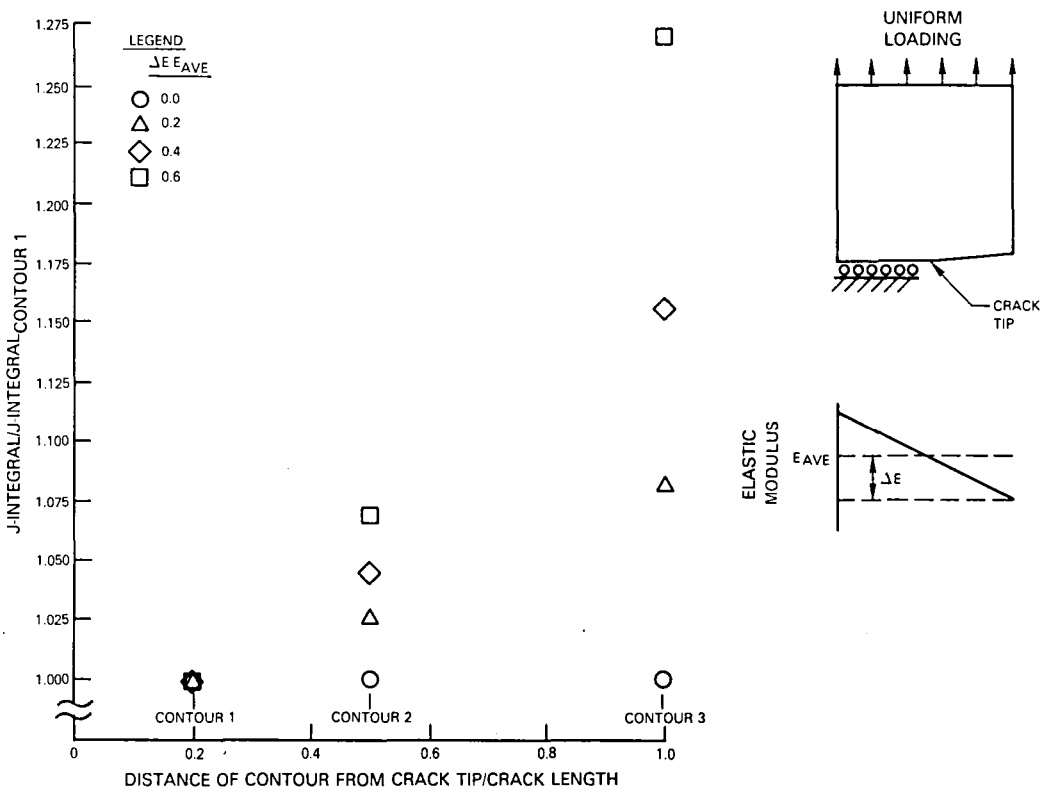

Figure 25 Effect of Elastic Modulus Variation on J-Integral Calculation using Coarse Grid.

Test cases involving a linear temperature gradient in the crack direction were also run for the Figure 24 geometry. All material properties were held constant. A linear temperature gradient applied to this geometry should introduce no thermal stresses, so that the J-Integral value should depend only upon the traction loading. However, the results in Figure 26 show this to not be the case. Here T_{AVG} = 1/2 (T_{MAX} + T_{MIN}) is the same value for all cases at the crack tip and Δ T = (T_{MAX} - T_{MIN}) measures the temperature variation in the body. For the contours considered, the MARC internal calculations of J can vary by more than 20 percent depending upon the contour chosen.

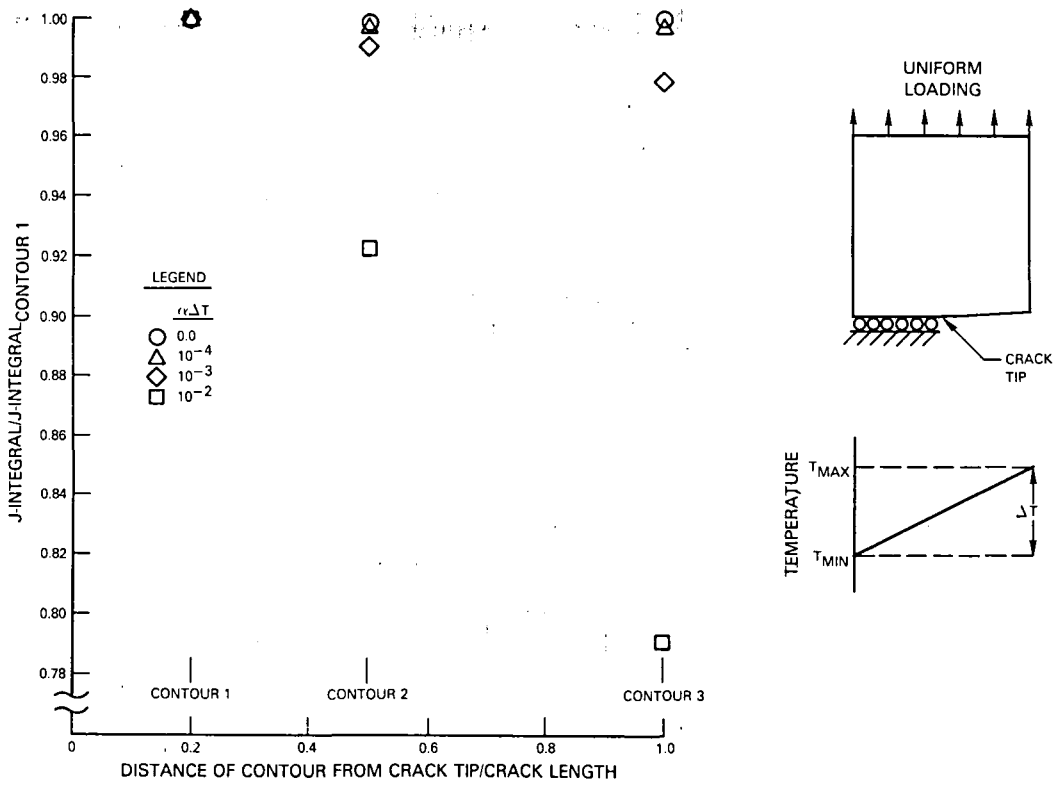

Figure 26 Effect of Linear Temperature Gradient on J-Integral Calculation Using Coarse Grid.

From these results, it was concluded that the MARC internal calculation of J exhibited significant path dependence for nonisothermal, nonhomogeneous cases and that these differences were unacceptable, at least for the geometry and grid breakup in the MARC sample case. In an attempt to overcome this obstacle, a rectangular body geometry was developed with a fine grid breakup in the crack tip region, Figure 27. This breakup was more representative of that expected to be used in the final combustor liner analysis, where the spatial variation in material properties and temperatures is not as severe as in the first series of cases just discussed. As before, the Barsoum special crack tip elements enclosed the crack tip node. The MARC internal J calculations were taken on contours 1, 2 and 3 in Figure 27 which were very close to the crack tip. In fact, this approach may be considered as a numerical approximation to the J*-Integral definition of Blackburn (11).

Elastic isothermal J-Integral calculations were performed on a double edge-crack plate simulation for the Figure 27 geometry with uniform opening mode tractions. The results in Figure 28 indicate that for a realistic elastic modulus variation, i.e., $\Delta E/E_{AVG} = 0.176$, the variations in the MARC calculated values of J from contour to contour are no greater than in the pure homogeneous (i.e. $\Delta E = 0$) case. Thus, for the isothermal nonhomogeneous elastic case, the fine grid break-up appears to be acceptable.

An incremental cyclic elastic-plastic analysis of the plate in Figure 27, with incrementally changing uniform thermal loading, was next attempted. At the point in the analysis where the crack first begins to open, it was found that the strain concentration at the fine mesh integration point nearest the crack tip was approximately 30 times nominal value. The elastic-plastic algorithm in the J1 version of MARC is stable only for comparatively small changes in strain per increment anywhere in the body. In particular, based upon the MARC user guidelines, it was calculated that temperature increments of about 1.1°C (2°F) would be required for stability with the fine grid breakup. This constraint was unacceptable because of the excessively large number of increments required to perform a full cyclic thermal-elastic-plastic analysis.

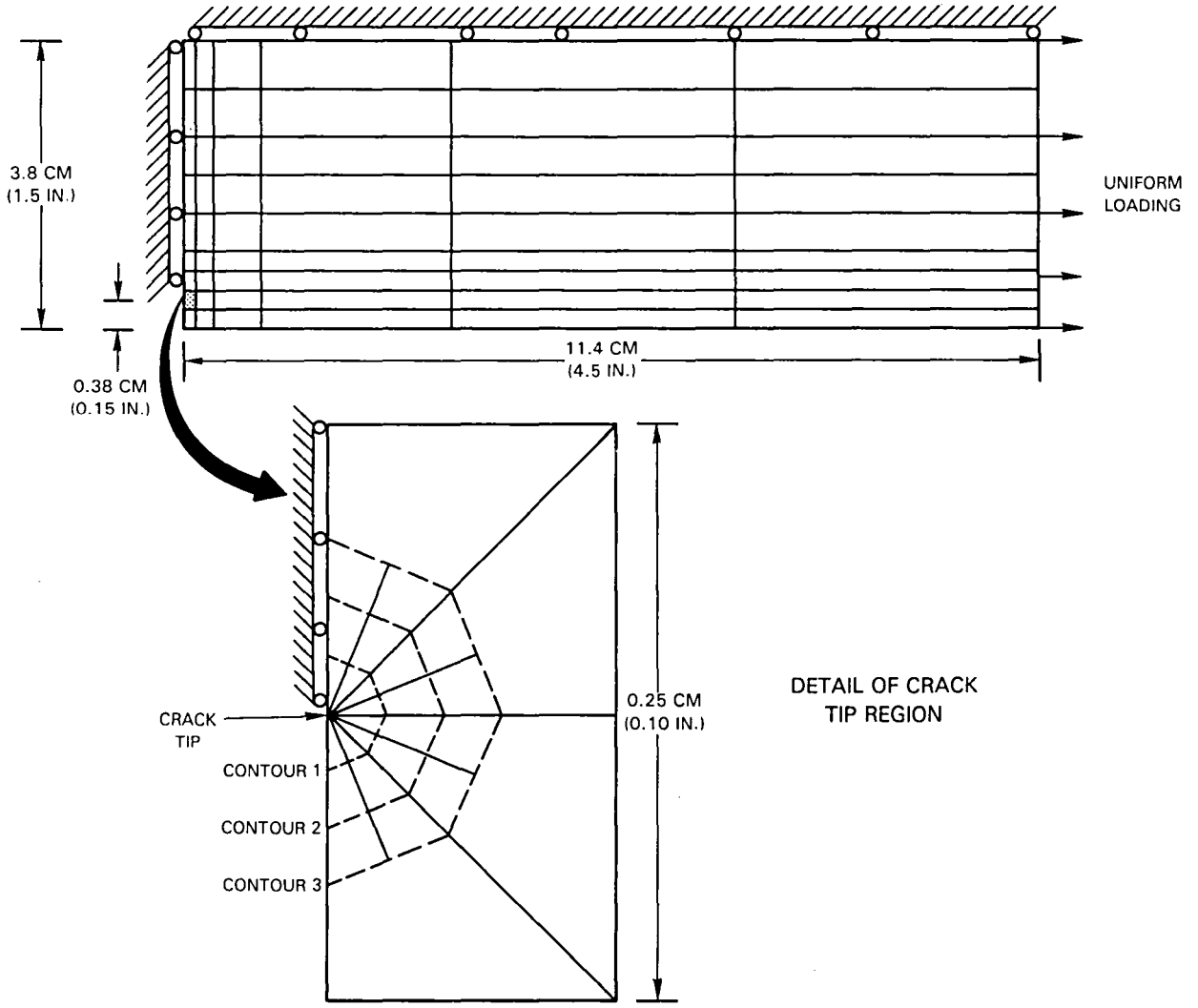

Figure 27 Refined Grid Finite Element Mesh for J-Integral Test Cases.

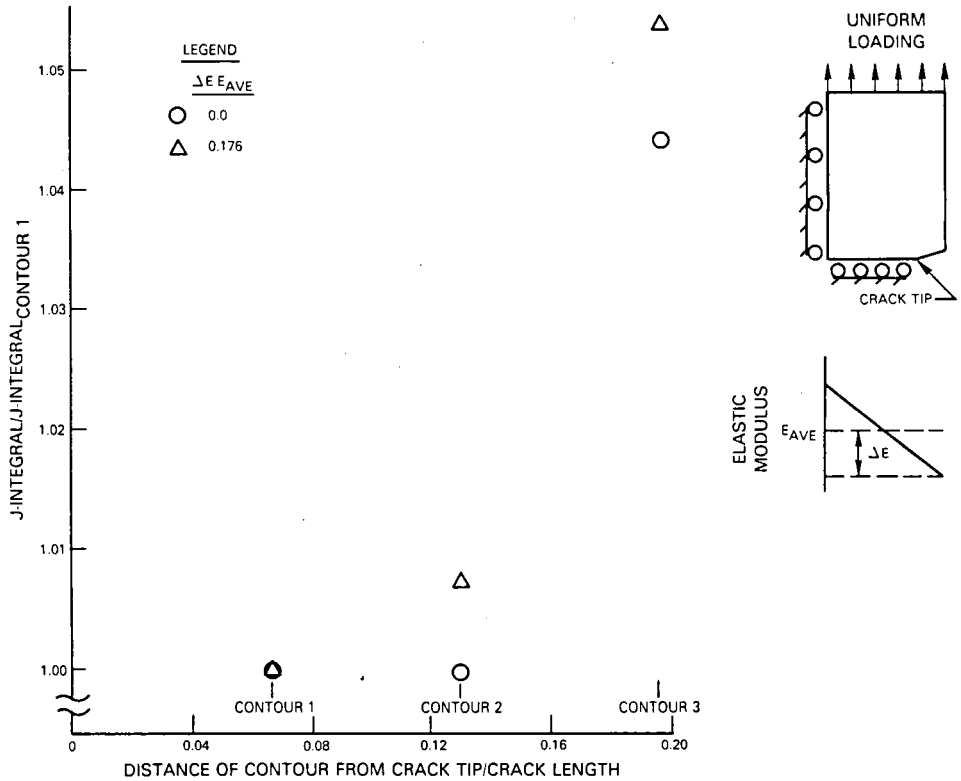

Figure 28 Effect of Elastic Modulus Variation on J-Integral Calculation using Refined Grid.

Consequently, the fine grid breakup was abandoned in favor of a coarser, more efficient grid breakup, Figure 29. Special element technology was not employed for elements containing the crack tip node; we are thus sacrificing accuracy of results near the crack tip in order to perform a full cyclic analysis. As a result, an alternative technique to the MARC internal J-Integral calculation was required; this was developed using a modified Begley-Landes (3) approach for load-displacement values at the right side boundary in Figure 29. For the actual burner liner cases run, the input loading at the right side boundary was in the form of uniform total nodal displacements δ . Consequently, a mechanical nodal displacement value δ_{MECH} can be defined for each node by

$$\delta_{MECH} = \delta - \Delta(\alpha T)\ell$$

where α is the coefficient of thermal expansion, T the temperature and ℓ the specimen length.

We can then consider a representative plot of P versus δ_{MECH} for different crack lengths, Figure 30. A complete thermomechanical cycle involves movement in this figure from 0 to A (maximum compressive strain) and then on reversal to B where the crack starts to open (the same in all cases). After point B, the cycle is completed by movement along one of the three curves indicated, depending upon crack length ($a_1 < a_2 < a_3$). The mechanical work done, W, during one complete cycle for a given crack length, a, can be written as

$$W(a) = \sum_{\substack{\text{Right} \\ \text{Side} \\ \text{Boundary} \\ \text{Nodes}}} \int_{\substack{\text{one} \\ \text{cycle}}} P \, d\delta_{MECH}$$

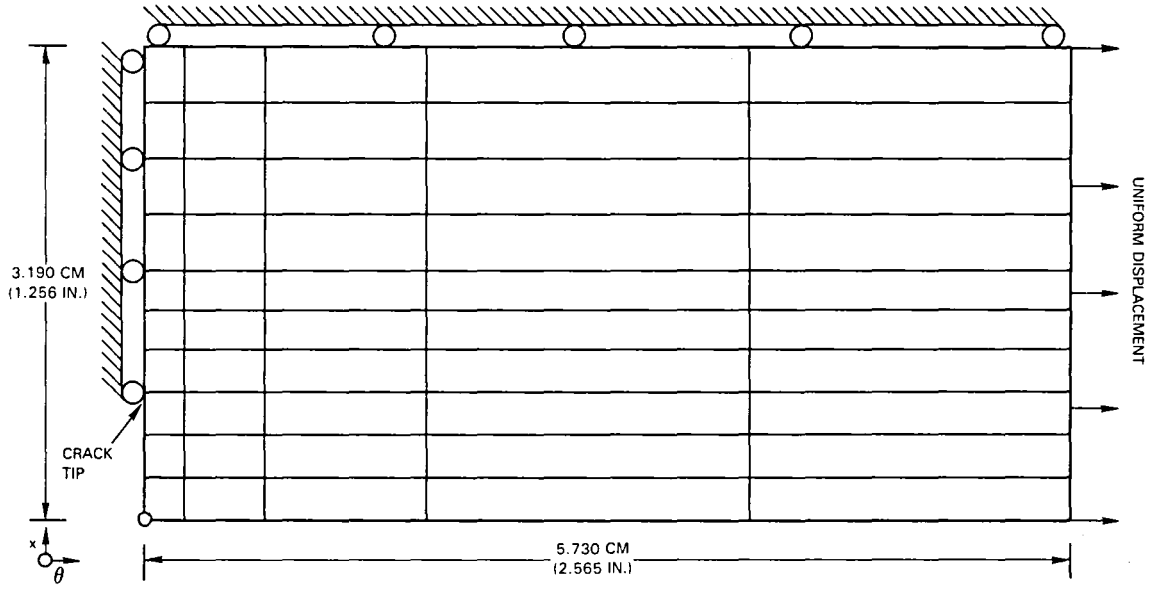

Figure 29 Finite Element Mesh for Combustor Liner J-Integral Calculation.

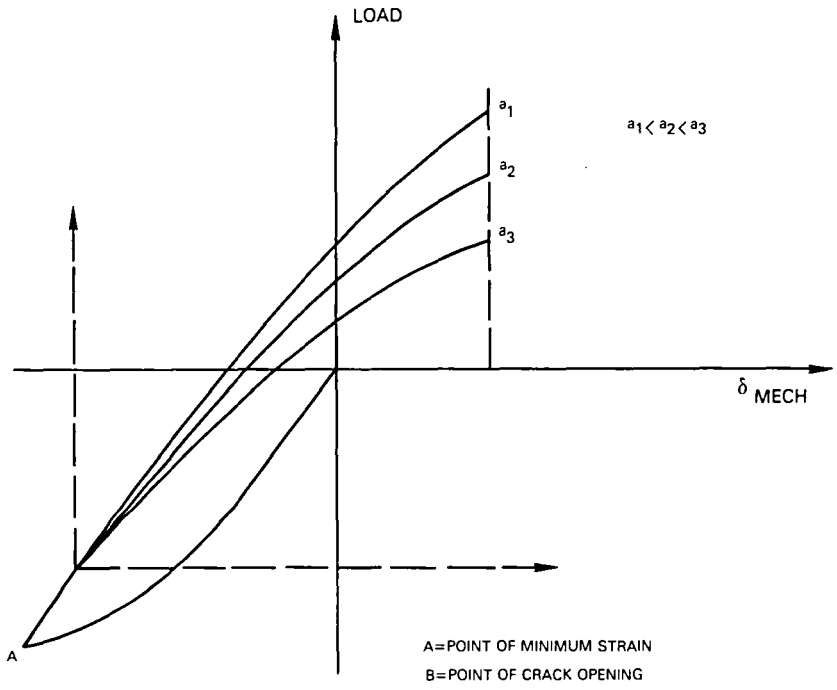

Figure 30 Schematic of Load - Displacement Information Obtained from Finite Element Analysis.

so that analogous to the Begley-Landes approach, we can write

$$J = -\frac{dW(a)}{d(at)}$$

where t is the out-of-plane thickness for the plane stress case.

To implement this approach, a post-processor was developed for the nodal point loads, displacements and temperatures at the right side boundary, Figure 29. Test cases were run with uniform thermal loading, constant material properties and opening mode traction loads. Full cycle calculations were made for two different crack lengths (0.99123 and 1.133 cm(0.39025 and 0.446 in)) and the results postprocessed to determine the mechanical work done per cycle:

Crack Length cm(in)	Mechanical Work Done per Cycle Joules(in.-lb)
0.991(0.390)	545.7(4829)
1.133(0.446)	529.3(4684)

The average crack length is a_{AVG} = 1.061 cm(0.418 in) and the change in crack length is Δa = 0.142 cm(0.056 in). For a plate of unit thickness, J can be approximated from

$$(-J)(\Delta a) = W(a = 1.133 \text{ cm}(0.446 \text{ in})) - W(a = 0.991 \text{ cm}(0.390 \text{ in})),$$

so that the value of J calculated is

J_{CALC} = 45.29 Joules/cm^2(2588 in-lb/in^2) for a_{AVG} = 1.061 cm(0.418 in).

A theoretical value of J can be found for this case from handbook formulas:

J_{TH} = 48.35 Joules/cm^2(2763 in.-lb/in^2)

Thus, J_{CALC}/J_{TH} = 0.94; this result is quite satisfactory considering the fact that $\Delta a/a_{AVG}$ = 4/30 and also that differentials are being approximated by finite differences in the calculation. The accuracy of the solution using the above approach justifies its use for the combustor component analysis, the results of which are presented below.

5.3.2.3 Cyclic Component Analysis

A cracked combustor liner represents a full three-dimensional structural analysis problem. However, a three-dimensional, cyclic, thermal elastic-plastic analysis was not considered feasible for this contract from both a time and cost standpoint. Consequently, an alternative two-step approach was developed. In the first step, a complete axisymmetric burner configuration, without an axial crack, was modeled, as shown previously in Figure 12. A full cyclic thermal elastic-plastic analysis was performed on this configuration. The results of this analysis were then used to generate the input loading for the second step of the procedure, a plane stress analysis of an axially cracked burner liner, Figure 29. The uniform incremental displacement input is

obtained from the hoop strain results of the axisymmetric analysis. In addition, the temperature input was obtained from an axisymmetric combustor liner thermal analysis. An efficient preprocessor computer program was developed for generating both input temperatures and displacements in the required MARC format.

The location of the axial crack is shown in Figure 29. Nodes on the crack surface are connected to ground via special "gap" elements in the MARC program. These elements keep the crack from overclosing due to a compressive load across the crack surface, but allow the crack to open normally due to a tensile load. Roller boundary conditions were used for the remainder of the crack plane, including the crack tip node. In addition, the double thickness at the seam weld in the Figure 12 axisymmetric model was accounted for in the plane stress model by giving the corresponding elements in Figure 29 twice the out-of-plane thickness of the rest of the elements.

The geometry in Figure 29 was run through a full thermomechanical cycle for three different crack lengths. The Hastelloy X material property information used in the analysis is shown in Figure 31. A bilinear representation of the material stress-strain curves was employed. In the course of running the analysis, stability problems were initially encountered for temperatures above 760°C(1400°F). The problem was traced to the way in which the temperature

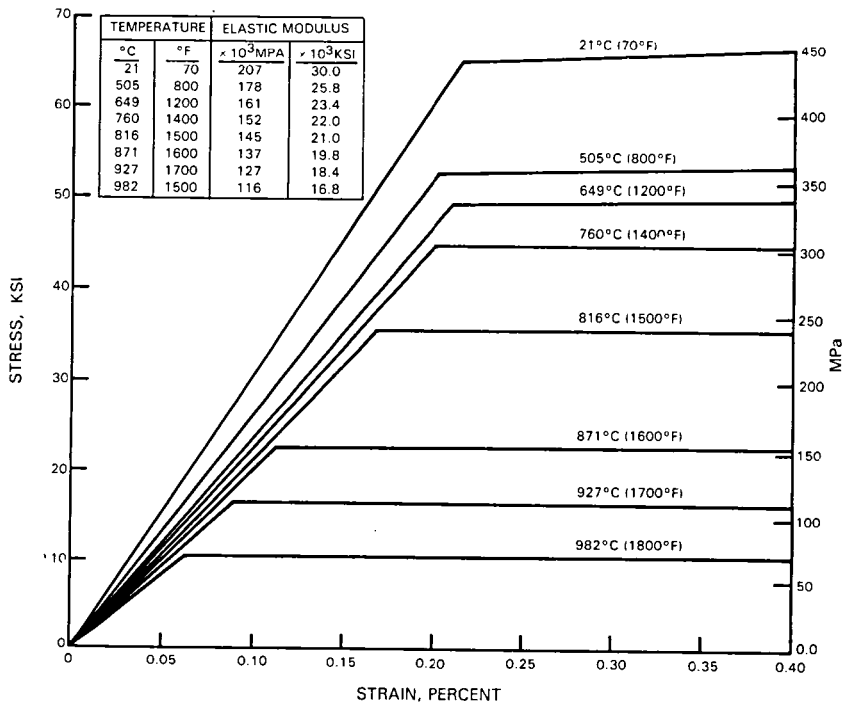

Figure 31 Hastelloy X Stress - Strain Representation for MARC Combustor Liner Analysis.

dependent plastic stress-strain data was input. An instability occurred when the direct MARC input stream was used; however, a satisfactory stable solution was obtained when the stress-strain curves were input via the user subroutine WKSLP.

For the nodes at which displacements were applied to the model, the temperature, load and displacement results were input into a post-processor (as described previously) to determine the mechanical work done W per cycle for each crack length. The work done from the point in the cycle where the crack opens (the same in all cases) to the end of the cycle is plotted in Figure 32. A least-squares best fit parabola was determined for W(a), with the constraint of having a zero slope for zero crack length. The value of J is then found by differentiating the parabola, and is thus found to be linear. Extrapolation of J beyond the range of crack lengths shown in the figure is not recommended.

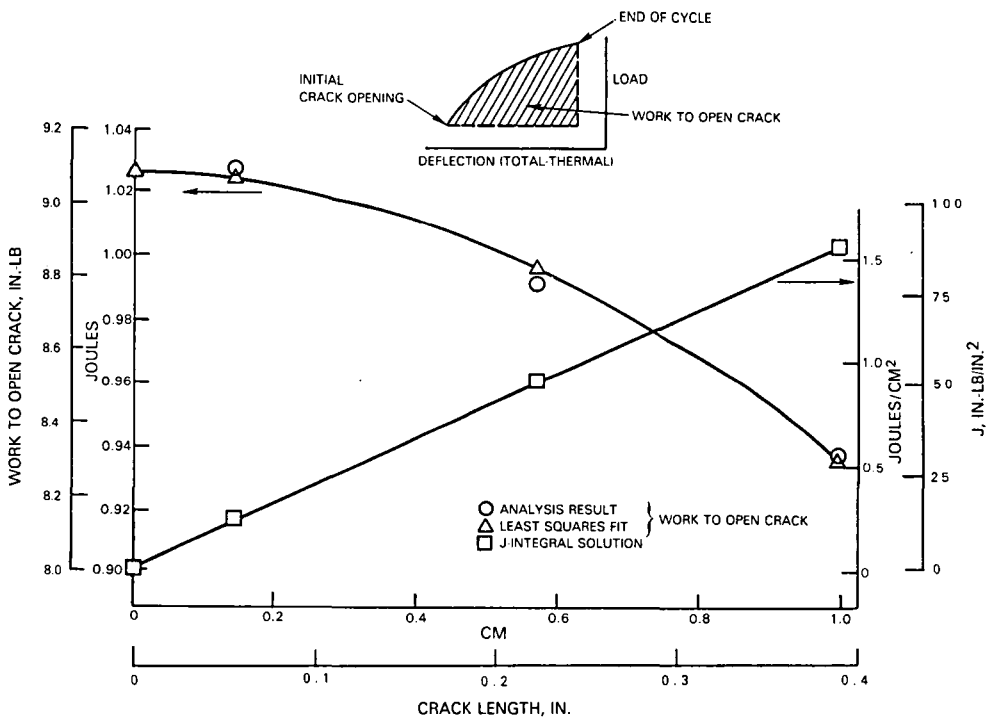

Figure 32 J-Integral Solutions from Combustor Liner Structural Analysis.

It should also be pointed out that the limitations of the analysis are as follows. First, the crack lengths analyzed are reasonably small compared to the plate width. The top and right side boundary conditions will therefore be only slightly affected by the crack. Second, the presence of the crack does not appear to affect the results at the right side boundary far from the

crack. Finally, the modified Begley-Landes J-Integral type approach allows us to calculate a reasonable J-type value for thermomechanical cycling; it is still unclear, however, whether this approach can be used successfully for other types of loadings, geometries or materials.

5.3.3 Specimen-Component Analysis Comparisons

The J-Integral analysis of the tubular specimen and the combustor liner component were described in Sections 5.3.1 and 5.3.2, respectively. In this section, J-Integral analyses of a typical specimen test and for the combustor liner are compared. As opposed to the strain intensity factor solutions, which are a function only strain range and crack lengths (Figure 15), the J-Integral solutions are different for each specimen test. These differences occur because J is a function of the material stress-strain response, which is different for each testing situation. For comparison purposes, the analyses chosen were for the 426 to 926°C(800°F to 1700°F) thermomechanical fatigue tests. The result of the comparison is shown in Figure 33. As was the case with the strain intensity factor solutions (Section 5.2.3), the range of J values from the specimen testing is large enough to include the range of values for the combustor liner.

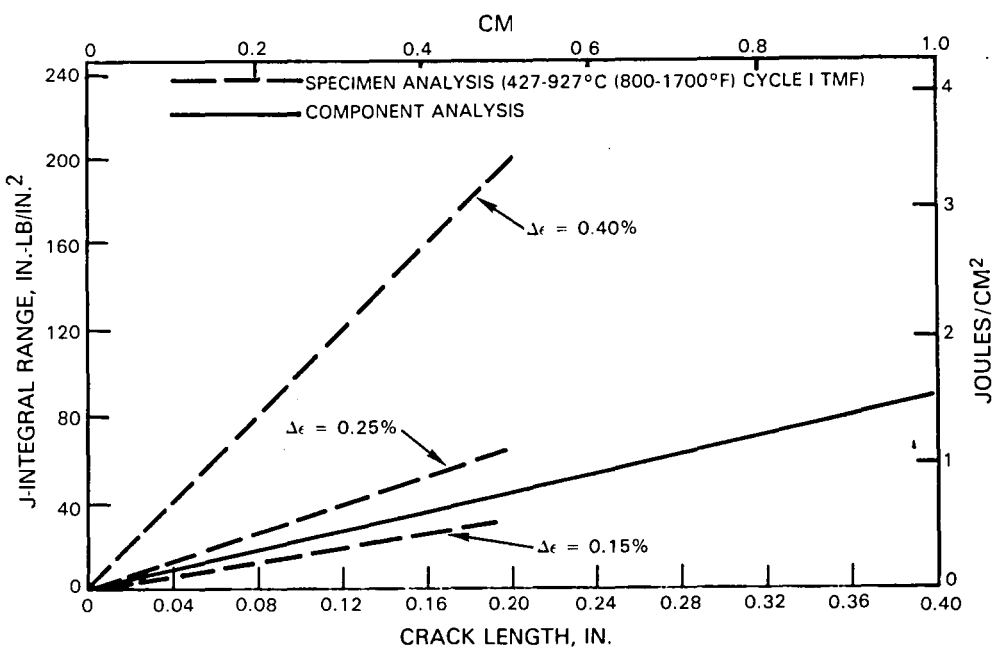

Figure 33 Comparison of Combustor Liner Component and Tubular Test Specimens using J-Integral.

It must be noted here that the "J-Integral" analysis of the component was performed using a compliance approach similar to that used previously by Begley and Landes. However, the combustor situation is different from theirs in the following respects. First, analytical load-displacement records are

used rather than those obtained from testing. Analytical results, which are dependent on material modeling accuracy, cannot be expected to be as accurate as testing results. Second, the same compliance definition that holds for isothermal situations is also assumed to hold for the case of TMF cycling. Third, the combustor liner has temperature and strain gradients which were not present in the original definition. The above observations indicate that the component analysis should not be termed a J-Integral solution in the strict sense. A "J-Integral"-like parameter has been calculated, but in fact the definition of J for the complex loading situation described is not clear.

It should also be noted that the approach for calculating J for the specimen is similar to that suggested by Shih and Hutchinson (4). Again, the concept developed for isothermal testing has been extended and is assumed to hold for TMF cycling. It is unclear whether this approach is completely valid.

In summary, it is evident that a better theoretical framework for calculating nonlinear crack propagation parameters such as the J-Integral needs to be built, for the case of TMF cycling. This appears to be an appropriate subject for future research.

SECTION 6.0

TASK IV - DEVELOPMENT OF CRACK PROPAGATION DATA

6.1 PURPOSE OF SPECIMEN TESTING

The overall purpose of this portion of the program was to define a testing program and carry out crack propagation testing on a typical material used in combustor liners of advanced aircraft engines in commercial service. This section describes the rationale for the specimen testing carried out in the program. The crack growth data reduction techniques and results are presented in Section 7.

The goals of the specimen testing program were defined to address two major features which are important in crack growth of combustor liners. The first feature is the extent of nonlinear material behavior, caused by a combination of high temperature levels, high strain levels, and low yield strength characteristics of current Pratt & Whitney Aircraft combustor material. Standard fracture mechanics techniques, which assume nominally linear elastic material behavior, may not be applicable under these conditions. Nonlinear techniques may be required. Thus, the first goal of the testing program was to assess the applicability of several linear and nonlinear parameters to correlate crack growth data under temperatures and strain levels encountered in typical combustor liner service application.

The second important feature is the presence of a complex variable temperature or thermomechanical cycle. This cycle is defined as one in which the temperatures and strains both change as a function of time. This aspect is not accounted for in simple specimen testing carried out under constant temperature (isothermal) conditions. The relationship of crack growth rates obtained from isothermal specimen testing to the rates obtained under thermomechanical conditions is not clear. Thus, a second goal of the testing program was to perform a prediction of crack growth rates obtained under thermomechanical cycling, using crack growth data obtained from isothermal specimen tests. The predictions would then be compared to specimen test data obtained under thermomechanical conditions.

The development of the testing plan to meet the above goals, and a description of the testing conditions used in this program, are given below.

6.2 SPECIMEN TESTING PROGRAM

6.2.1 Specimen Material

The material used was Hastelloy-X, which is used extensively at Pratt & Whitney Aircraft in commercial aircraft engine combustor liners. Hastelloy-X is a nickel-base alloy strengthened in solid solution by chromium and molybdenum. Current combustor liners are constructed of sheet metal. However, due to the types of testing required in this program, specimens made of sheet material could not be used. Instead, one inch diameter bar stock, manufactured

in a way to produce a grain size consistent with the sheet material, was used. Prior specimen testing has shown plasticity, creep and fatigue characteristics of the bar and sheet material to be similar.

The table below gives the chemical comparison of the material used in the testing.

Element	C	Cr	Co	Mo	W	Fe	Mn	Si	P	S	Ni
Percent by weight	0.10	22.0	1.5	9.0	0.6	18.5	1.0	1.0	0.040	0.030	remainder

6.2.2 Types of Tests

All tests in this program were conducted in laboratory air environment. Two types of tests were performed. The first type were isothermal tests in which the specimen was placed in an electric furnace and strain cycled at constant temperature. The second type were variable temperature (thermomechanical fatigue or TMF) tests in which the specimen was simultaneously strain cycled and temperature cycled. Transient heating was provided by an induction coil wrapped around the specimen. Transient cooling was provided by convective cooling of room temperature air. Further information concerning the specimen testing was previously described in Section 4 (see Table V).

6.2.3 Specimen Geometry

Tubular, strain-controlled specimens were used which have a crack initiating starter slot placed in the center of the specimen, perpendicular to the loading direction. The starter slot was nominally 0.101 cm(0.040 in) long by 0.012 cm(0.005 in) wide and is placed in the specimen using an EDM (Electrical Discharge Machining) technique. Tubular specimens were chosen in favor of flat sheets due to the capability of the tubular specimens to support both the compressive and tensile loading associated with typical combustor liner cracking. Two types of tubular specimens were used, as shown in Figure 34. The major difference between the two specimen types is the location of the extensometry ridges. External ridge specimens were used for the isothermal tests, internal ridge specimens were used for the TMF tests. Internal ridge specimens are the more costly of the two specimens to machine. However, in-house experience has shown internal extensometry to be required in the TMF tests due to the use of induction heating and forced air cooling.

6.2.4 Component Conditions

The dominant loading in the combustor liner arises as a result of temperature gradients. The gradients produce varying degrees of thermal growth in the structure, which result in thermally induced mechanical strains. The mechanical strain is here defined as the difference between the total strain and the free thermal strain. The thermal loading results in a structural response which is displacement (i.e., strain) controlled rather than load controlled. Because of this situation, the specimen testing in this program was also performed under strain control.

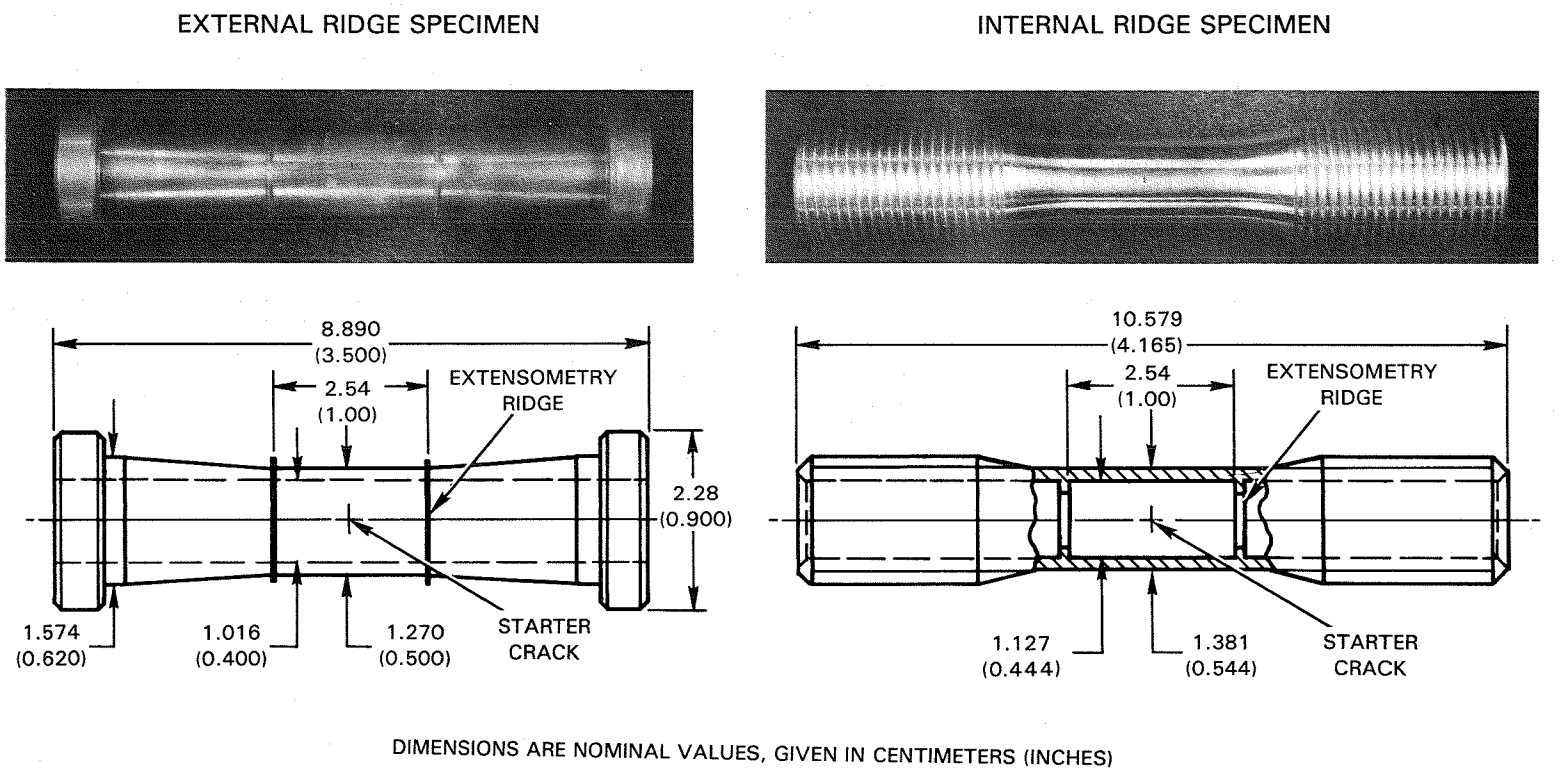

Figure 34 Tubular Strain-Controlled Crack Propagation Specimens.

Each point in the combustor liner undergoes its own strain-temperature response as a result of the change of temperature gradient as a function of time into the engine cycle. Figure 13 shows the predicted response at several locations in a typical combustor liner. The results shown were taken from a MARC nonlinear finite element analysis; the second cycle of the analysis is illustrated. Temperature ranges and strain ranges for the test specimens are based in a general way on thermomechanical cycles shown. The following conclusions can be drawn from the figure: 1) the maximum strain range is no greater than 0.4 percent, 2) the maximum temperature is no greater than 982°C(1800°F), with the maximum temperature at most locations being on the order of 926°C(1700°F).

6.2.5 Specimen Loading

A detailed description of the specimen testing conditions conducted in this program is given in Tables VI and VII. There were a total of 12 TMF tests and 24 isothermal tests performed. The following comments are made concerning the various test parameters.

Temperature

Tests were conducted in the temperature range of 426 to 982°C(800°F to 1800°F). The low temperature is set by the ability of the cooling air in the TMF test to cool the specimen in a reasonable time (about 30 seconds). In addition, 426°C(800°F) roughly corresponds to a ground idle engine condition. The peak temperature is set by the maximum temperature expected in combustor service. The testing concentrated on a peak temperature of 926°C(1700°F), since this is typical of most areas of the combustor. Other peak temperatures are used in the TMF testing to correspond to other locations to determine the sensitivity of crack growth rate to the peak temperature.

TMF Cycle Shape

Several types of strain-temperature cycles were used in the TMF tests to determine sensitivity to cycle shape, as shown in Figure 35. "Cycle I" with a linear strain-temperature relationship, was used in most of the testing since it is the simplest type of TMF cycle. To check for sensitivity of the response to cycle shape, other types of TMF tests were conducted. One of these was a "faithful cycle" which more closely models the actual strain-temperature path seen by a particular point (the point of crack initiation) on the combustor. The faithful cycle used in the test was obtained from an analytical loop similar to that shown in Figure 13 by 1) truncating the parts of the loop which are less than 426°C(800°F) or greater than 926°C(1700°F); 2) shifting from a negative mean strain to a zero mean strain; 3) linearizing the strain temperature loop to facilitate set-up of the test. Cycle I and faithful cycle tests were run both with and without a strain hold time at peak temperature to simulate the steady-state condition. The other type of test is a "Cycle II" type which has a linear strain-temperature relation like Cycle I, but where the peak temperature occurs in the tensile, rather than the compressive, part of the cycle. The 426 to 926°C(800°F to 1700°F) Cycle II test was to test the sensitivity of the crack growth rate to a cycle that is dissimilar to Cycle I and faithful cycle.

TABLE VI

CONDITIONS FOR ISOTHERMAL TESTING*

Test No.	Temperature (°C)	Temperature (°F)	Strain Range (%)	Minimum Strain (%)	Maximum Strain (%)	Cyclic Rate (cpm)	Average Strain Rate (cm/cm)/min ((in/in)/min)	Comments
I-1	427	800	0.15	-0.075	0.075	60	0.18	
I-2	427	800	0.40	-0.20	0.20	10	0.08	Mean Strain=
I-3	427	800	0.40	-0.45	-0.05	10	0.08	-0.25%
I-4	427	800	0.25	-0.125	0.125	10	0.05	
I-6	649	1200	0.15	-0.075	0.075	2.0	0.006	
I-7	649	1200	0.40	-0.20	0.20	1.0	0.008	Mean Strain=
I-8	649	1200	0.40	0.05	0.45	1.0	0.008	+0.25%
I-9	760	1400	0.15	-0.075	0.075	1.0	0.003	
I-10	760	1400	0.25	-0.125	0.125	0.5	0.005	
I-11	760	1400	0.40	-0.20	0.20	1.0	0.004	
I-13	760	1400	0.25	-0.125	0.125	0.5	0.005	1 minute Hold Time
I-14	871	1600	0.15	-0.075	0.075	1.0	0.003	
I-15	871	1600	0.175	-0.0875	0.0875	1.0	0.0035	
I-16	871	1600	0.40	-0.02	0.02	0.5	0.004	
I-18	927	1700	0.15	-0.075	0.075	1.0	0.003	
I-19	927	1700	0.25	-0.125	0.125	1.0	0.005	
I-20	927	1700	0.40	-0.20	0.20	0.5	0.004	
I-21	927	1700	0.25	-0.125	0.125	1.0	0.005	Mean Strain =-0.25%
I-22	927	1700	0.25	-0.125	0.125	0.5	0.005	1 minute Hold Time
I-23	982	1800	0.15	-0.075	0.075	1.0	0.003	
I-23a	982	1800	1.50	-0.75	0.75	1.0	0.030	Large Strain Range
I-24	982	1800	0.25	-0.125	0.125	1.0	0.005	
I-25	982	1800	0.40	-0.20	0.20	0.5	0.004	
I-26	982	1800	0.40	-0.20	0.20	0.5	0.004	Triangular Wave Shape

* All tests had a sinusoidal wave shape, zero mean strain, and no hold time, except where indicated.

TABLE VII

CONDITIONS FOR THERMOMECHANICAL FATIGUE TESTING*

Test No.	Maximum Temperature (°C)	(°F)	Strain Range (%)	Minimum Strain (%)	Maximum Strain (%)	Cyclic Rate (cpm)	Average Strain Rate (cm/cm)/min ((in/in)/min)	Comments
T-1	927	1700	0.15	-0.075	0.075	0.83	0.0025	
T-2	927	1700	0.25	-0.125	0.125	0.83	0.0042	
T-3	927	1700	0.40	-0.20	0.20	0.44	0.0035	
T-4	927	1700	0.25	-0.125	0.125	0.83	0.0042	Cycle II
T-5	927	1700	0.40	-0.20	0.20	0.44	0.0035	Faithful Cycle
T-6	927	1700	0.40	-0.20	0.20	0.30	0.0035	Faithful Cycle; 1.125-minute Hold Time
T-7	982	1800	0.25	-0.125	0.125	0.83	0.0042	
T-8	871	1600	0.25	-0.125	0.125	0.83	0.0042	
T-9	760	1400	0.25	-0.125	0.125	0.83	0.0042	
T-10	649	1200	0.25	-0.125	0.125	0.83	0.0042	
T-11	927	1700	0.40	-0.20	0.20	0.30	0.0035	1.125-minute Hold Time
T-12	871	1600	0.40	-0.20	0.20	0.44	0.0035	

* All tests were Cycle I with no hold time except where indicated.

* All tests had a minimum temperature of 427°C (800°F) and zero mean strain.

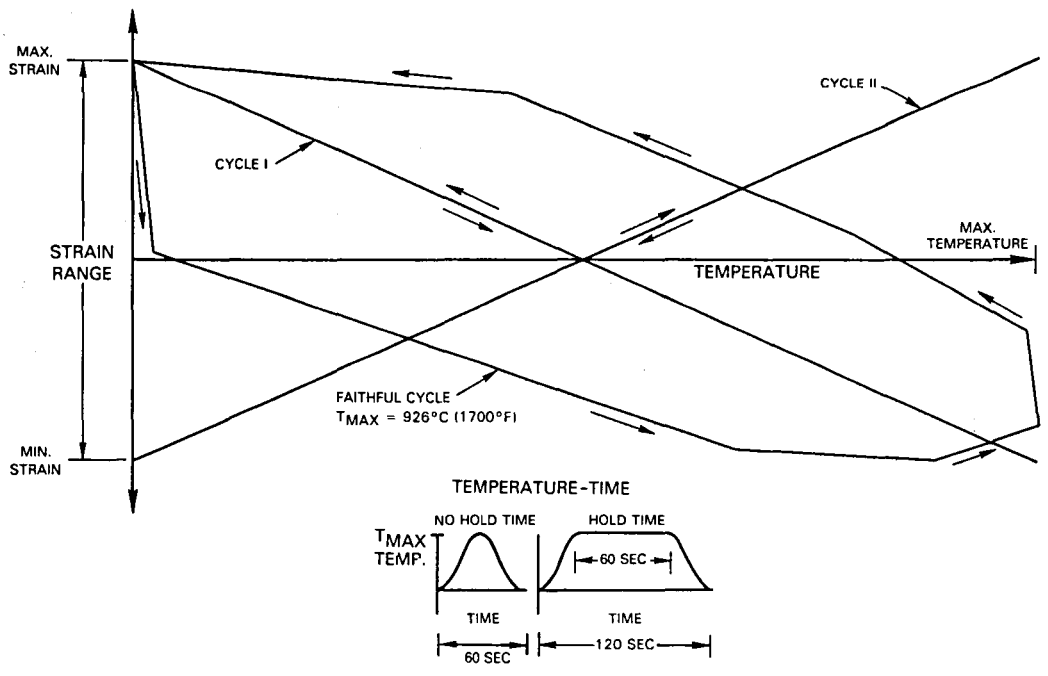

Figure 35 Strain-Temperature Cycles used in Thermomechanical Fatigue Testing.

Strain Range

Three strain ranges of 0.15, 0.25, and 0.40 percent were run. The material behavior in the specimen net section was fully elastic for the low temperature, low strain range tests, and fully plastic for the high temperature, high strain range tests. One of the specimens (#23a) was inadvertently tested at a strain range of 1.5%, rather than the desired value of 0.15%.

Mean Strain

To facilitate comparison of the crack growth data, most of the tests were run to the same mean strain. This mean strain was chosen to be zero even though the nonlinear analysis (Figure 13) indicates a negative mean strain, for two reasons. First, the analysis result shown applied to the second cycle. However, the mean strain changes cycle-to-cycle, according the the analysis; no analysis has yet been carried out to enough cycles to determine the stabilized mean strain value. Therefore, the choice of the mean strain is arbitrary; a zero value was chosen for convenience. Second, prior in-house TMF testing showed negligible change in material cyclic stress-strain response due to a mean strain change. Therefore, it is expected that TMF crack propagation rate would not be affected by mean strain. This situation is not necessarily the case in isothermal tests, however, so three isothermal tests were conducted with a mean strain to check this effect.

Strain Rate

The maximum cyclic rate for the TMF tests was set by the maximum transient heating and cooling rate that can be experimentally obtained. This rate is approximately 30 seconds each for heat-up and cool down, that is, a cyclic rate of 1 cycle per minute (cpm). At a strain range of 0.20 percent, a one cpm cyclic rate corresponds to an average strain rate of 0.004 (cm/cm)/min(0.004 (in/in)/min.) To maintain this strain rate for a strain range of 0.40 percent, a cyclic rate of 0.5 cpm is required. Prior in-house testing on Hastelloy X has shown significant strain rate sensitivity at temperatures of 760°C(1400°F) and above. Therefore, it was decided that all high-temperature isothermal and all TMF tests would be run at consistent as possible strain rates. However, low temperature tests were run at a much faster rate to minimize testing time and thus testing cost.

Both the temperatures and strain in a Cycle I TMF test change sinusoidally with time. The strain-time relation in the isothermal tests was also sinusoidal to maintain consistency with the TMF tests. One isothermal test, however, was run using a triangular wave shape to investigate the effect of cycle shape on crack growth rate.

Hold Time

A 1 minute compressive strain hold simulating time at steady-state conditions was applied on two TMF tests and two isothermal tests to determine the effect on crack growth rate.

6.2.6 Crack Length Measurements and Data Reduction

Crack measurements were made visually, using a 50X telescpe equipped with a calibrated micrometer graduated to 0.0012 cm(0.0005 in). Measurements were taken at no greater than 0.050 cm(0.020 in) intervals and were made at the point in the cycle of maximum tensile loading.

The crack growth rate was determined using the following procedure.

1. The measured crack length vs number of cycle data was smoothed.

2. The smoothed data was converted from a projected crack length as measured by the micrometer and telescope to a mean crack length for the tube using:

   $a = R \sin^{-1} (2a_p/D_o)$,

   where, as shown in Figure 11,

   a = mean crack length

   $R = (D_o + D_I)/4$ = mean radius of tube

   D_o, D_I = outer and inner diameter of tube, respectively

   $2a_p$ = total projected crack length

3. The crack growth rate at a crack length a_i and number of cycle point N_i is detrmined by a secant procedure. The slope of the a-N curve both immediately before and immediately after the point (a_i, N_i) is calculated. A weighted average of these slopes determines the crack growth rate. The following formula is used:

$$\frac{da}{dN} = \frac{\frac{a_i - a_{i-1}}{N_i - N_{i-1}} \times (N_{i+1} - N_i) + \frac{a_{i+1} - a_i}{N_{i+1} - N_i} \times (N_i - N_{i-1})}{N_{i+1} - N_{i-1}}$$

The specimens were not precracked prior to fatigue testing, since in the testing conditions employed, it was found that sharp fatigue cracks initiated from the EDM starter slot in a small number of cycles. Crack length measurements taken for the first 0.025 cm(0.010 in) of crack growth were not used in the data reduction.

SECTION 7.0

TASK V - DATA CORRELATION AND GENERALIZATION

7.1 DEFINITION OF CORRELATION PARAMETERS

The prediction of crack propagation rates in structural components from specimen data generated in the laboratory is only possible if a parameter which characterizes the severity of stress and strain cycles near the crack tip can be found. Such a parameter is needed to match a particular loading and crack length in a component with the correct equivalent specimen loading and crack length. For example, in cases of cyclic loading involving linear elastic deformation and small scale yielding, the stress intensity factor is a widely used and successful parameter. However, the stress intensity factor may not be applicable for use in combustor liners and some other hot section components, since in these areas cracks may grow through regions of substantial plastic deformation.

In this contract, data was generated for use in assessing the suitability of various parameters for correlating high temperature and thermomechanical crack growth rates. A parameter is sought which can correlate data for the full range of conditions from elastic strain cycling to substantially plastic strain cycling. The ultimate goal of establishing such a parameter is the prediction of the propagation life of real engine components. To be useful in reaching that goal, the parameter should have the following attributes:

1. Predict crack growth rate from a single crack growth rate vs parameter curve. In this way, cracks of different lengths loaded in such a way to yield the same value of the parameter experience the same crack growth rate.

2. Correctly predict fatigue crack growth rates independent of part geometry.

3. Be calculable for complex real part geometries.

Parameters not satisfying the above requirements would be of limited value since component or simulated component testing would always be required to obtain crack growth rate information.

The prediction of propagation life in engine components requires the consideration of thermomechanical fatigue (TMF) cycles. The problem of thermomechanically driven crack growth in the presence of significant inelastic strain is a challenging problem. In order for the parameter chosen to be useful for predicting thermomechanical crack growth in components, it should satisfy the above conditions. In addition, it is highly desirable that:

4. A parameter can be found that results in a temperature-independent growth rate plot.

Such a temperature-independent result is possible if all temperature effects on crack growth rate are a result of the change in material stress strain response and if the influence of the material response is correctly reflected in the chosen parameter.

Less desirable but useful attributes for a parameter to have when predicting TMF growth rates are:

5. A parameter for which a scheme of predicting TMF crack growth rates from isothermal data can be found.

6. A parameter that allows TMF growth predictions from TMF growth rate data for cycles that are in some sense similar.

The data generated was used to test the ability of five different parameters to correlate crack growth data with respect to the characteristics stated above. These parameters include the stress intensity factor, the strain intensity factor, the J-integral, crack opening displacement, and Tomkin's model. The first two parameters are generally accepted in cases where linear elastic material behavior prevails. The last three parameters have been proposed for situations in which there exists large scale yielding. None of the last three parameters have gained universal acceptance. Success in their use has been reported; however, in each case, there is also some evidence to the contrary. Accepting this fact, the major purpose of this effort was to assess the applicability of the parameters for non-isothermal, or TMF cycling, for which there has been very little data reported to date.

Stress Intensity Factor

The stress fields around crack tips in different linear elastic bodies show the same dependence on spatial variables if the coordinates are attached to the crack tip. However, different specimen geometries, crack lengths, and load levels result in different scale factors for the stress distribution. This scale factor is the stress intensity factor and may be written as follows.

$$K_\sigma = \sigma \sqrt{\pi a} \; f \text{ (geometry)}$$

Paris (13) proposed that the stress intensity factor range given as:

$$\Delta K_\sigma = \Delta\sigma \sqrt{\pi a} \; f \text{ (geometry)}$$

was the overall controlling factor in fatigue crack growth. For linear elastic deformation, two classical experiments (14, 15) and many others subsequently showed that this was a valid proposition. Despite its acknowledged limitations, the stress intensity factor was one of the parameters used in reducing the fatigue data for this report, even in the range where plastic strains dominate.

Strain Intensity Factor

The use of the strain intensity factor as a measure of crack tip conditions is based on an intuitive argument that strains should be characterized by a strain based parameter similar to the elastic stress intensity factor. The strain intensity factor is obtained by replacing the stress range with the strain range in the expression for the stress intensity factor as follows:

$$\Delta K_{\varepsilon} = \Delta\varepsilon \sqrt{\pi a} \; f \text{ (geometry)}$$

In the above expression, f is the same geometric correction term derived in connection with the stress intensity factor. In spite of the fact that the strain intensity factor lacks a rigorious mechanics interpretation, it has been shown to be useful in correlating crack growth data (16 through 19).

J-Integral

The J-Integral as originally proposed by Eshelby (20) and further developed by Rice (6) was originally used in the prediction of monotonic ductile fracture in a manner analogous to the way in which the stress intensity factor was originally used for brittle fracture. More recently, the J-Integral was proposed (21) for application to fatigue crack propagation prediction for general yielding in a manner also analogous to the way in which the stress intensity factor has been used for crack growth prediction for the case of small scale yielding. Since then, the application of J-Integral to fatigue crack propagation has been developed over the last five to ten years. Some impressive success has been achieved (22 through 27). However, some individuals claim the method is not successful for all situations. It should be noted that the application of J-Integral to fatigue crack growth should not be assumed a priori to be completely valid.

The definition of the J-Integral as a path-independent quantity is given in Section 5.3.2. The direct physical interpretation of this quantity is not trivial and has been the subject of several papers. Without going into details, two of the interpretations are given here. First, it is equal to the strain energy release per unit crack extension if non-linear or linear elastic behavior prevails (20). Second, J characterizes the local crack tip field in problems governed by deformation plasticity theory (28, 29). It has also been shown to describe the resulting stress and deformation fields when crack tip blunting is included, provided J is determined from a path which is not too near the crack tip (30). The case of cyclic loading does not appear to have been addressed directly in the literature. McMeeking (30) and others claim that it is the non-proportional nature of the straining that causes the path independence to J to break down. From this, one can conclude that the cyclic value of J is a valid characterizing parameter as long as the deformation behavior results in proportional straining. The amount of non-proportional strain in the specimens used in the crack growth testing can only be determined by detailed crack tip analysis, which was beyond the scope of this effort. However, for data reduction purposes, J was nevertheless defined in a particular manner, which was described in Section 5.3.1.

Crack Opening Displacement

Crack Opening Displacement, or COD, has also been proposed for use in monotonic fracture for cases in which there is a large amount of plastic deformation (31, 32). As with the J-Integral, the COD concept may also be extended to the case of fatigue crack propagation.

Crack opening displacement can be thought of as a measure of the strain in an imaginary tensile specimen at the crack tip and as such seems a reasonable candidate for characterizing ductile fracture and fatigue. In general, for monotonic fracture, COD is considered to be about as successful as J-Integral approaches. This may be explained by a finite element analysis for the case of small scale yielding which has shows that COD is equal to the J-Integral times some function of the strain hardening exponent (30).

COD can be considered a successful fatigue crack growth parameter if any two cracks with the same COD range have the same crack growth rate even if the two cracks have different lengths and applied strain ranges. There is some evidence that COD may be useful for this application, (33 through 37); however, lack of success has also been reported (38). An important reason for studying COD for TMF conditions is that plastic flow properties appear explicitly in expressions used for its calculation. This characteristic offers some hope of accounting for the effect of temperature through its influence on flow properties. Thus, COD might be a temperature insensitive parameter that would make the prediction of TMF crack growth simpler.

Tomkins' Physical Process Model

The Tomkins' crack growth model (38 through 41) is based on a physical picture of the cracking as a process of shear decohesion occurring in 45-degree shear bands emanating from the crack tip. There is evidence for this in the form of direct microscopic observation of the tips of growing fatigue cracks (42, 43). The physical notion of how cracks grow upon which Tomkin's model is based is well supported. The solid mechanics upon which the quantitative aspects of the model are based involve several approximations and assumptions. In spite of the limitations, the model has had some success in predicting crack growth data over a wide range of temperatures and strain rates (38, 44). However, there is also evidence that the model severely underpredicts crack growth rates for longer crack lengths (45).

To make the model quantitative, it is necessary to predict by some means what the COD will be and what fraction of COD will be accommodated by decohesion. Tomkins has done this for several different cases using some severe approximations and also using results from the Bilby, Cottrell and Swinden (46) (BCS) model of a crack under small scale yielding. Three formulas for predicting growth rates have been proposed, depending upon the ratio of applied stress to the limit stress of the material. All three formulas show the crack growth rate as proportional to crack length and plastic strain range. The explicit form of Tomkins' equations and the associated data reduction is given in Section 7.5.

General Comments

The crack growth data generated in this effort is presented in the following sections. The major emphasis is toward investigating those items described above which determine the acceptability of the data correlation parameters toward high temperature and TMF crack growth conditions. Other effects investigated, including hold time, mean strain, and TMF cycle shape, are also described. There was a large volume of data generated in this effort and the following comments are made. First, all the data was reduced based on the strain intensity factor range. However, only selected data reduction was performed for the other correlation parameters. Second, all of the data reduction is included for completeness in the appendix. Only that data considered to be the most significant in establishing the acceptability of the correlation parameters is included in the following sections.

7.2 STRAIN INTENSITY FACTOR

The following comments are made concerning the data presented in Figures 36 through 39.

1. The strain intensity factor range (ΔK_ϵ) correlates the data well for high temperature isothermal (982°C(1800°F)) and TMF (426 to 926°C(800 to 1700°F) Cycle I). There is little or no "strain range" effect.

2. The 426 to 871°C(800 to 1600°F) tests show the fastest crack growth rate of all the Cycle I TMF tests. This does not agree with the intuitive result that the higher the peak temperature in the TMF cycle, the faster should be the crack growth rate.

3. The spread in crack growth rate in isothermal tests from 426 to 982°C (800 to 1800°F) was about a factor of 5, for the strain range of 0.4 percent.

In addition to the above major effects, the following conclusions can be drawn from the data shown in Appendix A.

1. There is a mean strain effect only at the lowest temperature tested (426°C(800°F)); there is no mean strain effect at 648°C(1200°F) or 926°C (1700°F). The load deflection data from these tests shows that the shift in mean strain causes a shift in mean stress only at 426°C(800°F). The material shows significant work hardening only at the lower temperatures.

2. There is a substantial hold time effect at 760°C(1400°F) but very little for high temperature and TMF cycling. Although more stress relaxation of the net section occurred for the 926°C(1700°F) isothermal and the TMF test than for the 760°C(1400°F) isothermal test, the amount of net section material inelastic behavior was increased by a much higher percentage in the 760°C(1400°F) test.

3. The isothermal high temperature crack growth rate is not significantly affected by the shape of the deflection-time curve. A triangular wave shape imposed on the specimen gave comparable crack growth rates to the sinusoidal shape used in the majority of the testing.

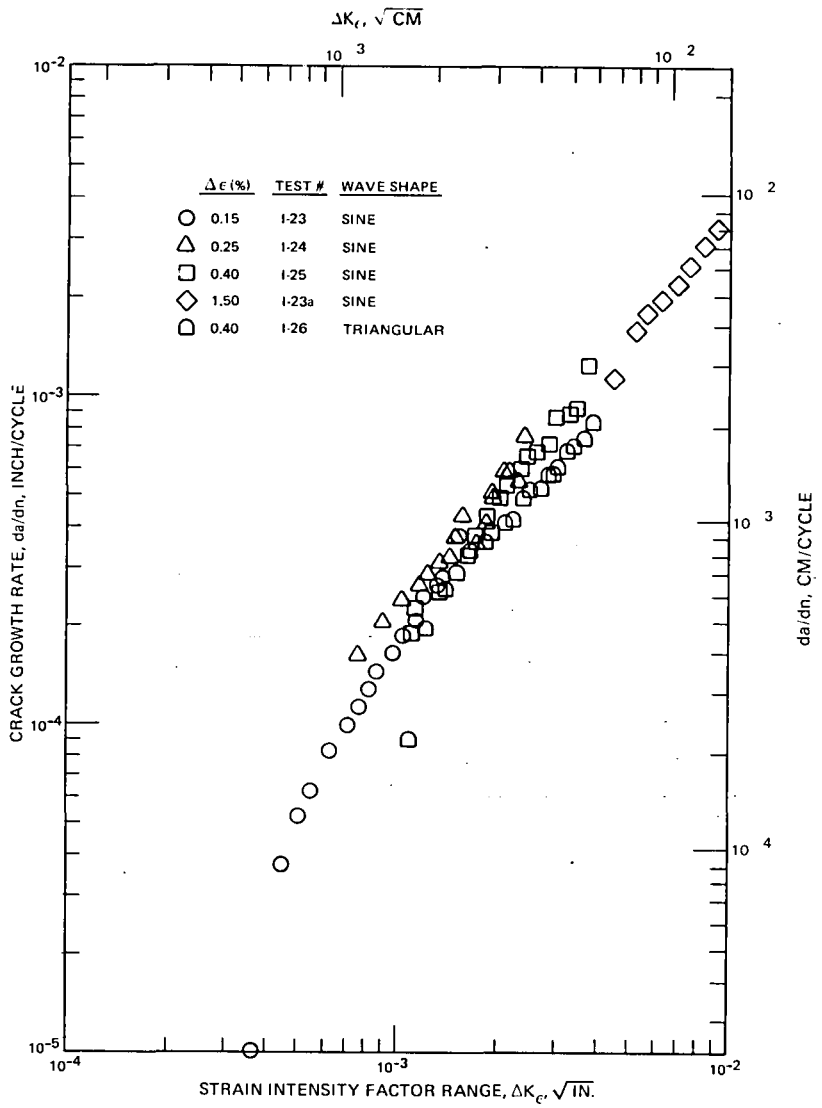

Figure 36 982°C(1800°F) Crack Growth Rates Based on Elastic Strain Intensity Factor Range.

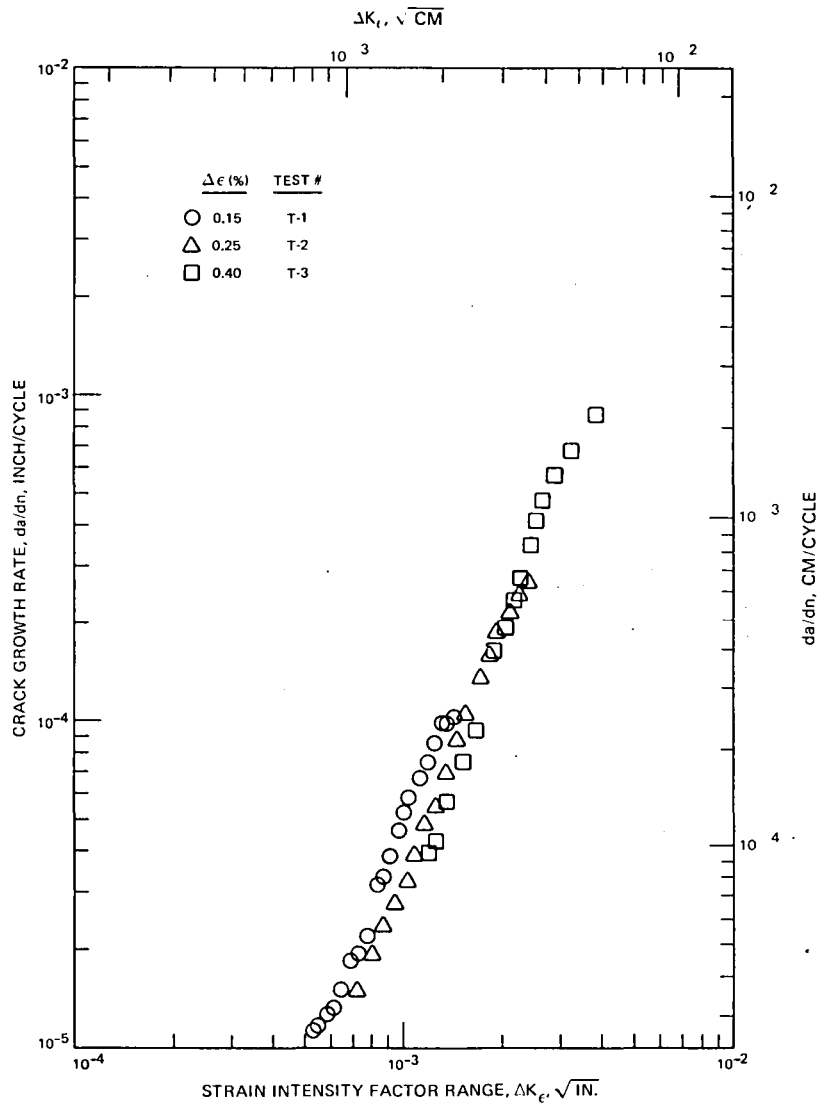

Figure 37 426°C(800°F) to 926°C(1700°F) Cycle I Crack Growth Rates Based on Elastic Strain Intensity Factor Range.

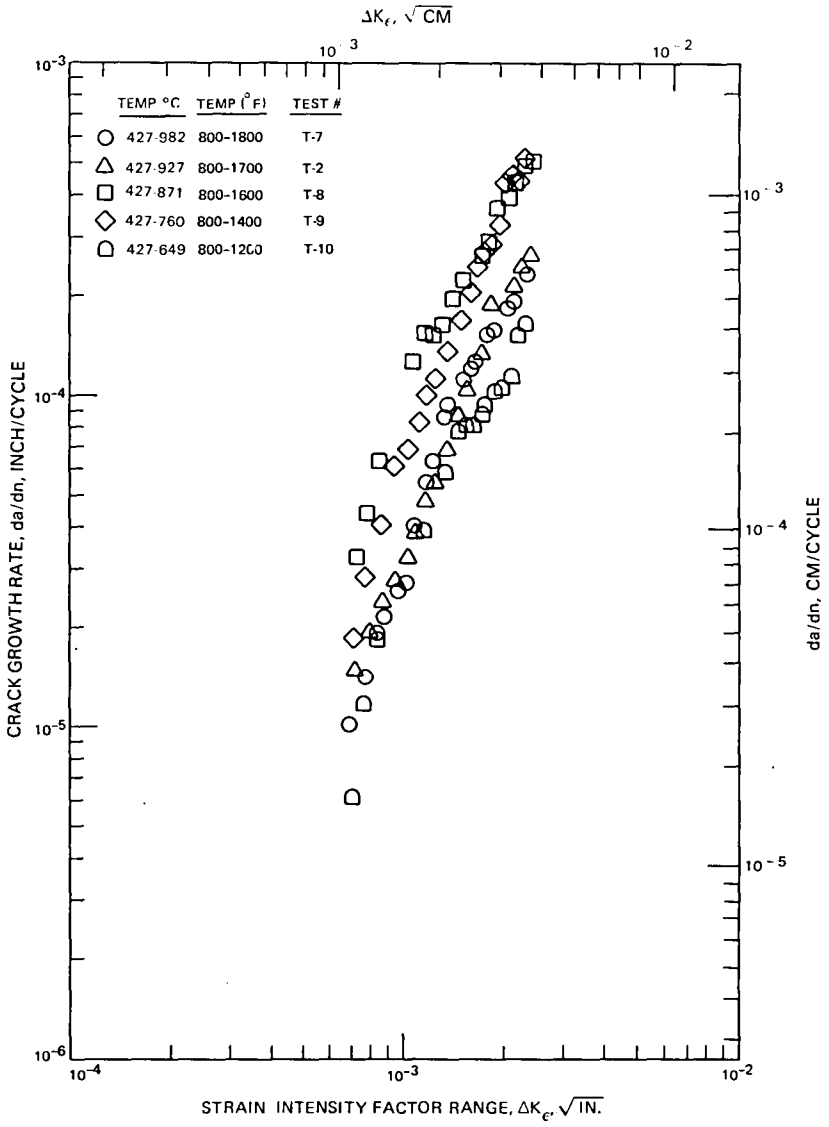

Figure 38 Cycle I, 0.25 Percent Strain Range Crack Growth Rates Based on Elastic Strain Intensity Factor Range.

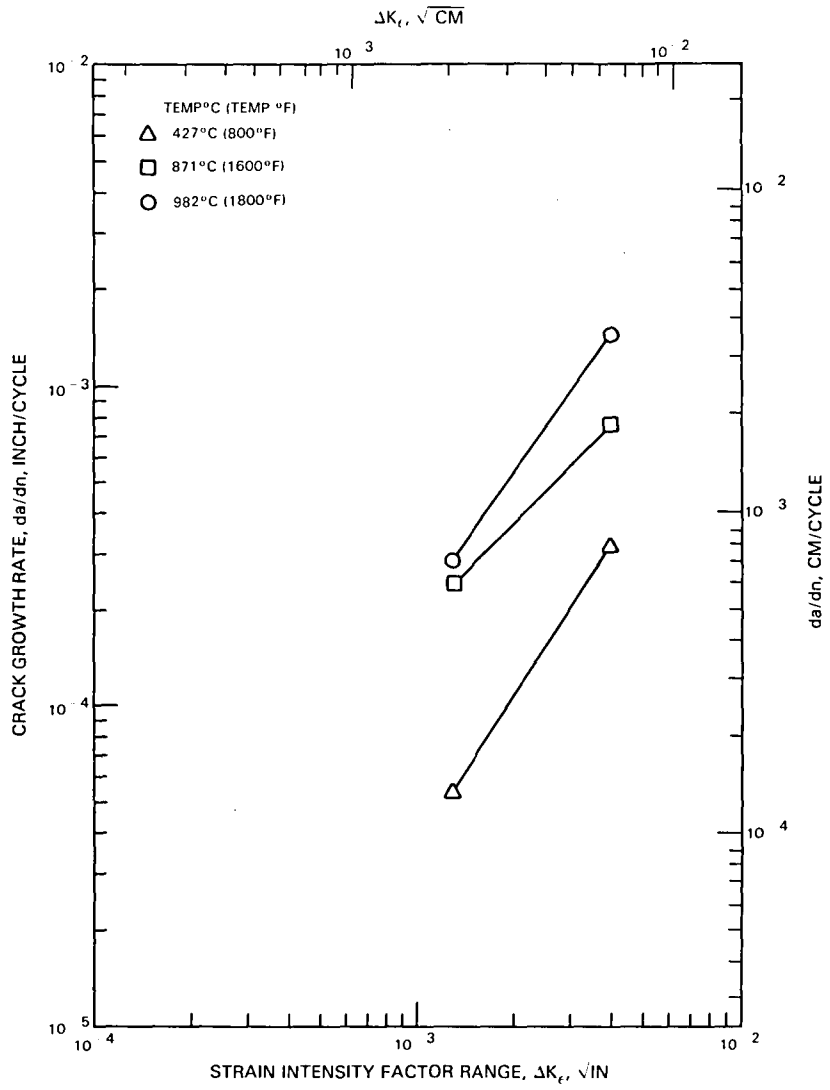

Figure 39 Spread in 0.4 Percent Strain Range Low- to High-Temperature Crack Growth Rates Based on Elastic Strain Intensity Factor Range.

4. The shape of the strain-temperature loop for TMF tests had an effect on crack growth rates. The "faithful cycle" data showed faster rates than the Cycle I data. The Cycle II rates were similar to the Cycle I rates on the average but had a shallower slope of crack growth rate vs ΔK_ϵ.

5. The slope of the da/dN- ΔK_ϵ curve is steeper for the Cycle I TMF tests than for the isothermal tests. The slope of the curve for the Cycle II and faithful cycle tests was comparable to the slope for the isothermal tests.

6. There is a "strain range" effect which is quite substantial at the lower temperature but disappears at the higher temperature. This effect may be due in part to the tests being run to a zero mean strain. The zero mean strain produces an R-ratio ($\sigma_{min}/\sigma_{max}$) of approximately -1. The "R-ratio" effect would be less severe at the higher temperature because crack tip residual stresses have a greater tendency to relax at the higher temperatures.

7.3 STRESS INTENSITY FACTOR

The following comments are made concerning the data presented in Figures 40 through 43.

1. The stress intensity factor range (ΔK_σ) does not correlate the high temperature (982°C 1800°F) data. However, excellent correlation of the TMF (426 to 926°C(800°F to 1700°F) Cycle I) data is achieved.

2. The Cycle I TMF crack growth rate data as a function of peak temperature is collapsed to a greater extent than is the case using ΔK_ϵ for peak cyclic temperatures from 760 to 982°C(1400 to 1800°F).

3. The spread in crack growth rates in isothermal tests was about a factor of 100, compared to a factor of 5 for ΔK_ϵ.

The above observations indicate that the stress range may be more important than the strain range in correlating TMF data.

The following conclusions can also be drawn from the data presented in Appendix B.

1. The effect of cycle shape is less using ΔK_σ than using ΔK_ϵ comparing the Cycle I and the faithful cycle.

2. The low temperature "strain range" effect is about the same using ΔK_σ as with ΔK_ϵ. This is because the low temperature nominal material behavior was predominately elastic, so there is little difference between the two correlating parameters.

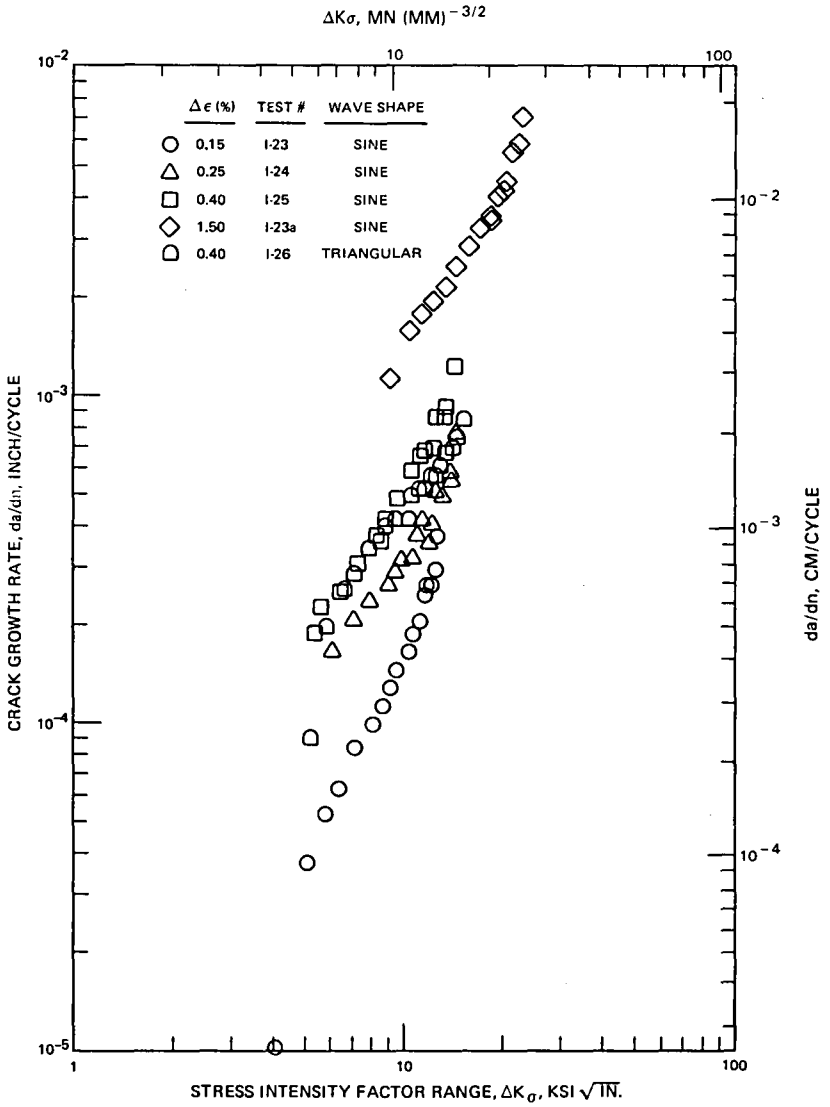

Figure 40 982°C(1800°F) Crack Growth Rates Based on Elastic Stress Intensity Factor Range.

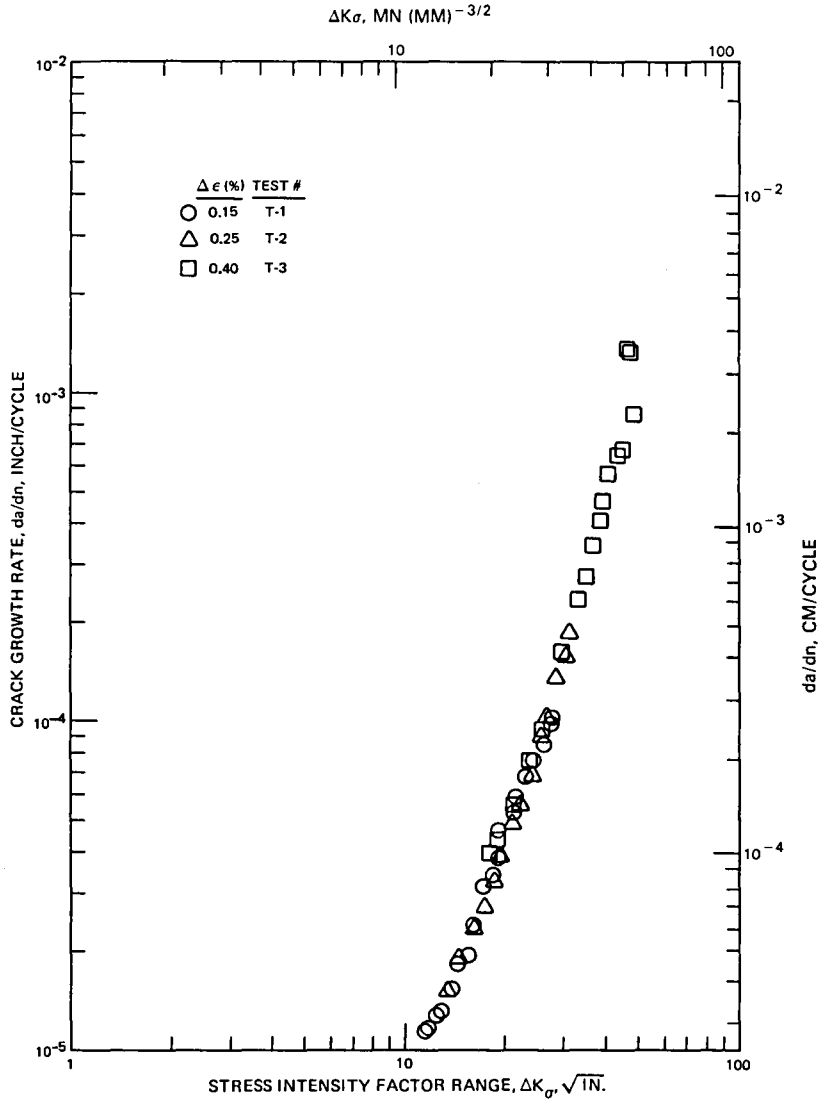

Figure 41 426°C(800°F) to 926°C(1700°F) Cycle I Crack Growth Rates Based on Elastic Stress Intensity Factor Range.

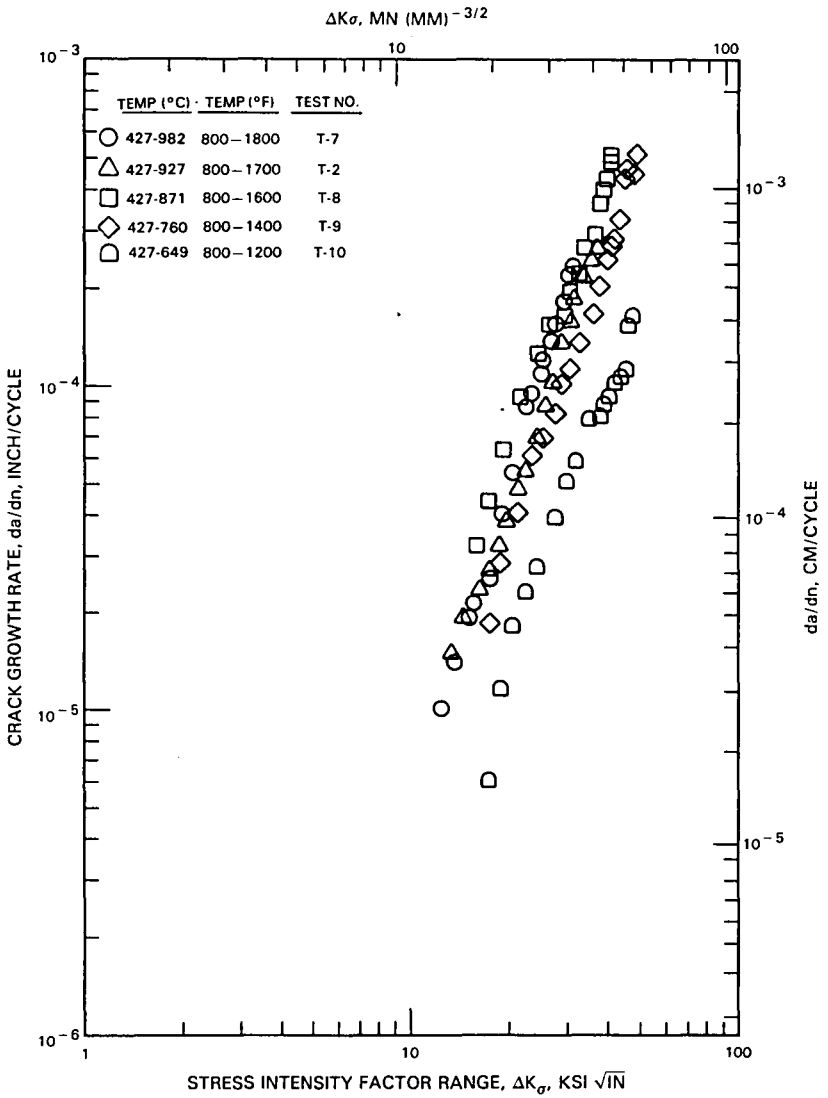

Figure 42 Cycle I, 0.25 Percent Strain Range Crack Growth Rates Based on Elastic Stress Intensity Factor Range.

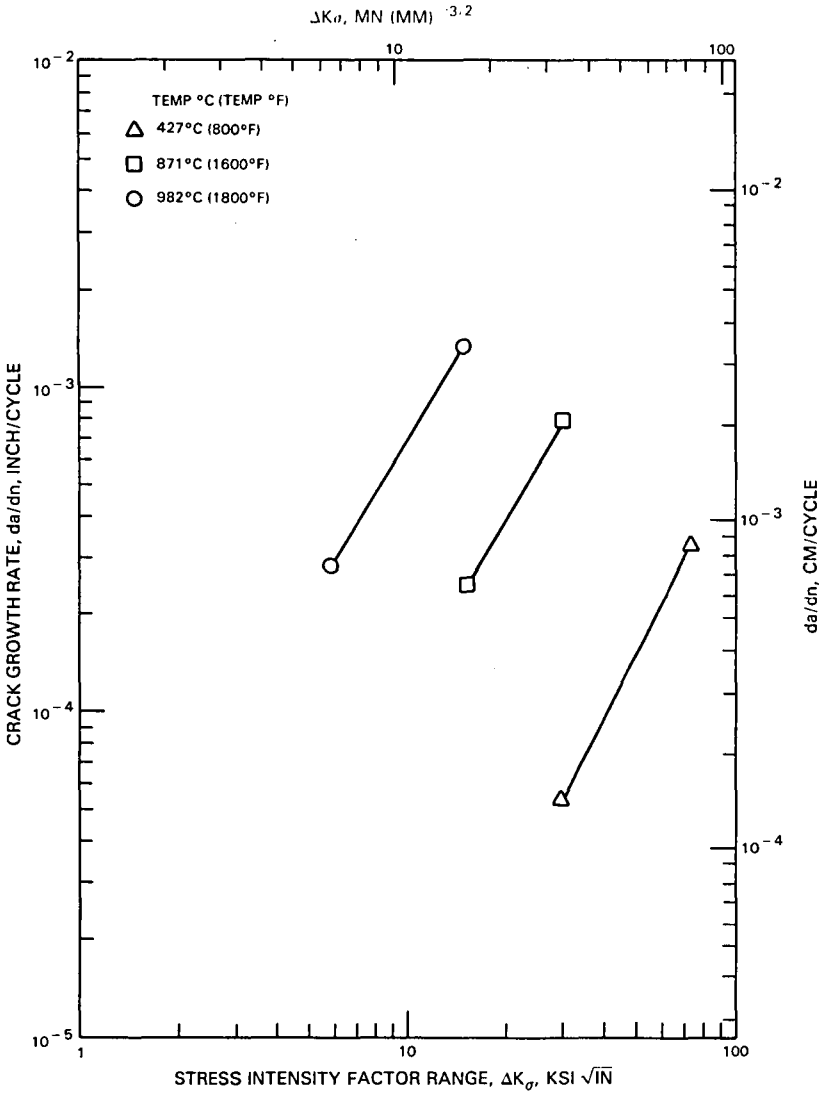

Figure 43 Spread in 0.4 Percent Strain Range Low- to High-Temperature Crack Growth Rates Based on Elastic Stress Intensity Factor Range.

7.4 J-INTEGRAL

The following comments are made concerning the data presented in Figures 44 through 47.

1. The J-Integral range (ΔJ) correlates the data well for both the high temperature isothermal (982°C(1800°F)) and Cycle I TMF testing.

2. The Cycle I TMF crack growth rate data as a function of temperature is collapsed to a greater extent than is the case with ΔK_σ and about the same as with ΔK_ϵ.

3. The spread in crack growth rates in isothermal tests was about a factor of 7, which is between the ΔK_σ and ΔK_ϵ result.

The above observations indicate that the area enclosed by the stress-strain loop in the nominal net section may be more important than either strain range or stress range in correlating the high temperature isothermal and TMF data.

In addition, it is noted in Appendix C that the low temperature "strain range" effect is also present in J-Integral data reduction to about the same degree as ΔK_ϵ or ΔK_σ.

7.5 CRACK OPENING DISPLACEMENT (COD)

As described in Section 7.1, COD is a possible parameter for describing fatigue crack growth. This parameter has the feature that formulas for its calculation explicitly contain the temperature-dependent material properties of elastic modulus, yield stress, and strain hardening exponent. Reduction of isothermal Hastelloy X data has shown a temperature dependence of crack growth rates when the data is reduced based on ΔK_σ or ΔK_ϵ . It is possible that this temperature dependence may be less significant or disappear when the COD is used for data reduction. If this were the case, the probability of the success of prediction of TMF crack growth rates from isothermal data would be greatly enhanced.

Several methods of calculating COD are possible. One of the methods is to measure COD directly by direct optical measurement, replication, or some type of COD gage. However, this method is impractical since the tubular specimen used has such a small amount of crack opening that direct measurement cannot be accurate enough. There are also a number of literature solutions for COD available, of varying levels of complexity. One of the simplest derived from the Dugdale model (47) is the following:

$$\text{C.O.D.} = \delta = \frac{K_\sigma^2}{2E\sigma_y}$$

where: σ_y = yield stress, and
E = elastic modulus.

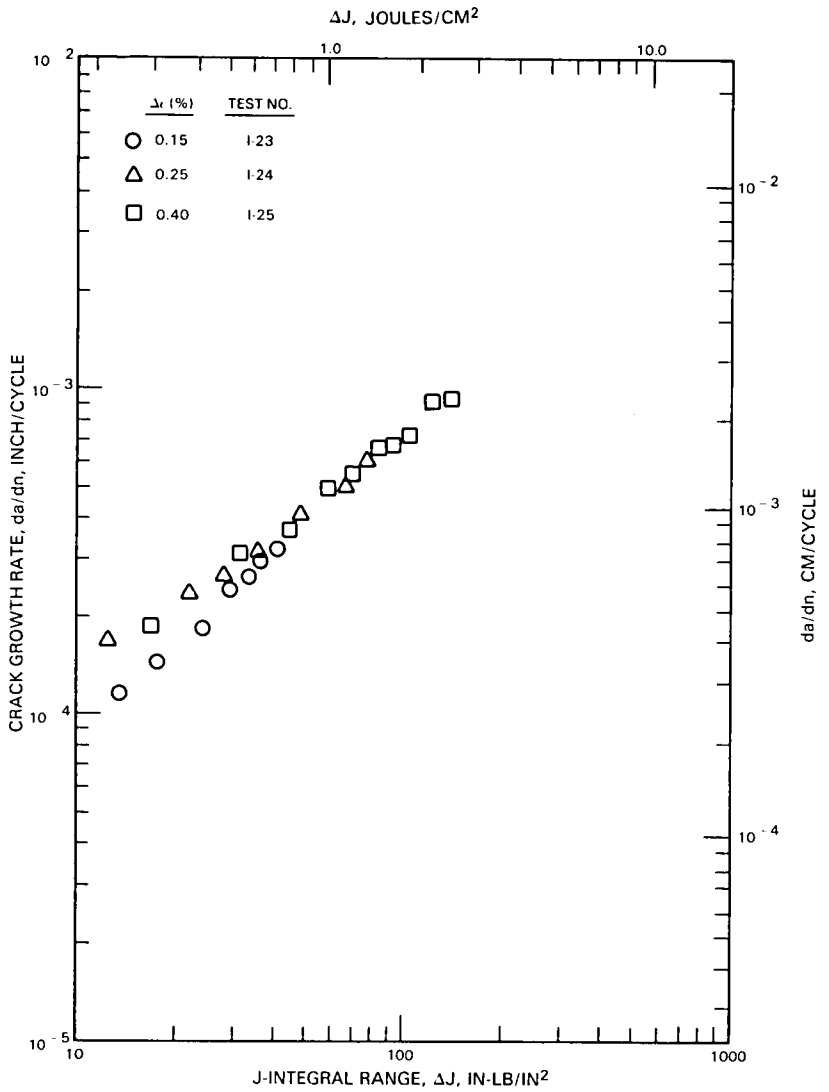

Figure 44 982°C(1800°F) Crack Growth Rates Based on J-Integral Range.

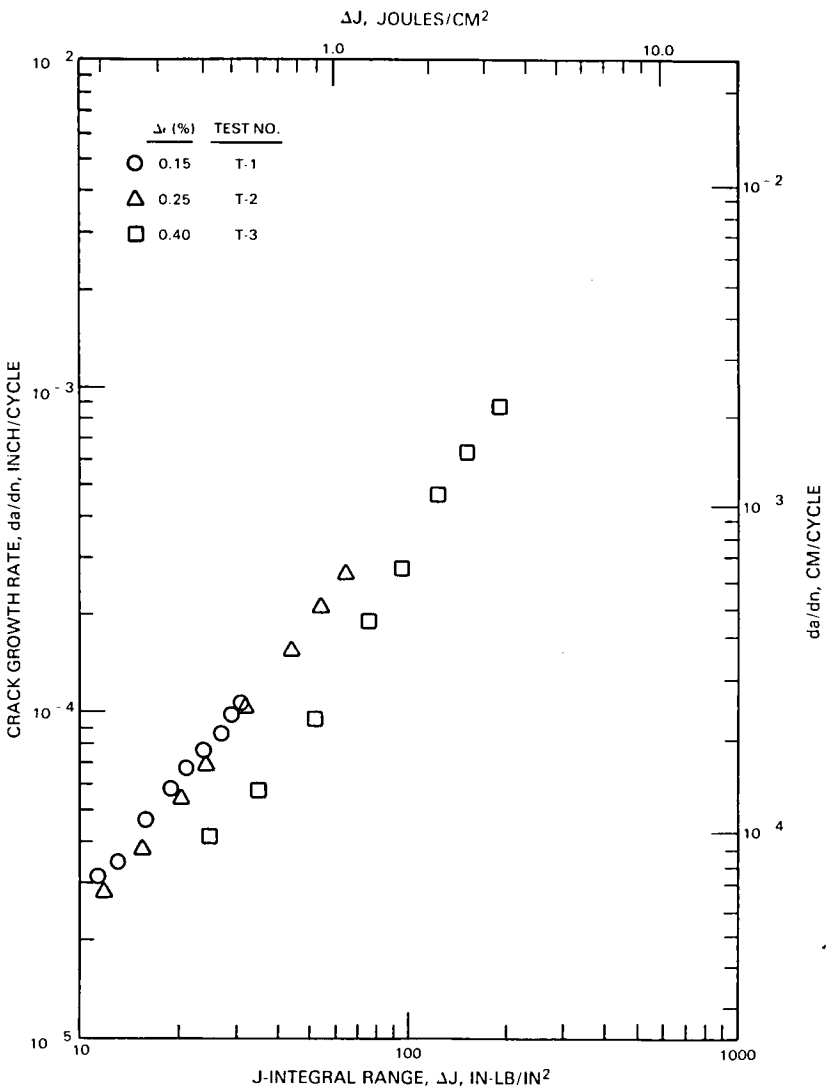

Figure 45 426°C(800°F) to 926°C(1700°F) Cycle I Crack Growth Rates Based on J-Integral Range.

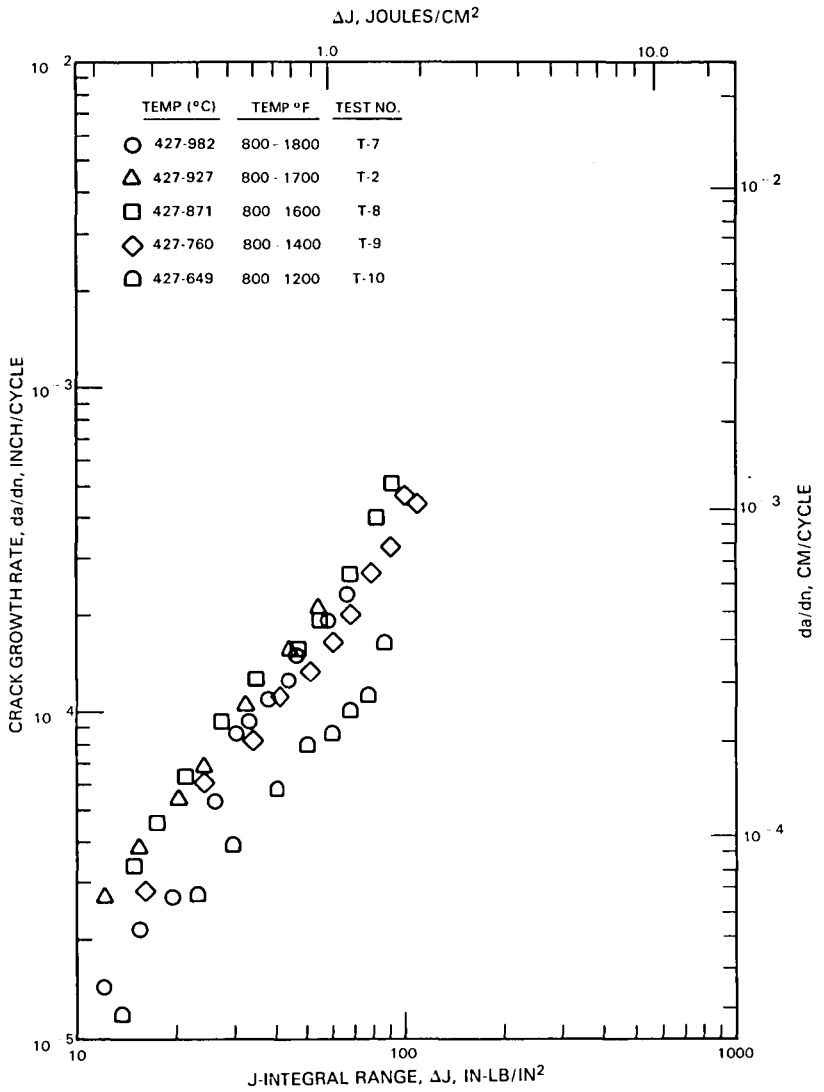

Figure 46 Cycle I, 0.25 Percent Strain Range Crack Growth Rates Based on J-Integral Range.

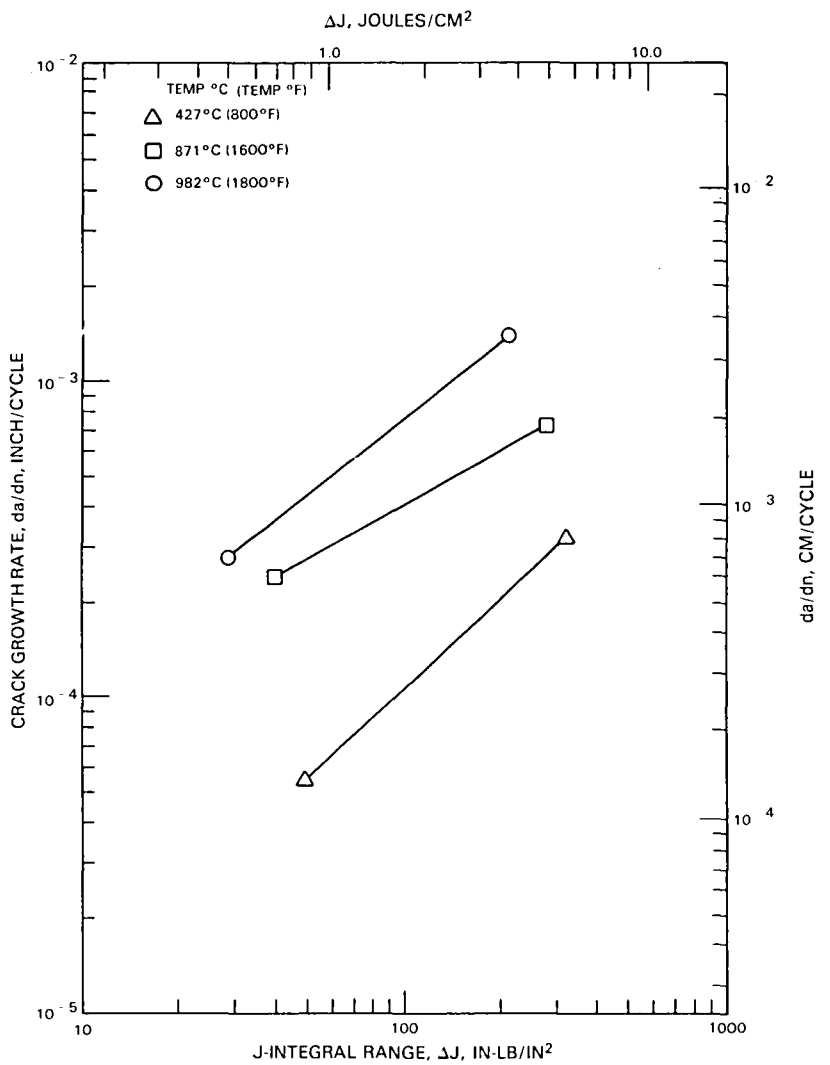

Figure 47 Spread in 0.4 Percent Strain Range Low- to High-Temperature Crack Growth Rates Based on J-Integral Range.

Some of the isothermal data was reduced on the basis of COD calculated from this formula. It is probable that for the conditions of many of the tests conducted in this investigation, this formula is not strictly valid. It is, however, the simplest to use and will give some indication of the effect of including temperature dependent material properties explicitly.

Data from tests at various temperatures at a strain range of 0.004 were plotted vs. COD on the basis of the above formula in Figure 48. For comparison, the same data plotted vs. ΔK_σ was shown in Figure 43. It is apparent that COD collapses the data with respect to temperature to a slight but not significant degree. This means that prediction of TMF growth rate from isothermal data using COD calculated from the above equation will probably have a similar level of success as that using ΔK_σ or ΔK_ϵ . The result of the TMF data prediction is given in Section 7.8.

Two other methods of calculating COD are possible by first finding the value of the J-integral and relating J to COD. Reduction of crack growth data based on J was successfully accomplished only toward the end of the time period allocated for this work. Therefore, a smaller amount of data reduction based on the COD-J relationship was performed than for the simple COD model. The results of these calculations are presented here because of the promising results found.

The first method involves relations between J and COD reported graphically by Shih in (48) for several values of strain hardening exponent. The comparison for three isothermal temperatures based on this relationship is shown in Figure 49. The spread in the crack growth rates has been reduced from a factor of 15 as seen in Figure 48 to a factor of 1.5 using this approximation.

The third method is based on finite element solutions reported by McMeeking (30) which give

$$\delta = 0.55 \frac{J}{2\sigma_y} \left\{ \frac{2}{\sqrt{3}} (1+\upsilon)(1+n) \frac{\sigma_y}{nE} \right\}^n$$

where: σ_y = yield stress
E = elastic modulus
ν = Poisson's ratio
n = strain hardening exponent

The result of COD calculated in this fashion for isothermal tests is given in Figure 50. The spread in crack growth rates for this model is also a factor of 1.5. The above formula was theoretically based on a small scale yielding assumption; however, the formula nonetheless does an excellent job of collapsing the high and low temperature data, even where fairly large amounts of plasticity prevail. Based on Figures 49 and 50, it is clear that further investigation of one or both of the above methods is warranted.

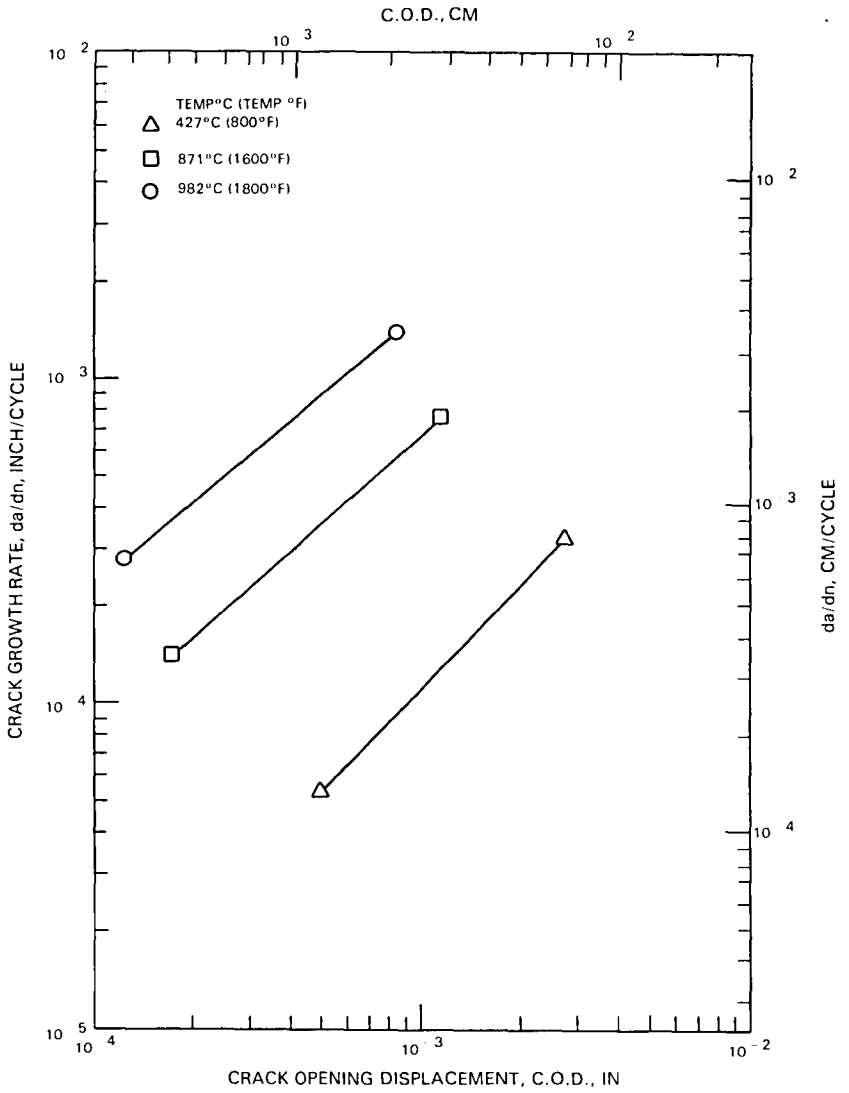

Figure 48 Spread in 0.4 Percent Strain Range Low- to High-Temperature Crack Growth Rates Based on Simplified COD Model.

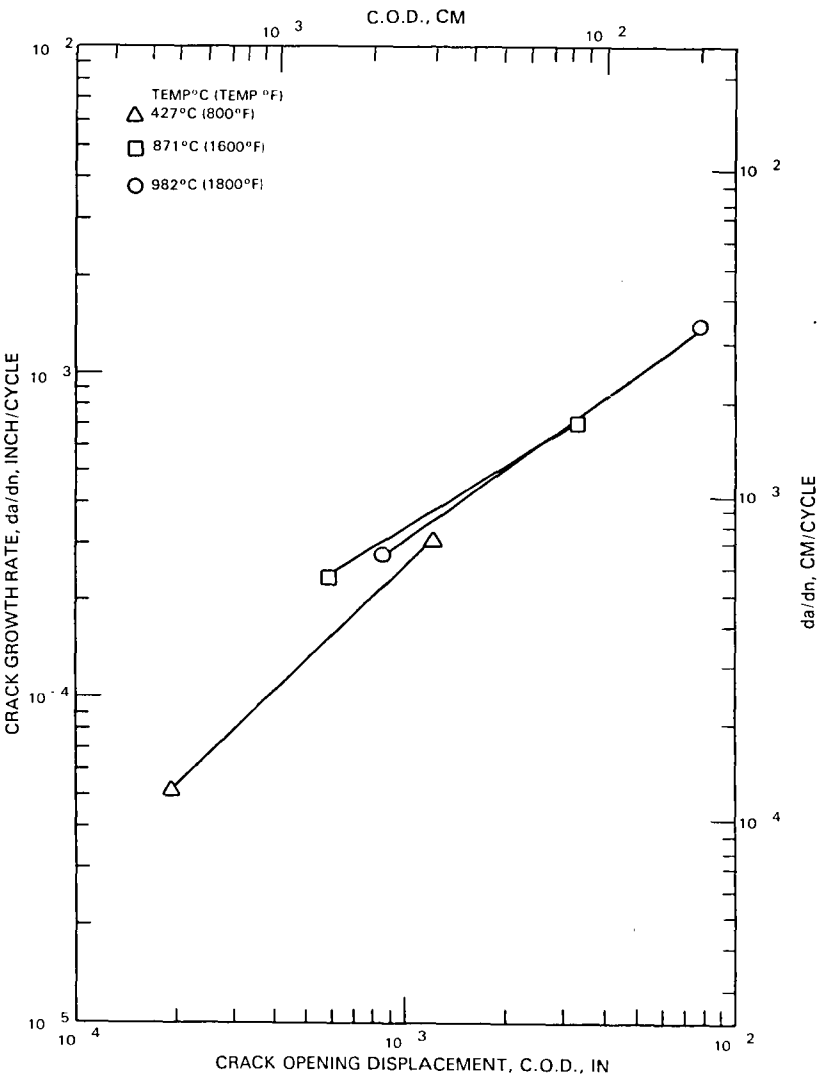

Figure 49 Spread in 0.4 Percent Strain Range Low- to High-Temperature Crack Growth Rates Based on COD Solutions by Shih.

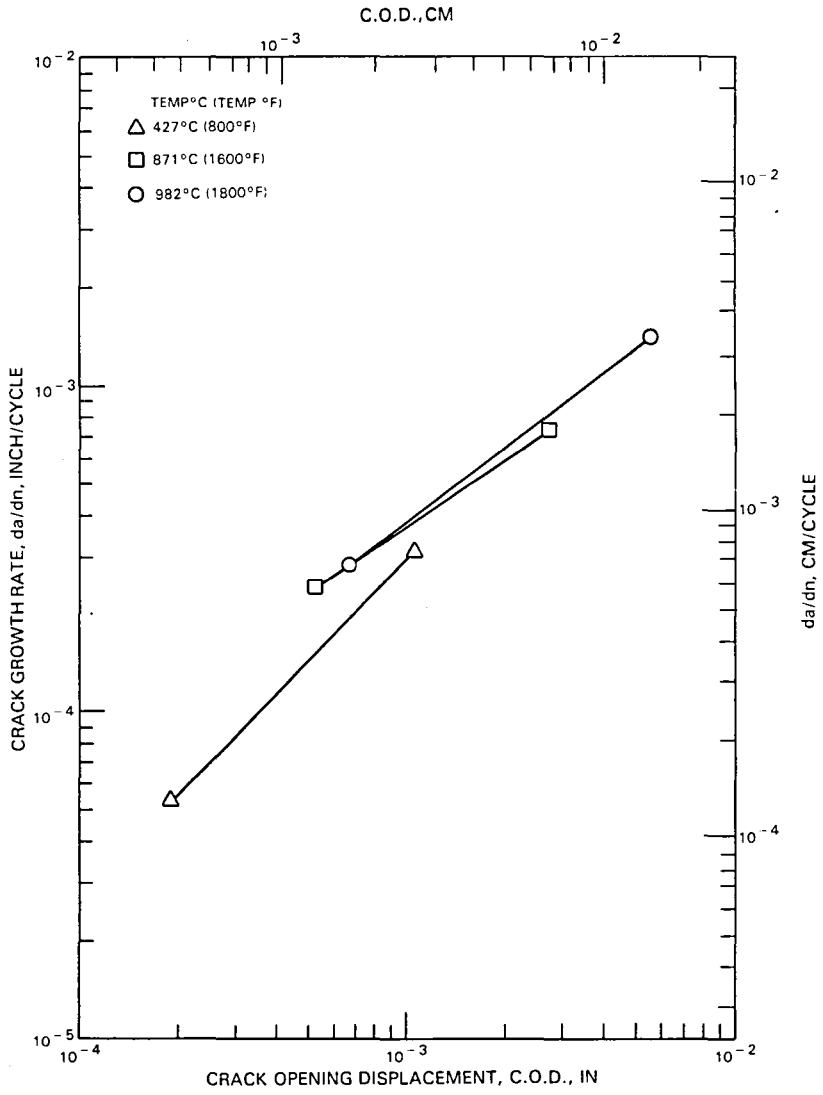

Figure 50 Spread in 0.4 Percent Strain Range Low- to High-Temperature Crack Growth Rates Based on COD Solutions by McMeeking.

7.6 TOMKINS' MODEL

As described in Section 7.1, three forms of Tomkins' model can be used for crack growth prediction, depending on the ratio of applied stress to yield stress of the material (38). In the first approximation, the crack tip field is approximated as two 45 degree plastic hinges. From this field, by matching some conditions with those predicted in the BCS model, the following crack growth law is deduced (here called "Model 1"):

$$\frac{da}{dN} = \frac{\pi^2}{8} \left(\frac{\Delta\sigma}{2T}\right)^2 \frac{\Delta\varepsilon_p}{2n+1} a$$

where: $\Delta\sigma$ = the stress range
T = the cyclic ultimate tensile strength
$\Delta\epsilon_p$ = the plastic strain range
n = the strain hardening exponent
N = number of cycles
a = crack length

Evidence presented by Tomkins suggests that this equation is applicable to moderate and high growth rate regimes.

A second form of the model arises from the same arguments if one assumes very high values of σ_{max}/T applicable to large plastic strains and/or high temperature. This form of the model gives the following growth law (Model 2):

$$\frac{da}{dN} = \left[\sec\left(\frac{\pi\sigma_{MAX}}{2T}\right) - 1\right] \Delta\varepsilon_p a$$

In the limiting case where the applied stress is nearly equal to the limit stress, the strain hardening is nearly zero, and a displacement controlled growth occurs which Tomkins claims gives rise to the following growth law (Model 3):

$$\frac{da}{dN} = (w-a)\ \Delta\varepsilon_p$$

w = length of ligament prior to cracking

The expressions for the above three models were evaluated for isothermal crack growth tests at three temperatures. The results of the data reduction are shown in Figures 51, 52, and 53 for temperatures of 982, 871, and 426°C(1800, 1600, and 800°F), respectively. The actual crack growth rate obtained from the testing is plotted against the rate predicted by the three models. The best prediction for all models was obtained for the highest temperature (982°C (1800°F)) data. Among the three models considered, Model 2 does the best in predicting the data for all temperatures. Only the Model 2 prediction is shown for 871°C (1600°F) and 426°C(800°F). It is worth pointing out that all models predict no crack growth for the case of zero plastic strain, so that the 426°C(800°F), 0.15 percent strain range test could not be considered.

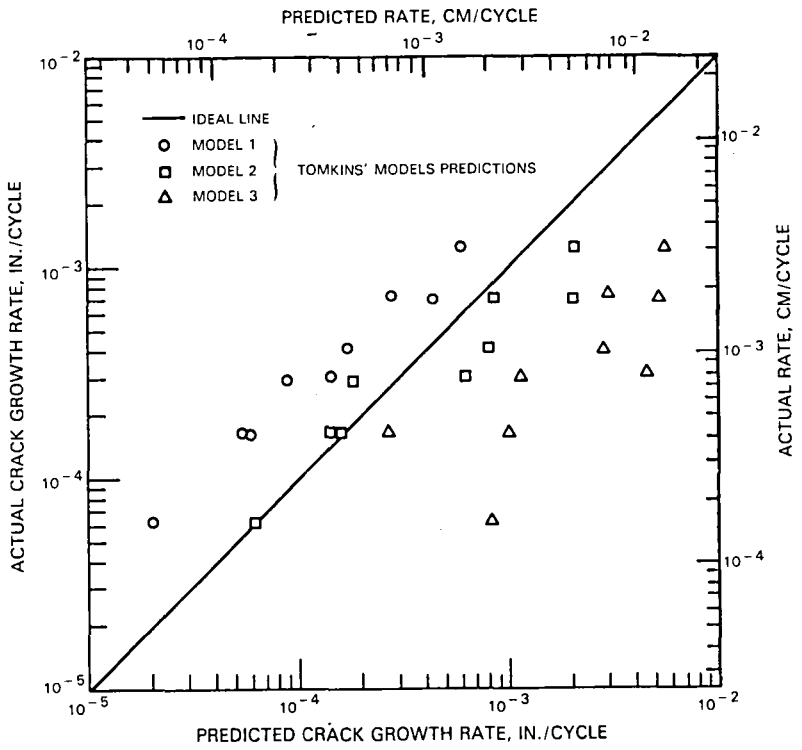

Figure 51 982°C(1800°F) Actual versus Predicted Crack Growth Rates Based on Tomkins' Model.

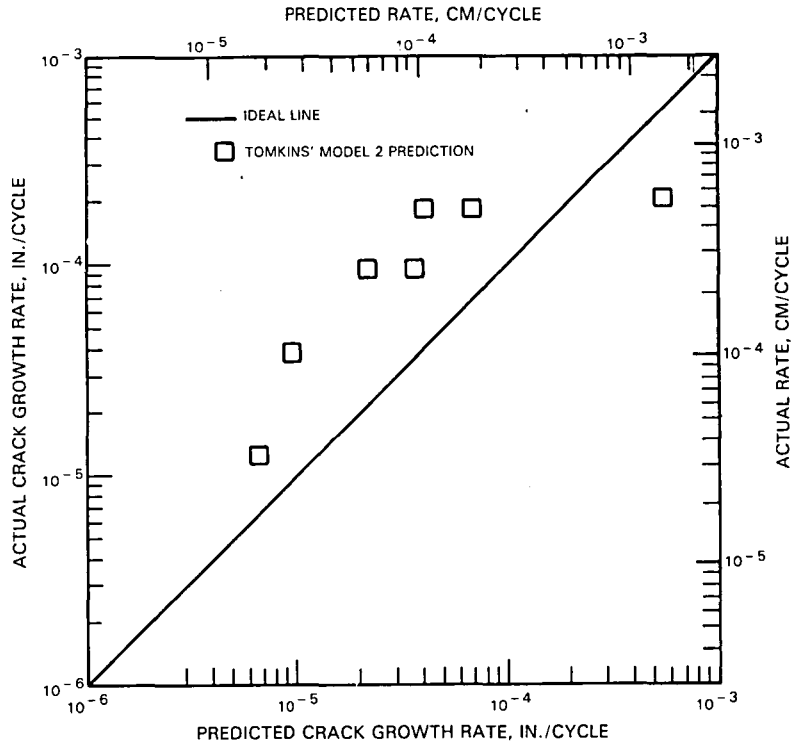

Figure 52 871°C(1600°F) Actual versus Predicted Crack Growth Rates Based on Tomkins' Model.

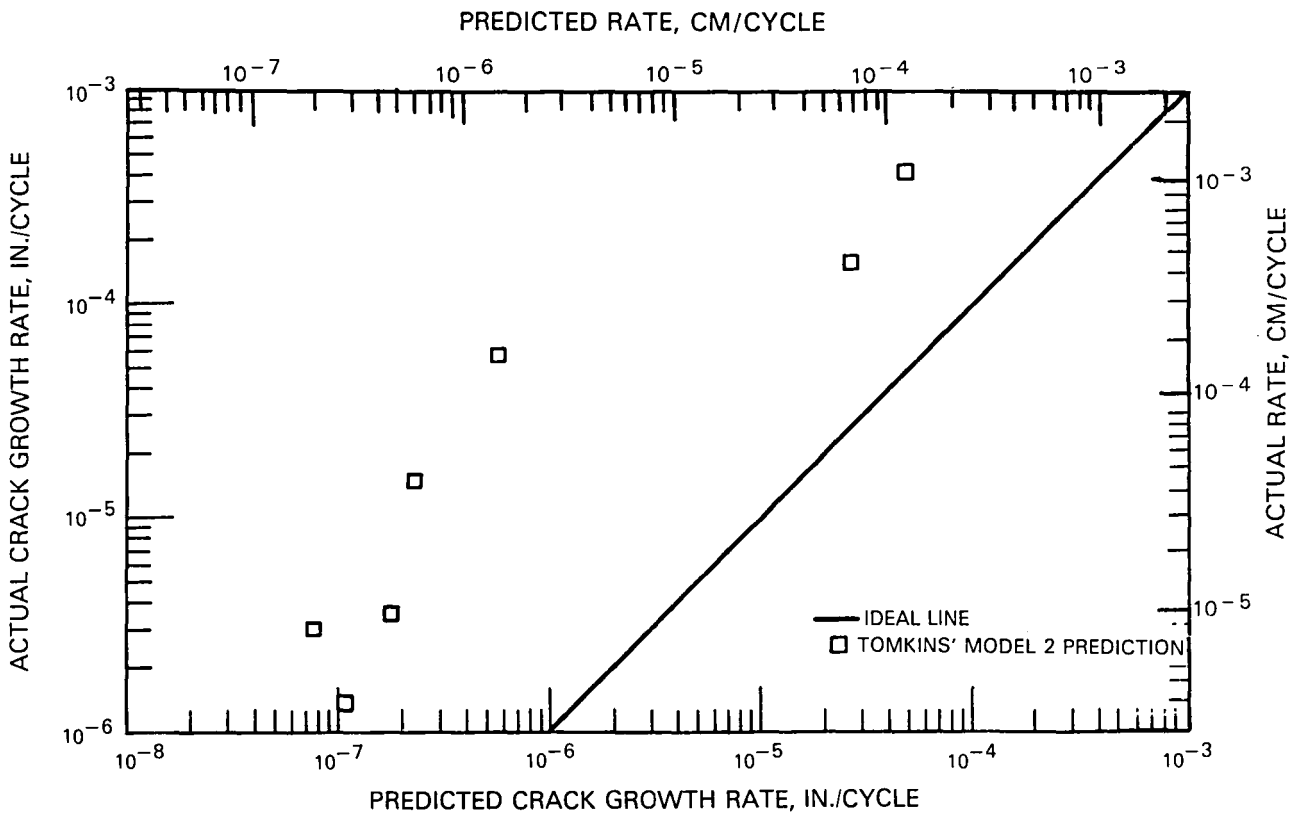

Figure 53 426°C(800°F) Actual versus Predicted Crack Growth Rates Based on Tomkins' Model.

It is apparent that for 871°C(1600°F) and 982°C(1800°F), Tomkins' Model 2 does a reasonable job of predicting growth rates while at 426°C(800°F) the prediction is very poor, being off by more than a factor of 10. Using the right-hand side of Tomkins equations as a parameter, it seems about as successful as K_ϵ in bringing different strain ranges and temperatures together. This is not surprising as Tomkins used the expressions of COD from the BCS model which is another small scale yielding model.

7.7 THERMOMECHANICAL FATIGUE (TMF) DATA PREDICTION

Motivation

The complete description of a thermomechanical cycle requires a definition of the relationship between strain and temperature. The prediction of the crack propagation life of an engine component ideally requires the correct prediction of crack growth rates at all locations along the crack growth path. A crack may grow through various regions with a range of different TMF cycles. For example, Figure 13 shows the strain-temperature relation at various locations along a combustor liner; an axial crack can propagate through all these locations. Solving the component problem requires the ability to predict the crack growth rates for many different strain temperature paths. If each

different TMF cycle requires independent crack growth data, the total data base required for making life predictions would be prohibitively large. Two possible strategies for dealing with this problem are as follows:

1. Develop a method of predicting TMF crack growth rates from isothermal data.

2. Develop a way of using TMF data for one type of TMF cycle to predict growth rates occurring as a result of different TMF cycles.

This section describes initial attempts to predict TMF growth rates from isothermal data. This approach is more desirable than strategy 2 above because isothermal data is both more commonly available and less expensive to generate.

A variety of TMF prediction schemes are possible. In this report, a particular scheme is described. The model philosophy could be applied to many other crack growth parameters. The prediction scheme is based on adding growth increments occurring within a single strain-temperature cycle.

Model Philosophy

In this section, the rationale for the models is presented. To make the derivation more understandable, the resulting equations for a model based on the strain intensity factor ΔK_ϵ will be presented. In addition, the generalized form of the equations for the model applied to an arbitrary mechanics para- meter X is presented. For the case of the model based on K_ϵ, the following isothermal growth law well represents the data:

$$\frac{da}{dN} = C(\Delta K_\varepsilon)^B$$

where C, B are temperature-dependent experimental constants.

In general, the following growth law is assumed:

$$da/dn=F(X)$$

The crack growth per cycle is usually given as the derivative da/dN. To avoid confusion, the derivative notation is abandoned in favor of incremental notation. The crack growth in a single cycle is thus designated by Δa. The model predicts TMF growth in one cycle by integrating the instantaneous growth rate within a cycle. To develop the model, the following assumptions are made.

1. The crack only grows during the tensile going part of the cycle.

2. The crack advances purely as a result of the tensile going change in the crack growth parameter and does not advance due to changes in other variables acting alone such as time and temperature.

3. The crack growth within a cycle can be treated as a continuous function of the parameter.

4. The total crack growth per cycle can be obtained by integrating the growth rate as a function of the parameter while correctly accounting for the effect of temperature on the instantaneous growth rate.

5. The crack growth rate for complete cycles is a certain function of the mechanics parameter X. The crack growth within a cycle is assumed to be the same function of the mechanics parameter. Thus,

$$\Delta a = f(\hat{X}), \text{ which gives } \frac{d\Delta a}{d\hat{X}} = \frac{df}{d\hat{X}}$$

$\hat{X}$ is measured from the strain reversal point, so that $\hat{X} = X - X_{MIN}$

For the case in which X is the strain intensity factor,

$$\frac{d\Delta a}{d\hat{K}_\varepsilon} = CB\hat{K}_\varepsilon^{\,B-1}$$

6. The instantaneous growth rate in a TMF test is a function of the current temperature and current value of the parameter and not a path function of these variables.

The final equation for prediction growth rate for the models is written as follows:

$$\Delta a = \int_o^{\Delta X} \frac{df}{d\hat{X}}\, d\hat{X}$$

or, where X is the strain intensity factor,

$$\Delta a = \int_o^{\Delta K_\varepsilon} CB\hat{K}_\varepsilon^{\,B-1}\, d\hat{K}_\varepsilon$$

where f, c, and B are functions of temperature.

Results

Strain Intensity Factor Model

Table VIII gives the values of C and B used in the above equation for the TMF data prediction. To evaluate the above integral, the crack growth constants were changed stepwise from one isothermal value to the next at a temperature halfway between the two temperatures at which the constants were determined.

TABLE VIII

CONSTANTS FOR

$$\frac{da}{dN} = C(\Delta K_\varepsilon)^B$$

Strain Range (%)	Temperature °C(°F)	Growth Law Constants B	C SI (CUSTOMARY)
0.25	426 (800)	2.96	2370(3706)
0.25	648(1200)	1.67	3.32(2.85)
0.25	760(1400)	1.40	0.90(0.68)
0.25	871(1600)	1.35	1.29(0.95)
0.25	926(1700)	1.17	0.76(0.52)
0.25	982(1800)	1.21	1.39(0.95)
0.40	426 (800)	1.57	2.22(1.82)
0.40	648(1200)	1.84	19.2(18.5)
0.40	760(1400)	1.53	4.58(3.68)
0.40	871(1600)	0.97	0.24(0.15)
0.40	926(1700)	1.22	1.09(0.76)
0.40	982(1800)	1.43	4.15(3.18)

The resulting predictions are shown in Figures 54 through 56. The following conclusions can be reached: 1) the levels of crack growth rate are reasonably predicted, with the exception of the 426 to 871°C(800 to 1600°F) test; 2) the prediction system is better than using the peak temperature data, again with the exception of the 426 to 871°C(800 to 1600°F) test; and 3) the slope of the Cycle I data is underpredicted, but the slopes of the Faithful Cycle and Cycle II data agree well with the prediction. The fact that the 426 to 871°C(800 to 1600°F) test is not well predicted is not necessarily a shortcoming of the prediction scheme itself, but the way in which the 426 to 871°C(800 to 1600°F) TMF data compares with that from the other Cycle I tests. As seen in Figure 38, the 426 to 871°C(800 to 1600°F) TMF test had the fastest crack growth rate, when compared on the basis of strain intensity factor. Thus, any technique which superimposes the isothermal crack growth rates could not correctly predict both the 426 to 871°C(800 to 1600°F) test and the slower 426 to 926°C(800 1700°F) test. The lack of success in predicting the 426 to 871°C(800 to 1600°F) data is likely a result of the use of the strain intensity factor as the correlation parameter.

Crack Opening Displacement Model

The simple formula which relates COD to stress intensity factor was used in the TMF data prediction. It was found that the isothermal data experiments can be reasonably well represented by the following equation:

$$\Delta a = C(\Delta\delta)^B$$

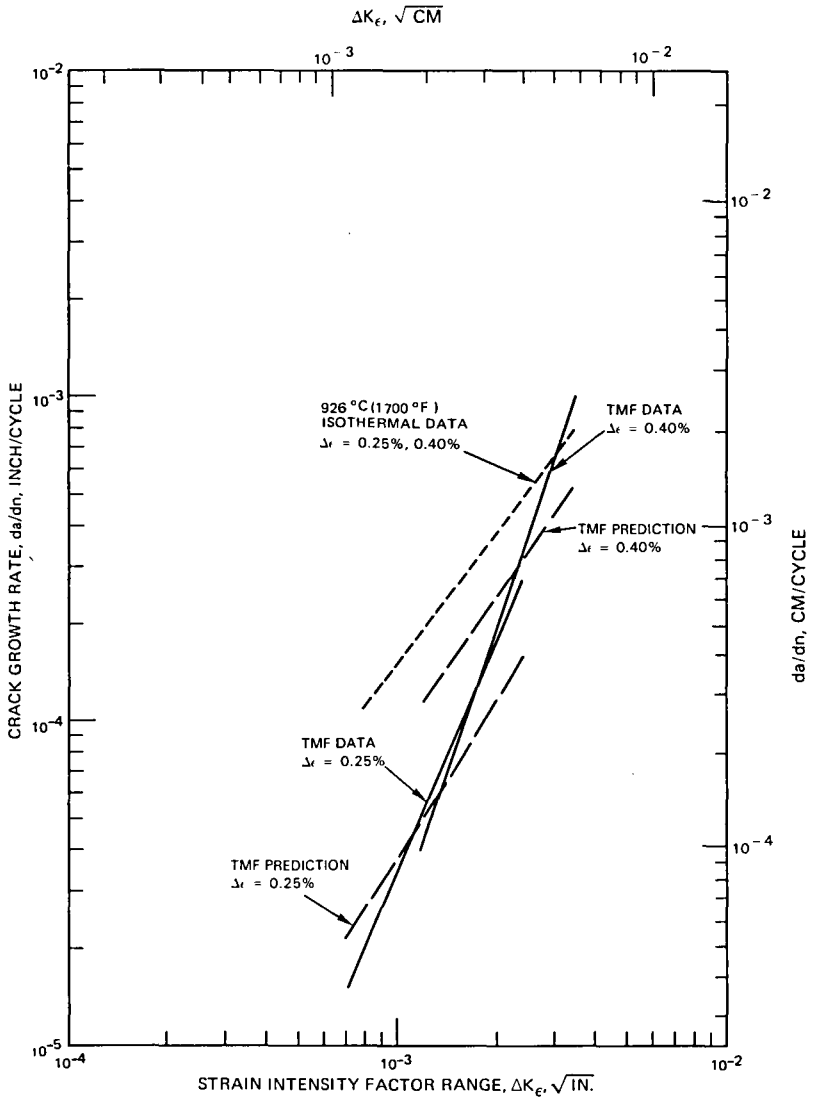

Figure 54 Prediction of 426°C(800°F) to 926°C(1700°F) Cycle I Crack Growth Data Using Elastic Strain Intensity Factor.

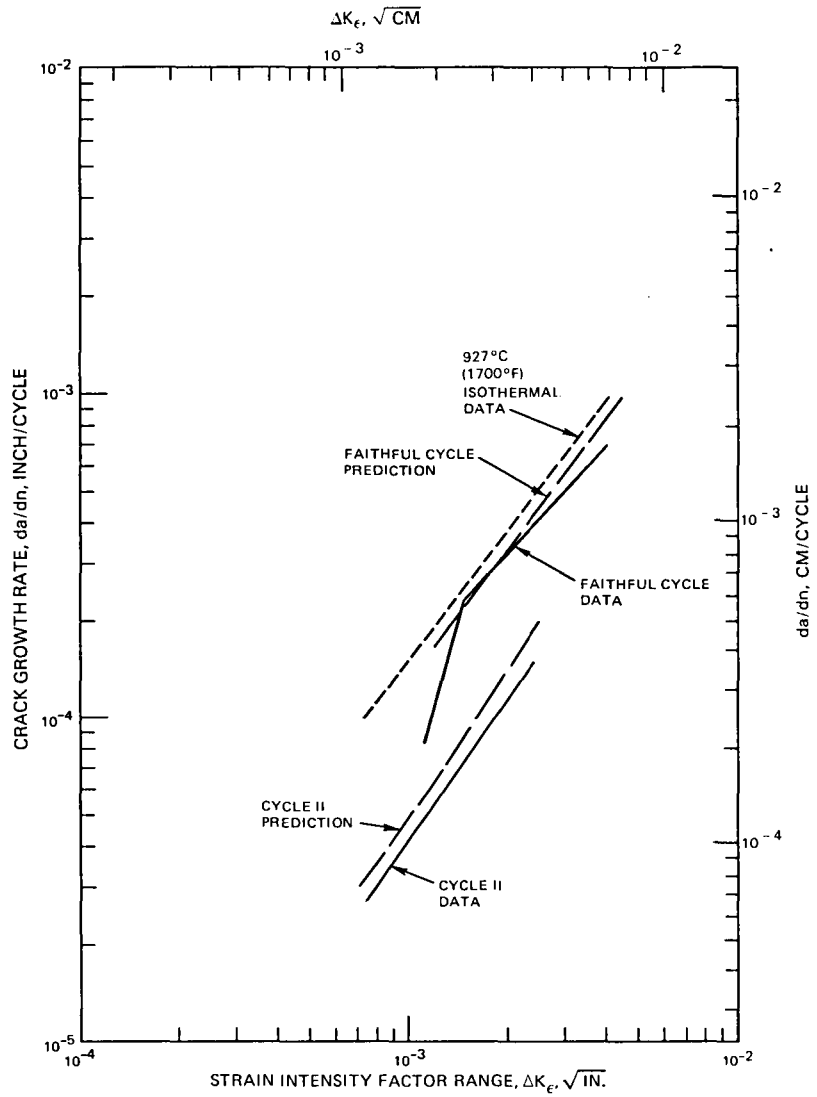

Figure 55 Prediction of 426°C(800°F) to 926°C(1700°F) Cycle II and Faithful Cycle Crack Growth Data Using Elastic Strain Intensity Factor.

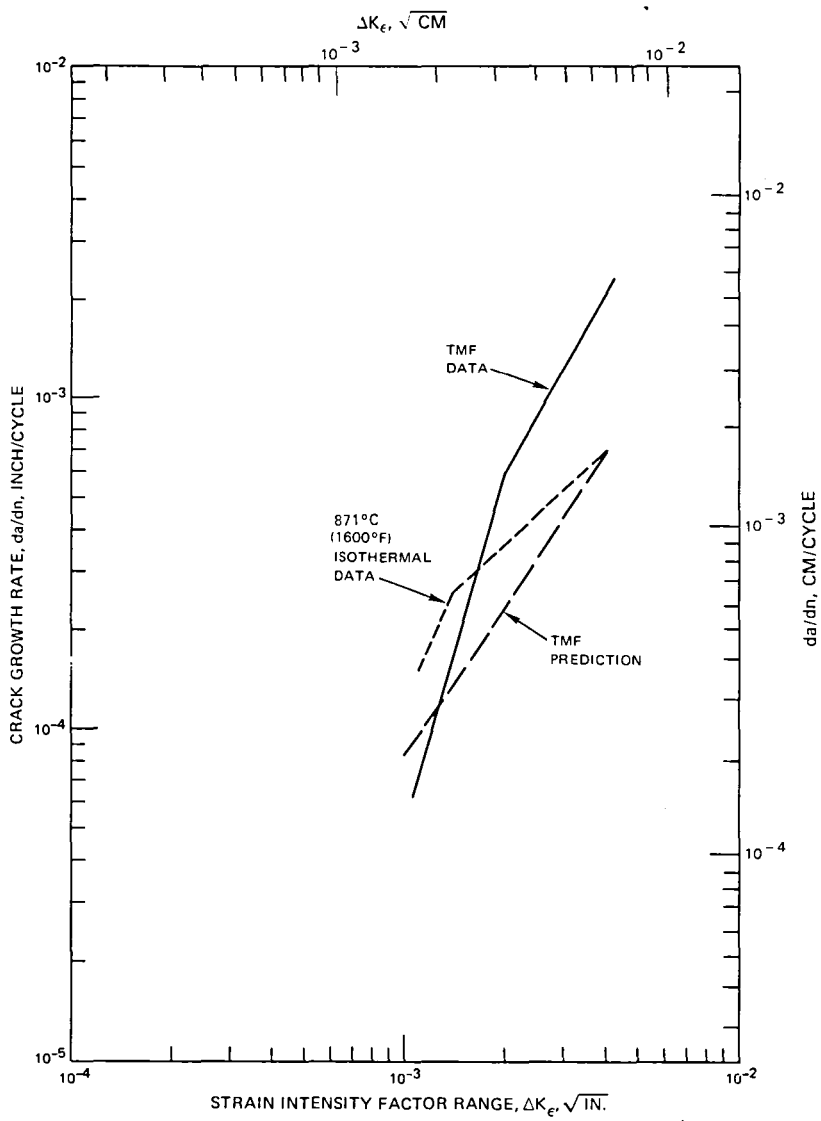

Figure 56 Prediction of 426°C(800°F) to 871°C(1600°F) Cycle I Crack Growth Data Using Elastic Strain Intensity Factor.

The data used in the TMF predictions was for the strain range of 0.40 percent, and it was found that a reasonable fit could be obtained using the constants listed in Table IX.

In determining the constants, the best fit was not used. A slight compromise was made to use a single value of the constant B which was chosen to equal 0.9 for all temperatures. Using a fixed value resulted in substantial simplification in evaluating the TMF cycles and insignificantly affected the fit of the equation to the data. TMF crack growth was predicted from the following equation.

$$\Delta a = \int_0^{\Delta\delta} C(T)(0.9)\hat{\delta}^{-0.1} d\hat{\delta}$$

This integral was then evaluated using Simpson's rule and using the following expressions for elastic modulus and yield strength:

SI Units:

$$E = [-69.6T + .206 \times 10^6] \text{ MPa}$$
$$\sigma_y = 220.5 \text{ MPa} \; ; \; T < 693°C$$
$$\sigma_y = [-0.634T + 670] \text{ MPa} \; ; \; T \geq 693°C$$

Customary Units:

$$E = [-5.61 \times 10^{-3}T + 30.1] \times 10^6 \text{ psi}$$
$$\sigma_y = 32{,}000 \text{ psi} \; ; \; T < 1280°F$$
$$\sigma_y = (-51.1\,T + 99{,}000) \text{psi} \; ; \; T \geq 1280°F$$

TABLE IX

CONSTANTS FOR

$$\Delta a = C(\Delta\delta)^B$$

Strain Range (%)	Temperature °C(°F)	Growth Law Constants B	C SI (CUSTOMARY)
0.40	426 (800)	0.9	0.0357(0.0325)
0.40	648(1200)	0.9	0.0512(0.0466)
0.40	871(1600)	0.9	0.2019(0.1839)
0.40	926(1700)	0.9	0.2806(0.2556)
0.40	982(1800)	0.9	0.4842(0.4411)

A bilinear curve was fit to actual hysteresis loop branches to represent the stress strain response.

The resulting predictions are shown in Figures 57 and 58. In these figures, the prediction is no more successful than that obtained using the model based on K_ϵ. This may be a result of the fact that the isothermal crack growth rates show an even greater spread from the lowest to the highest temperature using COD than using K_ϵ. A better prediction may have been possible had the COD based on the J-Integral been used rather than the simplified formula.

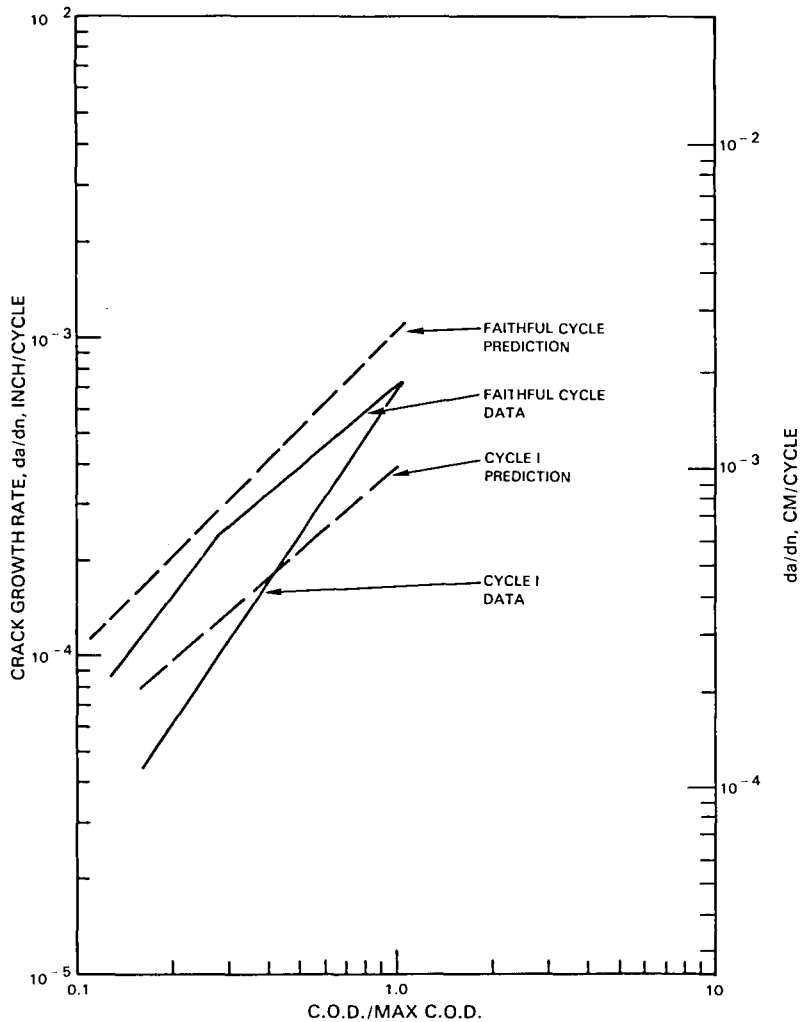

Figure 57 Prediction of 426°C(800°F) to 926°C(1700°F) Cycle I and Faithful Cycle Crack Growth Data Using Simplified COD Model.

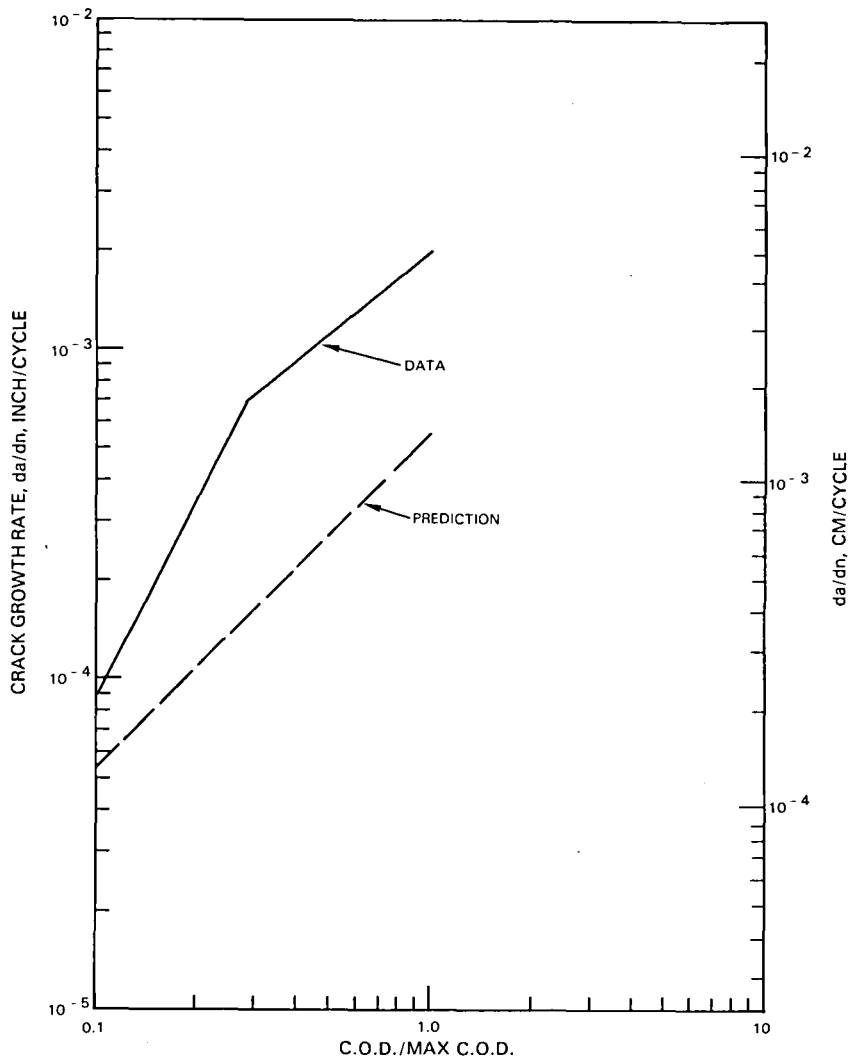

Figure 58 Prediction of 426°C(800°F) to 871°C(1600°F) Cycle I Crack Growth Data Using Simplified COD Model.

A choice must be made in the case of TMF cycles because the peak strain and peak stress do not coincide. The predictions shown were based on the assumption that the tensile going damaging part of the cycle started at the strain rather than the stress reversal.

Conclusions

The scheme developed here for predicting TMF crack growth rates is an improvement over using the crack growth rates associated with the peak temperature in the TMF cycle. Specifically, using peak temperature data to predict TMF da/dN results in a maximum error of a factor of 5.5 in da/dN compared to a maximum error of 2.7 using the model. There are some differences between the predictions and the actual TMF data. These differences may be the result of one or more of the following factors not included in the present model:

1. High temperature compressive loading may relax crack tip residual stresses. This effect produces larger COD's and plastic zones than if no residual stresses were present. This effect is included implicitly in the growth rates derived from high temperature data but neglected in the growth rates derived from low temperature data.

2. The effect of material ageing on the fatigue crack growth rate is not included explicitly. This effect is included implicitly for high temperature data but neglected in low temperature data.

3. Temperature change during straining may result in crack growth mechanisms that do not occur isothermally. Damage due to differential expansion of the oxide layer relative to the base metal is one possible mechanism of this type.

4. The success of the prediction may depend on the mechanics parameter chosen and the method used for its calculation. The promising result in Figures 49 and 50 indicates that the best parameter for predicting TMF crack growth may be COD, based on the J-Integral. Whether or not this is the case must be left for future work.

The TMF crack growth predictions made are an advancement over using isothermal data at the peak temperature. More importantly, the results suggest that TMF prediction from isothermal data is possible. Models that account for the factors cited above should give improved crack growth predictions. The ultimate accuracy of these predictions is limited primarily by the extent to which TMF crack growth is produced by unique TMF mechanisms.

7.8 METALLURGICAL EXAMINATION

The fracture surfaces of the failed specimens were examined with the goal of establishing trends in the surface appearance as a function of various test parameters, including strain range, temperature and TMF cycle shape. The major emphasis was to determine the similarities and differences between isothermal and TMF crack growth. The specimens were examined to determine whether the

crack growth was planar or non-planar; the extent of roughness of the fatigue surfaces, and the transgranular or intergranular nature of the crack growth. The following observations were made concerning the above effects.

Planar vs. Non-Planar Crack Growth

Isothermal Tests

The degree of nonplanar crack growth was a function of both strain range and temperature. The largest amounts of nonplanar growth were evident for the lower temperatures and the greater strain ranges. At 426°C(800°F) the growth was planar for the small strain range but very nonplanar for the larger strain ranges. At 648°C(1200°F) and 760°C(1400°F), the growth was planar for the smaller strain ranges and slightly nonplanar for the large strain range. At 871°C(1600°F), 926°C(1700°F) and 982°C(1800°F) growth was planar for all strain ranges. For the temperatures tested, there was no effect of either mean strain or hold time.

TMF Tests

The degree of nonplanar growth was a function of strain range, peak cyclic temperature and cycle shape. For the Cycle I tests at medium strain ranges, growth was planar for a peak temperature of 982°C(1800°F), slightly nonplanar for 926°C(1700°F) and 871°C(1600°F), and very nonplanar for 760°C(1400°F) and 648°C(1200°F). Growth for the 871°C(1600°F), large strain range test was more nonplanar than that for either the 871°C(1600°F), medium strain range test or the 926°C(1700°F), large strain range test. Growth for the Cycle I hold time test was slightly more planar than that for the test with no hold time. The Cycle II and faithful cycle tests exhibited planar growths.

Extent of Surface Roughness

Isothermal Tests

The extent of surface roughness was greater the higher the temperature and the larger the strain range. The 426°C(800°F) and 648°C(1200°F) specimens exhibited very smooth surfaces. The 760°C(1400°F) specimen surfaces were smooth for the small strain ranges but slightly rough for the large strain range. The 871°C(1600°F), 926°C (1700°F) and 982°C(1800°F) specimen surfaces varied from a smooth to slightly rough appearance at the small strain range to a very rough appearance at the large strain range.

TMF Tests

For the Cycle I tests, the extent of surface roughness was greater the higher the peak temperature and the greater the strain range. Surfaces were smooth for peak temperature of 648°C(1200°F), 760°C(1400°F), and 871°C(1600°F), rough for 926°C (1700°F) and 982°C(1800°F). The larger strain range tests at 871°C (1600°F) and 926°C(1700°F) had a rougher surface appearance than that for the smaller strain range tests. The hold time had no apparent effect on the degree of roughness. The Cycle II tests surface roughness was comparable to the 926°C (1700°F) isothermal test. The surfaces of the faithful cycle tests were smooth.

Transgranular vs. Intergranular Growth

Isothermal Tests

Only specimens with the largest strain range were studied. Crack growth was transgranular for the low temperature tests (426°C(800°F), 648°C(1200°F) and 760°C(1400°F)), and intergranular for the high temperature tests (871°C (1600°F), 926°C (1700°F) and 982°C(1800°F)).

TMF Tests

The mode of growth was a function of cycle shape. The Cycle I tests run in the intermediate strain range were all transgranular, with a small amount of intergranular growth only in the 426 to 982°C(800°F to 1800°F) test and the 426 to 926°C(800 to 1700°F) large strain range test. The faithful cycle growth was transgranular.

Discussion

It is observed that for the three types of surface features studied, there was a "transition" temperature from one mode of crack growth at the lower temperatures to a different mode of the higher temperatures. In all cases, this transition temperature for isothermal tests was a lower value than for the TMF tests. For a strain range of 0.4 percent, the transition temperature under isothermal conditions from nonplanar to planar growth, from a smooth to a rough fracture surface, and from transgranular to intergranular growth, all occurred at about 760°C(1400°F) to 871°C(1600°F). For Cycle I TMF conditions, the transition temperature for all features was for a peak temperature of around 926°C(1700°F).

Examples of surface features for low temperature isothermal, high temperature isothermal, and Cycle I TMF test specimens are shown in Figures 59 and 60. The degree of nonplanar growth and the extent of surface roughness for the TMF tests fall between the features observed for the high and low temperature isothermal tests.

The observations presented above suggest that crack growth under TMF conditions is in some sense an average of that experienced in isothermal tests over the temperature range of the TMF tests. This evidence offers hope that some type of superposition model as described in Section 7.7 may eventually well predict TMF crack growth.

Crack growth in service combustor lines tends to be nonplanar, of moderate level of surface roughness, and chiefly transgranular, similar to the TMF tests. However, high temperature isothermal growth tends to be planar, very rough, and intergranular. This observation reinforces the notion that isothermal tests run at the peak service hardware temperature do not duplicate service conditions, as well as TMF tests do.

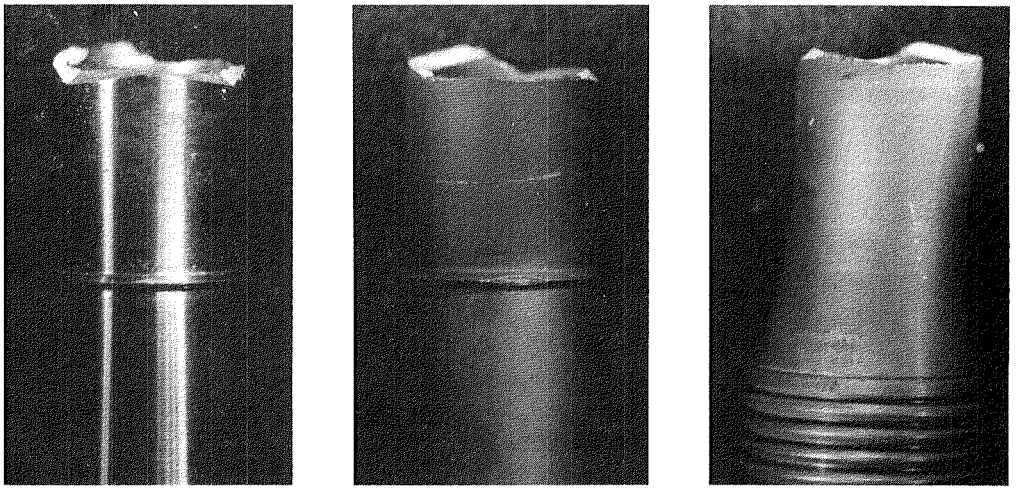

2X

TEMPERATURE °C	426	926	426-926
TEMPERATURE °F	(800)	(1700)	(800-1700)
STRAIN RANGE, %	0.40	0.40	0.40

Figure 59 Degree of Nonplanar Crack Growth for Low-Temperature, High-Temperature, and TMF Specimen Tests.

In addition, it is worth noting the effect of cycle shape on the mode of growth. The Cycle II test was different than the Cycle I test but similar to the isothermal test at the peak temperature in that the crack growth in the Cycle II test was planar, rough, and intergranular. The Faithful Cycle test also differed from the Cycle I test in that the Faithful Cycle growth was planar, and smooth; however, the mode of growth was transgranular similar to the Cycle I test. This evidence shows that not only is the temperature range and strain range important in a TMF test, but the cycle shape is also important.

7.9 CONCLUSIONS ON DATA CORRELATION PARAMETERS

The major purpose of the data reduction described in the previous sections was to assess the usefulness of fracture mechanics parameters for correlating high temperature and TMF crack growth, and for using isothermal data to predict TMF results. To quantitatively establish the applicability of the various parameters, several criteria were identified as being significant. The criteria consisted of evaluating the "spread" in crack growth rate data as a function of various test parameters as given below.

1. The spread in high temperature isothermal crack growth rates as a function of strain range.

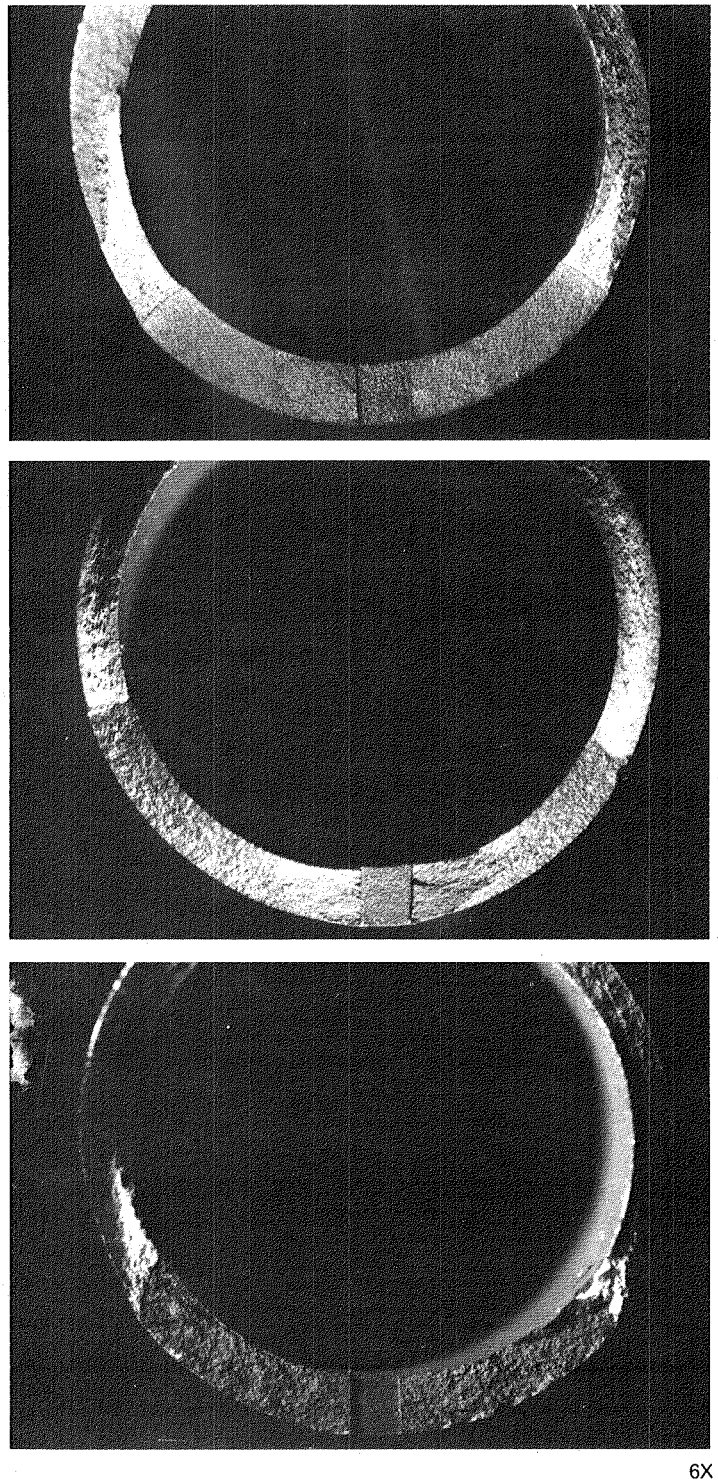

TEMPERATURE °C (°F)	STRAIN RANGE %
649 (1200)	0.40
926 (1700)	0.40
426-871 (800-1800)	

6X

Figure 60 Extent of Surface Roughness for Low-Temperature, High-Temperature, and TMF Specimen Tests.

2. The spread in Cycle I TMF crack growth rates as a function of strain range.

3. The spread in crack growth rates from low temperature to high temperature isothermal testing, at a given strain range.

4. The spread in crack growth rates as a function of peak temperature in a TMF cycle,at a given strain range.

The smaller the spread in growth rates as a function of the above conditions, the better the parameter is judged to be.

The crack growth data was assessed with the above criteria in mind. The spread in the data was defined by dividing the faster growth rate by the slower growth rate at the same value of the correlation parameter. The spread was calculated for both small and large values of the parameter and the numbers averaged.

The result of these calculations is shown in bar chart form in Figure 61. In this chart, a spread of 1.0 is considered "ideal". The following conclusions are drawn:

1. Crack opening displacement offers the most promise as a data correlation parameter, from the standpoint of predicting TMF results from isothermal data. Although there was no actual prediction of TMF crack growth performed for the COD based on J, the manner in which the temperature-dependent material flow properties have the effect of collapsing the low and high temperature isothermal data makes the COD appear attractive.

2. The J-Integral also performs well as a parameter in collapsing the high temperature and TMF data as a function of strain range, and in collapsing the TMF Cycle I data for various peak temperatures. However, J has a fairly large spread from the low to high temperature crack growth rates, which makes it unattractive in predicting TMF crack growth from isothermal data.

3. The stress intensity factor correlates the TMF data well as a function of strain range and peak temperature. However, the large spread in growth rates as a function of strain range make it undesireable for high temperature life prediction, and the large spread in growth rates from low to high temperature make it undesireable for prediction of TMF crack growth from isothermal data.

4. The strain intensity factor correlates the data well for high temperature isothermal tests and for Cycle I TMF tests. Also, the spread of crack growth rates from low to high temperature is not too great to provide a reasonable prediction of TMF crack growth. However, the spread in growth rates as a function of peak temperature in the Cycle I TMF tests make its use questionable as the best correlation parameter.

5. The Tomkins' model was assessed only from the standpoint of the crack growth prediction showing a better potential than the other parameters. Therefore, the results are not shown in the chart. However, the isothermal data reduction that was performed indicated that the Tomkins' model shows no particular advantage over the other parameters in predicting or correlating the isothermal or TMF crack growth data.

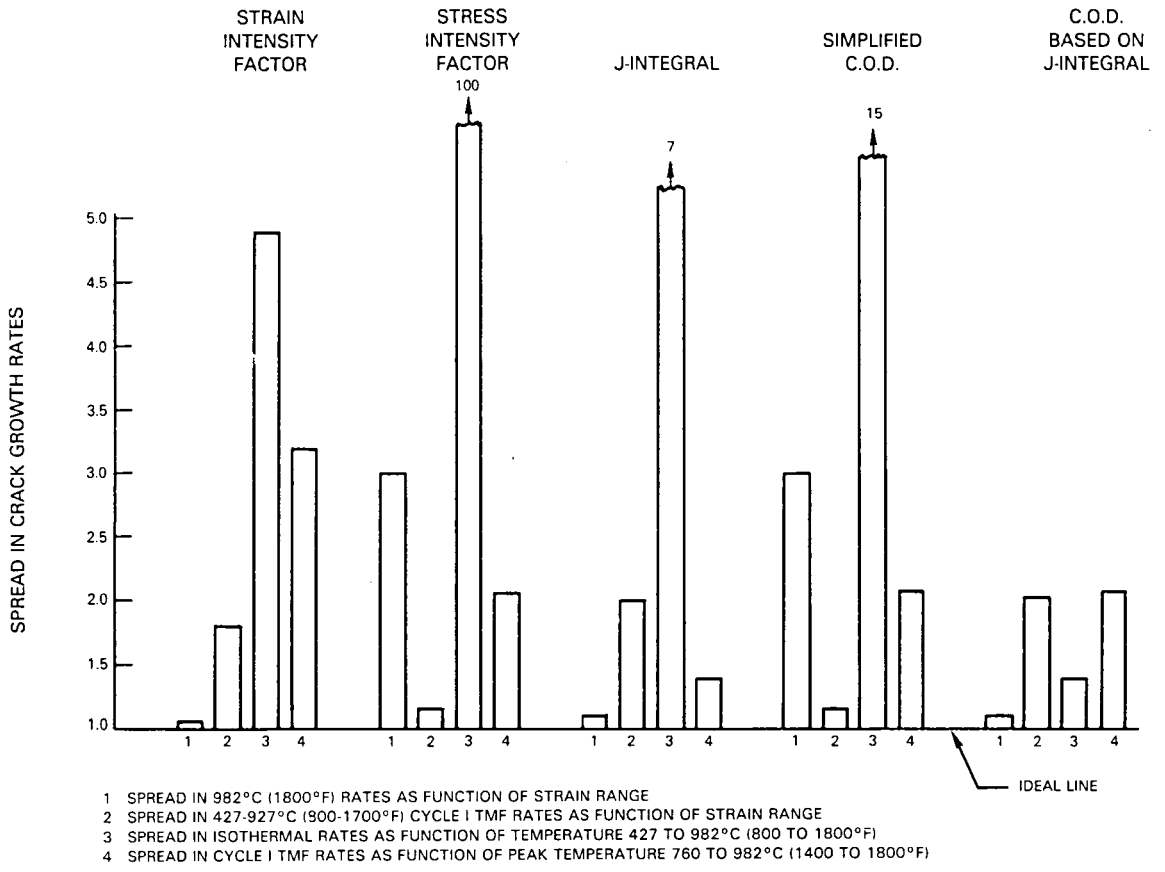

Figure 61 Spread of Crack Growth Rates for Fracture Mechanics Data Correlation Parameters.

This Page Intentionally Left Blank

SECTION 8.0

SUMMARY OF RESULTS

The problem of crack growth in hot section engine components was extensively examined, using the combustor liner as an example component. The major areas investigated included an engine survey, nonlinear fracture mechanics analysis techniques, evaluation of data correlation parameters, and prediction of crack growth under thermomechanical cycling. The following are the major observations, conclusions, and recommendations from this effort.

1. The engine survey suggested that there are some components in the engine hot section in which conventional approaches to crack propagation life prediction may not be appropriate. Due to the high temperature and thermal-mechanical fatigue (TMF) cycling, conventional liner elastic fracture mechanics techniques using using isothermal crack growth data may not be completely applicable in some locations. These locations include combustor liners, turbine blades, and turbine vanes. On the other hand, stress and temperature levels seen in turbine disks, turbine seals, turbine spacers, and turbine cases are not of a sufficient magnitude to produce significant amounts of cyclic inelastic material behavior. This makes the use of conventional elastic approaches appropriate for the above locations.

2. A procedure was developed for calculating the cyclic value of the J-Integral (ΔJ) for the tubular specimen used in the crack propagation testing. The procedure requires adding together the elastic and plastic components of ΔJ. The technique was originally developed for isothermal testing. In this effort the approach was used for both isothermal testing and extended to thermomechanical cycling. Further investigation into the use and calculation of ΔJ for TMF cycling situations is recommended.

3. A cyclic nonlinear fracture mechanics analysis of a simplified model of the combustor liner was performed. The analysis, although performed on a relatively coarse two-dimensional finite element model, still required a larger investment in man hours and computer time than would be appropriate for routine analyses. Further development of cyclic nonlinear fracture mechanics capability is recommended.

4. The finite element fracture mechanics analysis used a compliance approach to calculate a value for the correlation parameter. The compliance approach was originally developed for isothermal testing to obtain an experimental value of the J-Integral. The compliance approach was extended here for a more complicated situation, which includes a thermomechanical cycle, spatially varying temperatures, and temperature-dependent material properties. Thus, the parameter calculated cannot be termed a "J-Integral" in the strictest sense. Further assessment of other parameters which are both theoretically justified and calculable for structural components is recommended.

5. The crack propagation testing and data reduction for combustor liner material showed the necessity of the use of nonlinear data correlation parameters. The elastic stress and strain intensity factors showed several results which make their use undesirable for TMF crack growth prediction. There was some strain range dependence on crack growth rates using both linear and nonlinear parameters. Of the parameters extensively studied, the J-Integral was the best all-around approach for correlating high temperature and TMF data. The crack opening displacement (COD) calculated from the J-Integral shows the most promise in correlating the data over a range of temperatures and in performing predictions of TMF crack growth from isothermal data. Extensive evaluation of the COD for TMF cycling is recommended for future work. Data supporting the above conclusions were given in Figure 61.

6. A prediction scheme developed for using isothermal data to predict TMF crack growth was moderately successful, using both the strain intensity factor and a simplified COD approach. Better predictions may be achieved using more sophisticated approaches, such as COD calculated from the J-Integral.

7. There were marked differences in the specimen crack growth surface features as a function of temperature and TMF cycle. Low temperature isothermal growth was nonplanar, smooth, and transgranular. High temperature isothermal growth was planar, rough, and intergranular. Cycle I TMF crack growth was moderately nonplanar, moderately rough, and chiefly transgranular, with a small amount of intergranular growth. The surface features of the TMF growth could thus be considered an "average" of those seen for low and high temperature isothermal tests. This observation lends hope to the ultimate success of an isothermal to TMF data prediction scheme. However, the final degree of success of the scheme will be determined by the degree to which TMF crack growth is governed by unique TMF mechanisms not present under isothermal conditions.

REFERENCES

1. Erdogan, F., and Ratwani, M., "Fatigue and Fracture of Cylindrical Shells Containing a Circumferential Crack," International Journal of Fracture Mechanics, Vol. 6, 1970, pp. 379-392.

2. Rau, C. A., Jr., Gemma, A. E., and Leverant, G. R., "Thermal Mechanical Fatigue Crack Propagation in Nickel and Cobalt Base Superalloys Under Various Strain Temperature Cycles," Fatigue at Elevated Temperature, ASTM STP 520, American Society for Testing and Materials, 1973, pp. 166-178.

3. Labbens, R., Pellissier, - Tanon, A., and Heliot, J., "Practical Method for Calculating Stress-Intensity Factor Through Weight Functions," Mechanics of Crack Growth, ASTM STP 590, American Society for Testing and Materials, 1976, pp. 368 - 384.

4. Begley, J. A., and Landes, J. D., "The J-Integral as a Fracture Criterion," Fracture Toughness, Proceedings of the 1971 National Symposium on Fracture Mechanics, Part II, ASTM STP 514, American Society for Testing and Materials, 1972, pp. 1-20.

5. Shih, C. F., and Hutchinson, J. W., "Fully Plastic Solutions and Large Scale Yielding Estimates for Plane Stress Crack Problems," Journal of Engineering Materials and Technology, October 1976, pp. 289-295.

6. Rice, J. R., "A Path Independent Integral and the Approximate Analysis of Strain Concentration by Notches and Cracks," Transactions of the ASME, Journal of Applied Mechanics, Volume 34, 1968, pp. 379-386.

7. Rice, J. R., "Mathematical Analysis in the Mechanics of Fracture," Chapter 3 of Volume II, Fracture: An Advanced Treatise, ed. H. Liebowitz, Academic Press, 1968, pp. 191-311.

8. MARC General Purpose Finite Element Program-User Manual, Volumes A, B, C, MARC Analysis Research Corp.

9. Parks, D. M., "A Stiffness Derivative Finite Element Technique for Determination of Crack Tip Stress Intensity Factors," Int. Journal of Fracture, Volume 10, 1974, pp. 487-502.

10. Hellen, T. K., Price, R. H., and Harrison, R. P., "Thermal Analysis of Cracked Bodies Using Finite Element Techniques," Structural Mechanics in Reactor Technology 3rd Conference, 1975, Paper L7/4.

11. Blackburn, W. S., Jackson, A. D., and Hellen, T. K., "An Integral Associated with the State of a Crack Tip in a Non-Elastic Material," Int. Journal of Fracture, Volume 13, 1977, pp. 183-200.

12. Barsoum, R. S., "On the Use of Isoparametric Finite Elements in Linear Fracture Mechanics," Int. Journal for Numerical Methods in Engineering, Volume 10, 1976, pp. 25-37.

13. Paris, P. C., "Fatigue--An Interdisciplinary Approach," Proceedings of the 10th Sagamore Conference, Syracuse University Press, 1964, p. 107.

14. Swanson, S. R., Cicci, F., and Hoppe, W., "Crack Propagation in Clad 7079-T6 Aluminum Alloy Sheet under Constant and Random Amplitude Fatigue Loading," Fatigue Crack Propagation Symposium, ASTM STP 415, American Society for Testing and Materials, 1967, pp. 312-362.

15. Paris, P. C., and Erdogan, F., "A Critical Analysis of Crack Propagation Laws," Journal of Basic Engineering, Transactions of the ASME, Series D, Vol. 85, Dec. 1963, p. 528.

16. Boettner, R. C., Laird, C., and McEvily, A. J., "Crack Nucleation and Growth in High Strain Low Cycle Fatigue," Transactions of the Metallurgical Society of AIME, Vol. 233, 1965, pp. 379-387.

17. McEvily, A. J., "Fatigue Crack Growth and the Strain Intensity Factor," Proceedings of Air Force Conference on Fatigue and Fracture of Aircraft Structures and Materials, AFFDL-TR 70-144, p. 451.

18. Solomon, H. D., "Low Cycle Fatigue Crack Propagation in 1018 Steel", Journal of Materials, JMLSA, Vol. 7, No. 3, September, 1972, pp. 299-306.

19. Kitagawa, H., Takahashi, S., Suh, C. M., and Miyashita, S., "Quantitative Analysis of Fatigue Process Micro-cracks and Slip Lines Under Cyclic Strains," Symposium on Fatigue Mechanisms, ASTM STP 675, American Society for Testing and Materials, 1978, pp. 420-449.

20. Eshelby, J. D., Solid State Physics, eds. Seitz and Turnabil, Academic Press, 1956, p. 79.

21. Dowling, N. E., and Begley, J. A., "Fatigue Crack Growth During Gross Plasticity and the J-Integral," Mechanics of Crack Growth, ASTM STP 590, American Society for Testing and Materials, 1976, pp. 82-103.

22. Dowling, N. E., "Geometric Effects and the J-Integral Approach to Elastic-Plastic Fatigue Crack Growth," Cracks and Fracture, ASTM STP 601, American Society for Testing and Materials, 1976, pp. 19-32.

23. Dowling, N. E., "Crack Growth During Low-Cycle Fatigue of Smooth Axial Specimens," Cyclic Stress-Strain and Plastic Deformation Aspects of Fatigue Crack Growth, ASTM STP 637, American Society for Testing and Materials, 1977, pp. 97-121.

24. Brose, W. R., and Dowling, N. E., "Size Effects on the Fatigue Crack Growth Rate of Type 304 Stainless Steel," Elastic-Plastic Fracture, ASTM STP 668, American Society for Testing and Materials, 1979, pp. 720-735.

25. Sadananda, K., and Shahinian, P., "A Fracture Mechanics Approach to High Temperature Fatigue Crack Growth in Udimet 700," Engineering Fracture Mechanics, Vol. 11, 1979, pp. 73-84.

26. Sadananda, K., and Shahinian, P., "Application of J-Integral to High Temperature Fatigue Crack Growth in Cold Worked Type 316 Stainless Steel," Int. Journal of Fracture, Vol. 15, 1979, pp. R81-R84.

27. Mowbray, D. F., "Use of a Compact Type Strip Specimen for Fatigue Crack Growth Rate Testing in the High Rate Regime," Elastic-Plastic Fracture, ASTM STP 668, American Society for Testing and Materials, 1979, pp. 736-752.

28. Hutchinson, J. W., "Plastic Stress and Strain Fields at the Crack Tip," Journal of the Mechanics and Physics of Solids, Vol. 16, 1968, pp. 13-31.

29. Rice, J. R., and Rosengren, G. F., "Plane Strain Deformation Near a Crack Tip in Power-Law Hardening Material," Journal of the Mechanics and Physics of Solids, Vol. 16, 1968, pp. 1-12.

30. McMeeking, R. M., "Finite Deformation Analysis of Crack-Tip Opening in Elastic-Plastic Materials and Implications for Fracture," Journal of the Mechanics and Physics of Solids, Vol. 25, 1977, pp. 357-381.

31. Cottrell, A. H., "Theoretical Aspects of Radiation Damage and Brittle Fracture in Steel Pressure Vessels," Iron and Steel Special Report 69, 1961, pp. 281-296.

32. Wells, A. A., "Unstable Crack Propagation in Metals: Cleavage and Fast Fracture," Crack Propagation Symposium Proceedings, Cranfield College of Aeronautics, Vol. 1, 1961, pp. 210-230.

33. McClintock, F. A., discussion on paper by C. Laird entitled "The Influence of Metallurgical Struture on the Mechanics of Fatigue Crack Propagation," Fatigue Crack Propagation Symposium, ASTM STP 415, American Society for Testing and Materials, 1967, pp. 170-174.

34. Pelloux, R. M., "Fractographic Analysis of the Influence of Constituent Particles on Fatigue Crack Propagation in Aluminum Alloys," Transactions of the ASME, Vol. 57, 1964, pp. 511-518.

35. Lardner, R. W., "A Dislocation Model for Fatigue Crack Growth in Metals," Philosopical Magazine, Vol. 17, 1968, pp. 71-82.

36. Schwalbe, K. H., "Approximate Calculation of Fatigue Crack Growth," Eng. Fracture Mechanics, Vol. 9, 1973, pp. 381-396.

37. Edmondson, B., Formby, C. L., Jurevics, R., and Stagg, M. S., "Aspects of the Failure of Large Steel Pressure Vessels," Proceedings from the Second International Conference on Fracture, Chapman and Hall, 1969, pp. 192-203.

38. Tomkins, B., "The Development of Fatigue Crack Propagation Models fo Engineering Applications at Elevated Temperatures," Journal of Engineering Materials and Technology, October 1975, pp. 289-297.

39. Tomkins, B., "Fatigue Crack Propagation-An Analysis," Philosophical Magazine, Vol. 18, 1968, pp. 1041-1066.

40. Tomkins, B., and Biggs, W. D., "Low Endurance Fatigue in Metals and Polymers," Journal of Material Science, Vol. 4, 1969, pp. 344-553.

41. Tomkins, B., "Fatigue Failure in High Strength Metals," Philosophical Magazine, Vol. 23, 1971, pp. 687-703.

42. Neuman, P., "New Experiments Concerning the Slip Processes at Propagating Fatigue Cracks-I," Acta Metallurgica, Vol. 22, 1974, pp. 1155-1165.

43. Lankford, J., and Kusenberger, F. N., "On Crack Tip Yielding During Fatigue Cycling of a High Strength Steel," Philosophical Magazine, Vol. 26, 1972, pp. 1485-1490.

44. Wareing, J., Tomkins, B., and Sunner, G., "Extent to Which Material Properties Control Fatigue Failure of Elevated Temperatures," Fatigue at Elevated Temperature, ASTM STP 520, American Society for Testing and Materials, 1973, p. 123.

45. Huang, J. S., and Pelloux, R. M., "Low Cycle Fatigue Crack Propagation in Hastelloy-X at 25 and 760°C," Metallurgical Transactions A, Vol 11A, 1980, pp. 899-904.

46. Bilby, B. A., Cottrell, A. H., and Swinden, K. H., "The Spread of Plastic Yield From a Notch", Proceedings of the Royal Society, Series A, Vol. 272, 1963, p. 304.

47. Dugdale, D. S., "Yielding of Steel Sheets Containing Slits," Journal of the Mechanics and Physics of Solids, Vol. 8, 1960, pp. 100-104.

48. Shih, C. F., "Relationships between the J-Integral and the Crack Opening Displacement for Stationary and Extending Cracks," Journal of the Mechanics and Physics of Solids, Vol. 29, 1981, pp. 305-326.

APPENDIX A STRAIN INTENSITY FACTOR DATA REDUCTION

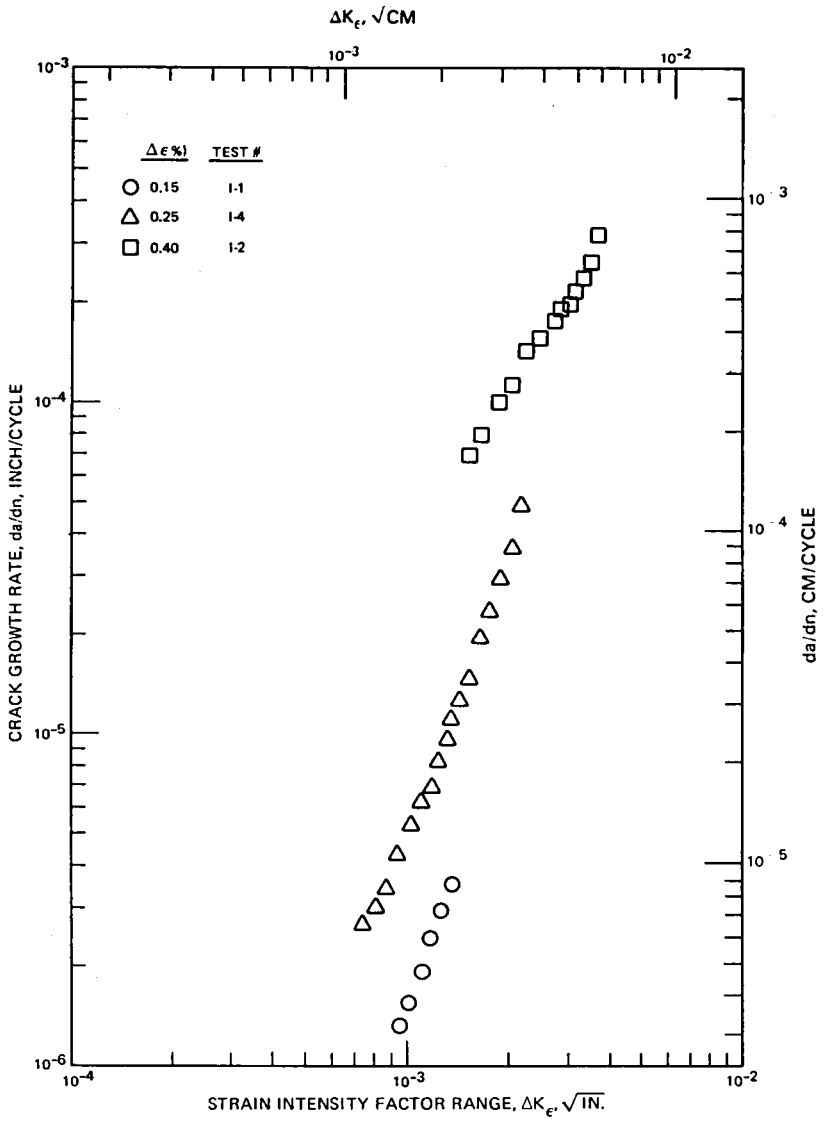

Figure A-1 427°C (800°F)

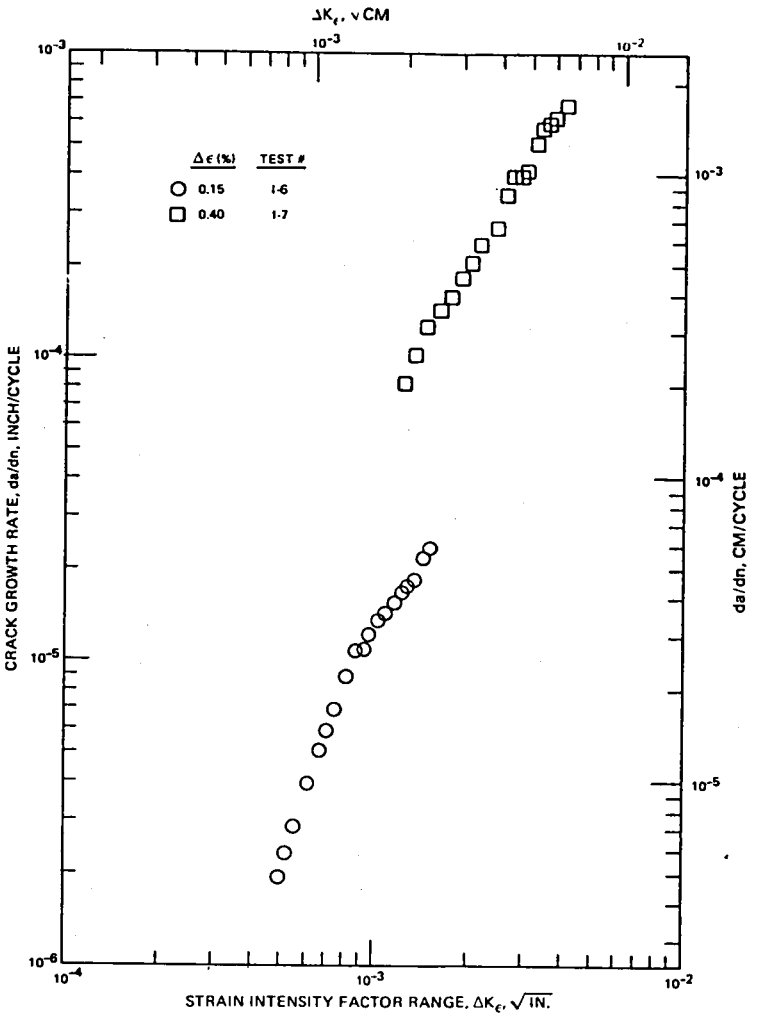

Figure A-2 649°C (1200°F)

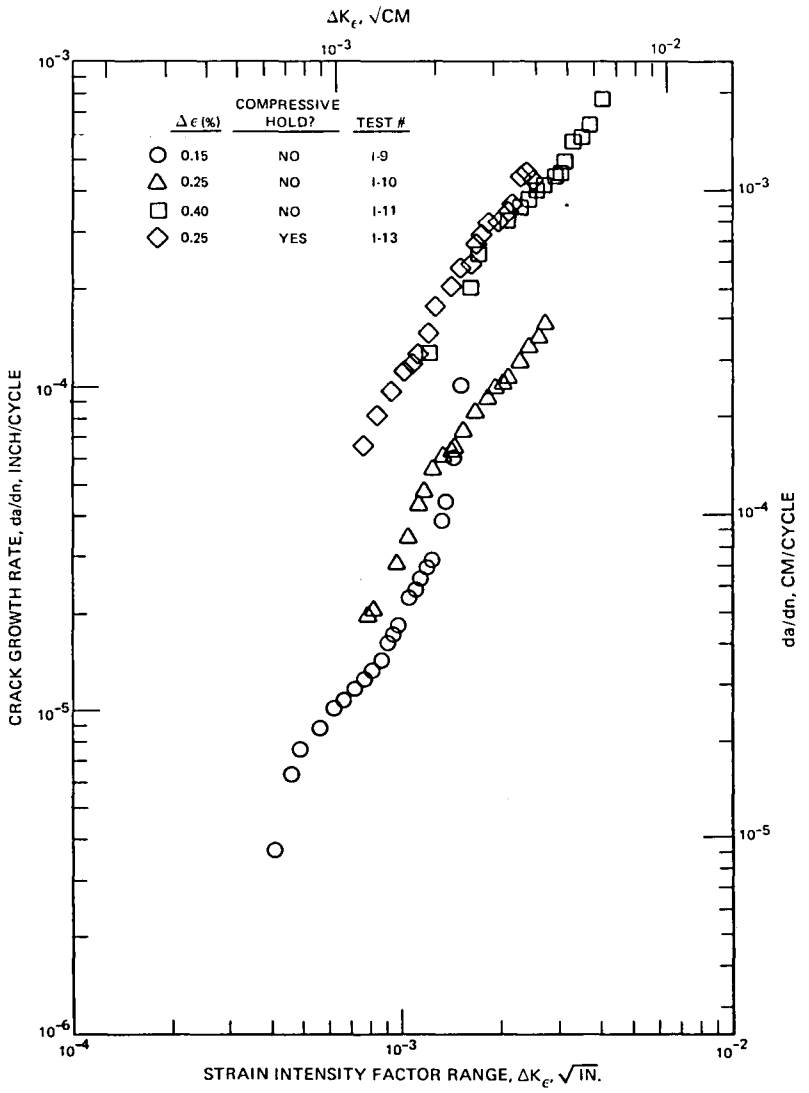

Figure A-3 760°C (1400°F)

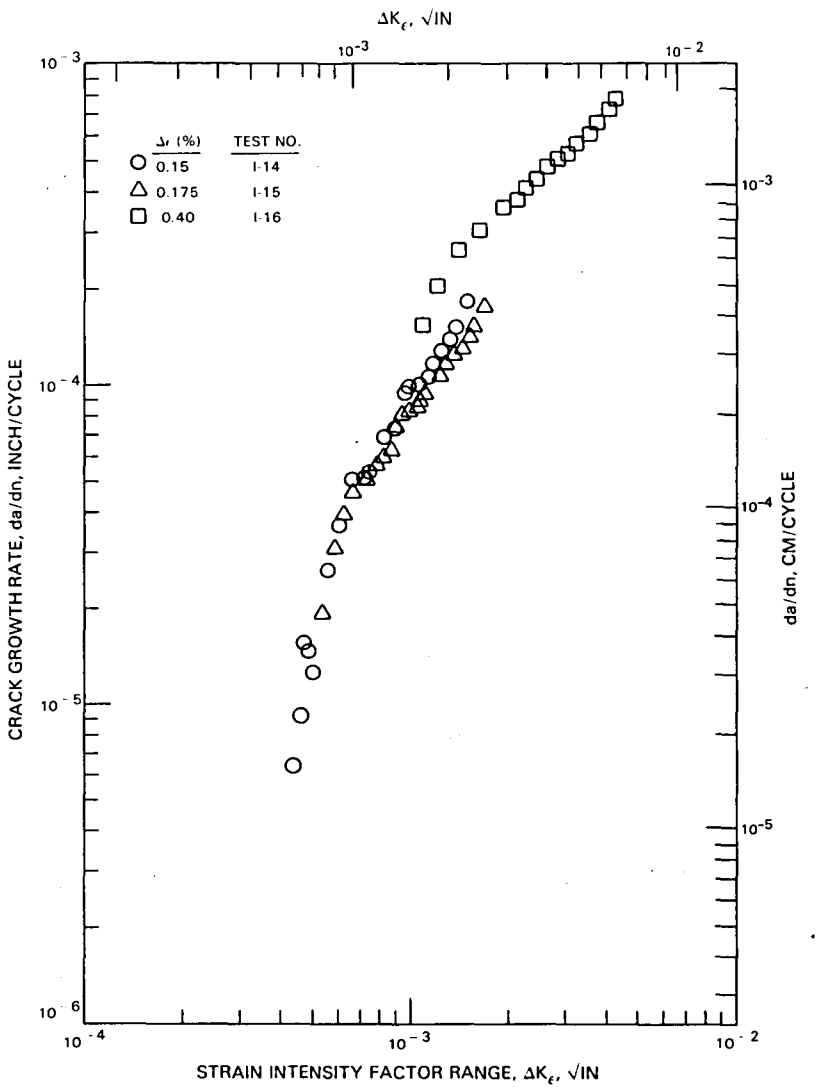

Figure A-4 871°C (1600°F)

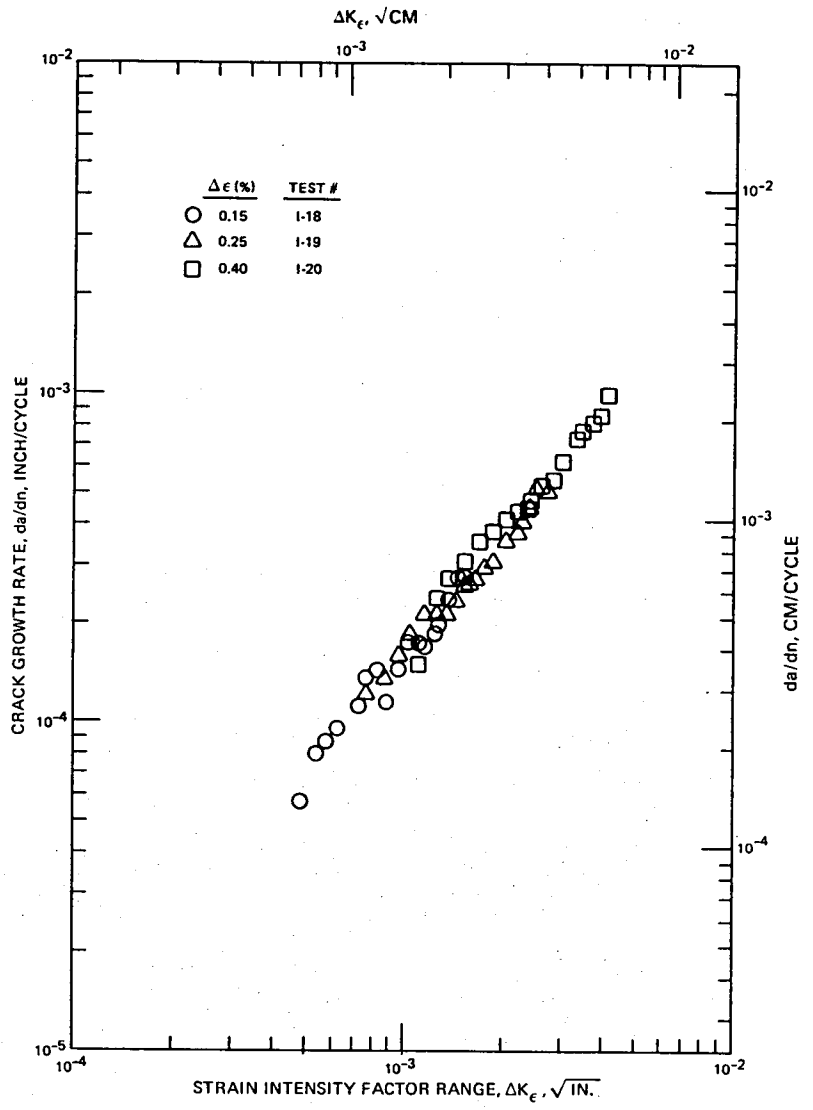

Figure A-5 927°C (1700°F)

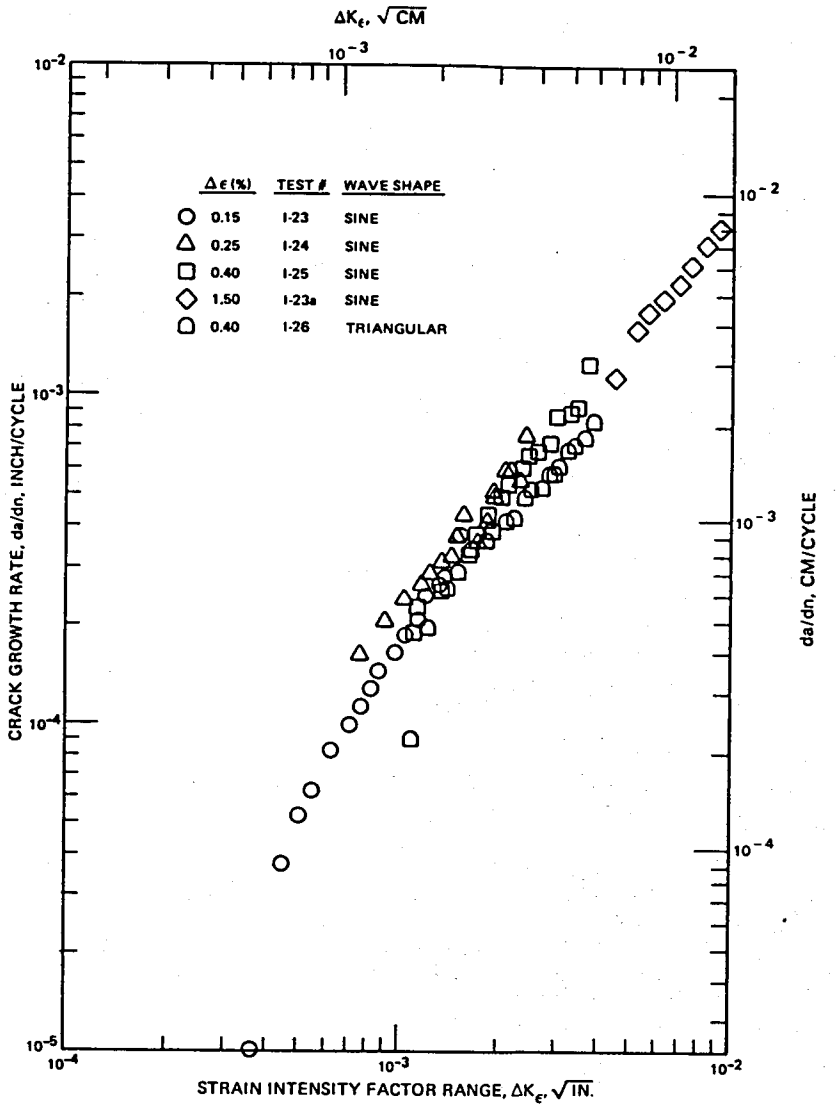

Figure A-6 982°C (1800°F)

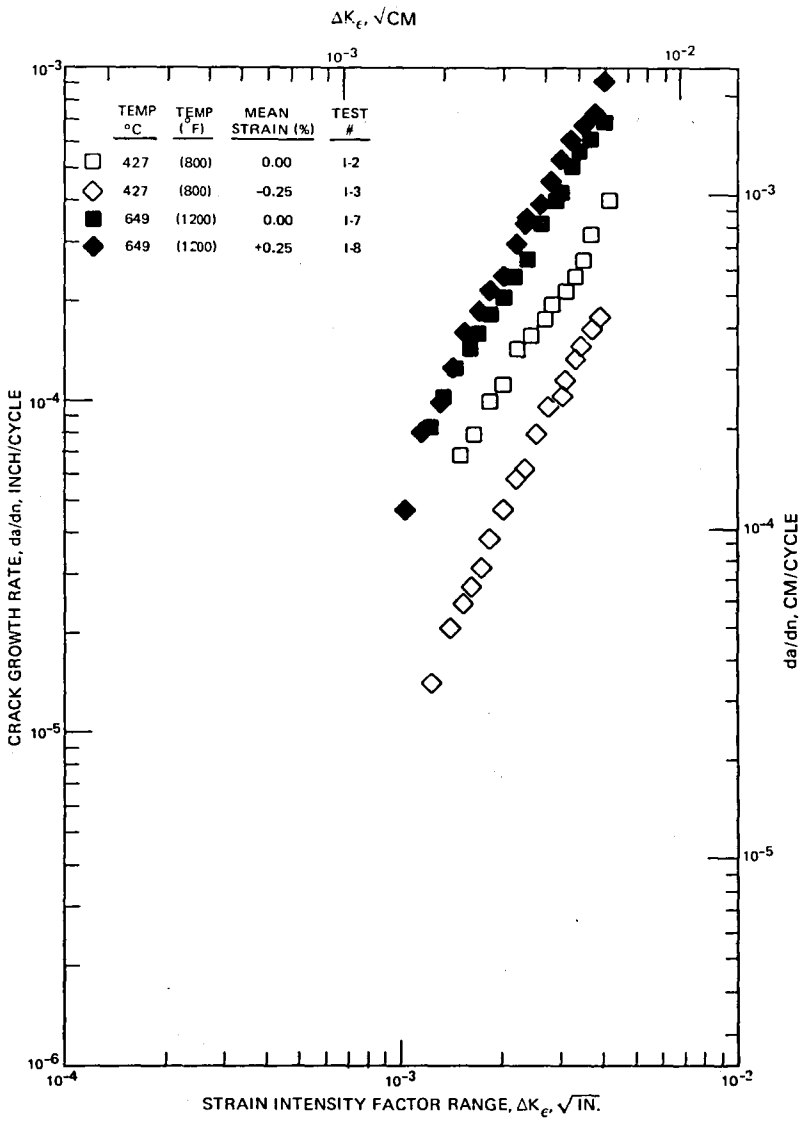

Figure A-7 Strain Range = 0.4%

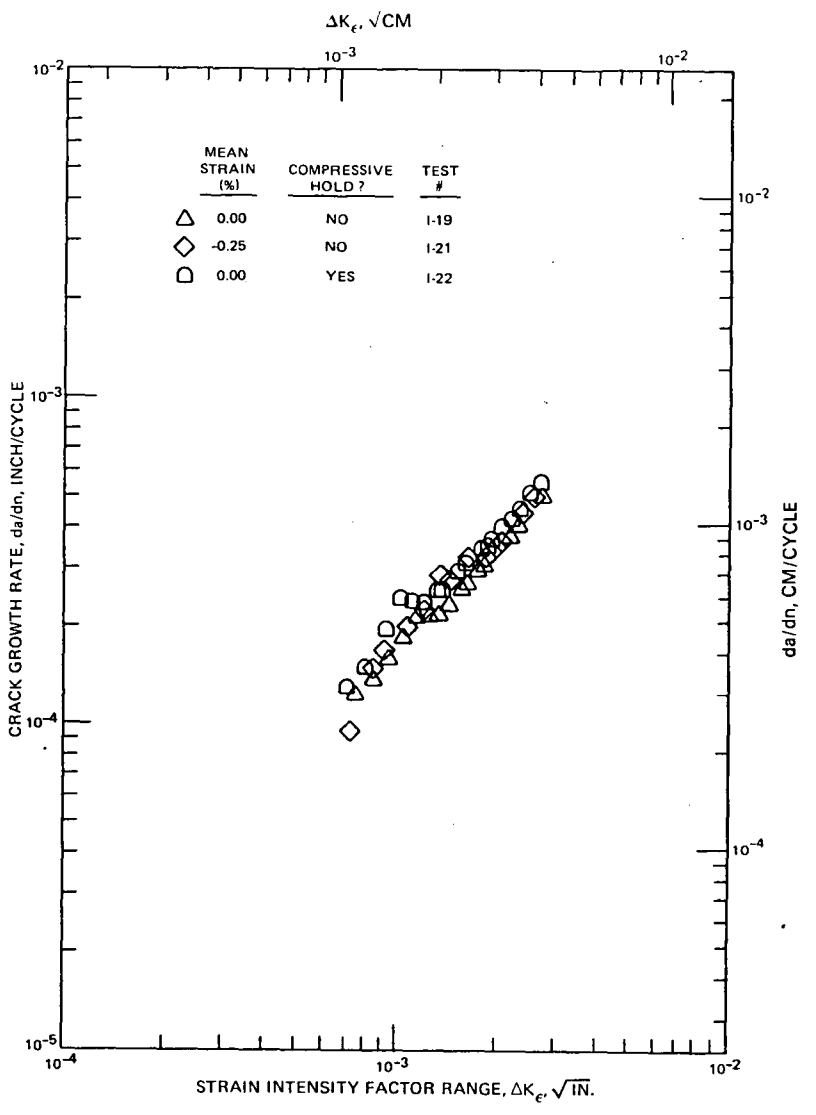

Figure A-8 927°C (1700°F) Strain Range = 0.25%

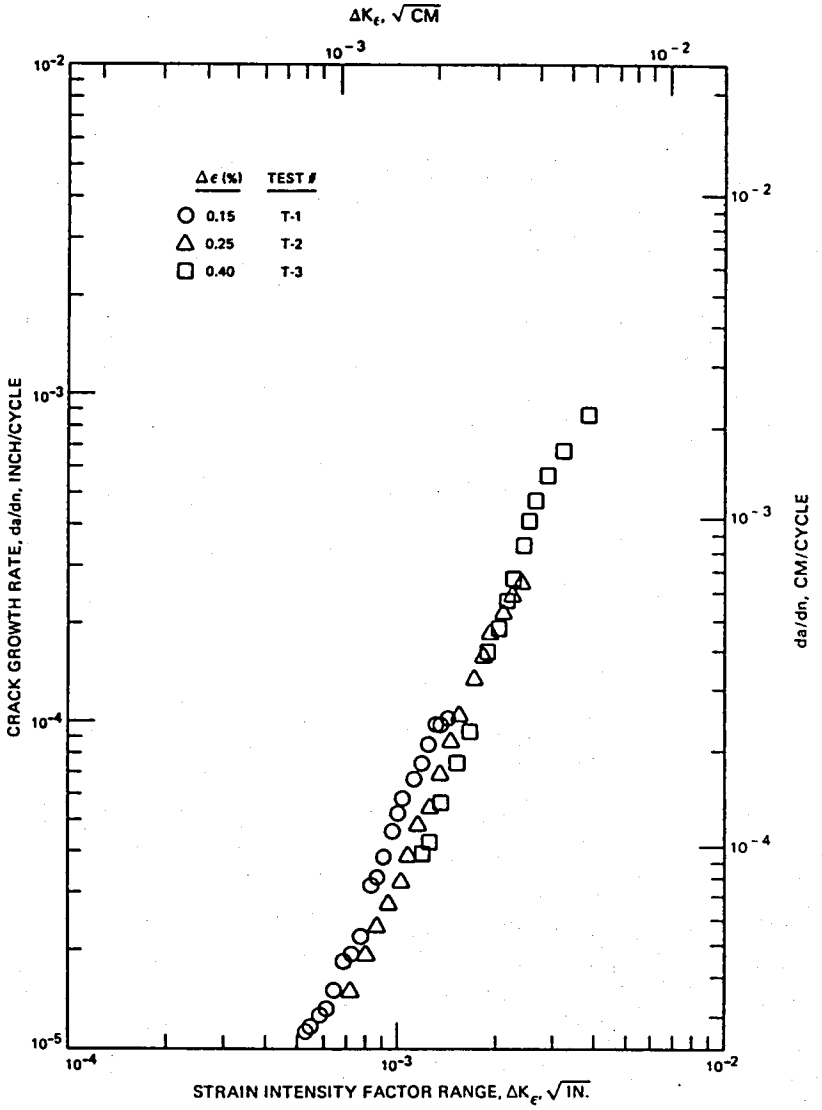

Figure A-9 427 to 927°C (800 to 1700°F) Cycle I

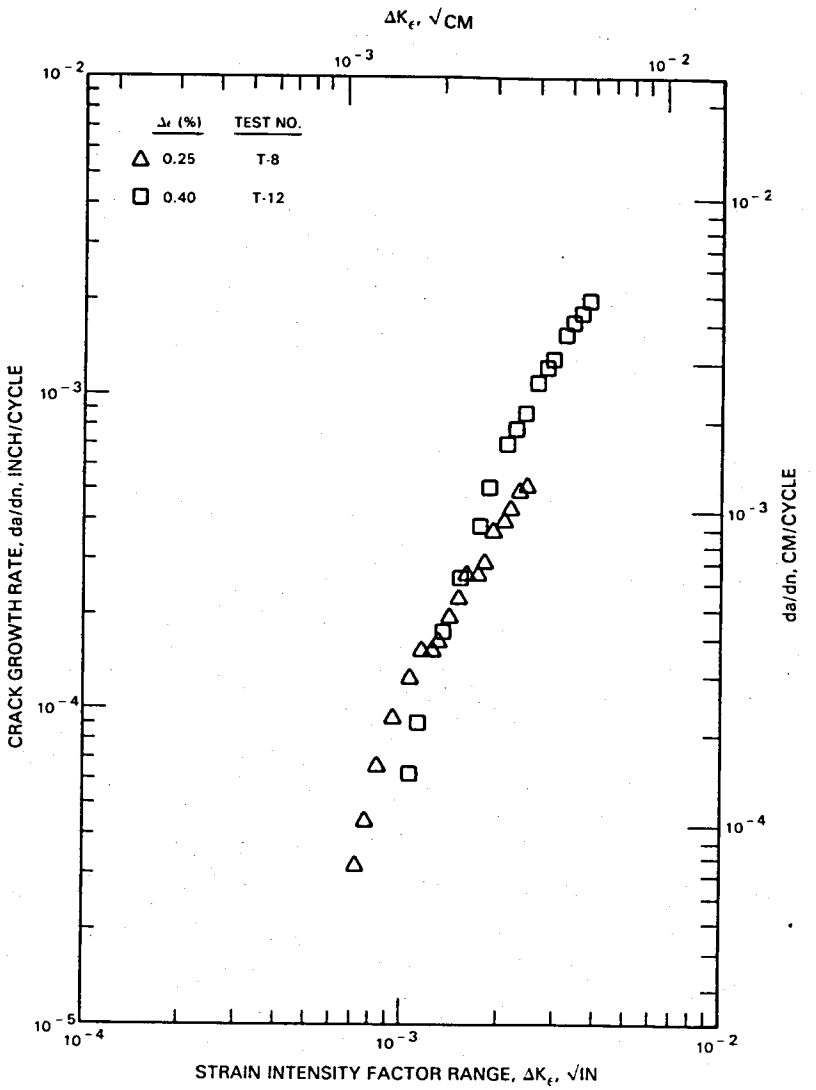

Figure A-10 427 to 871°C (800 to 1600°F) Cycle I

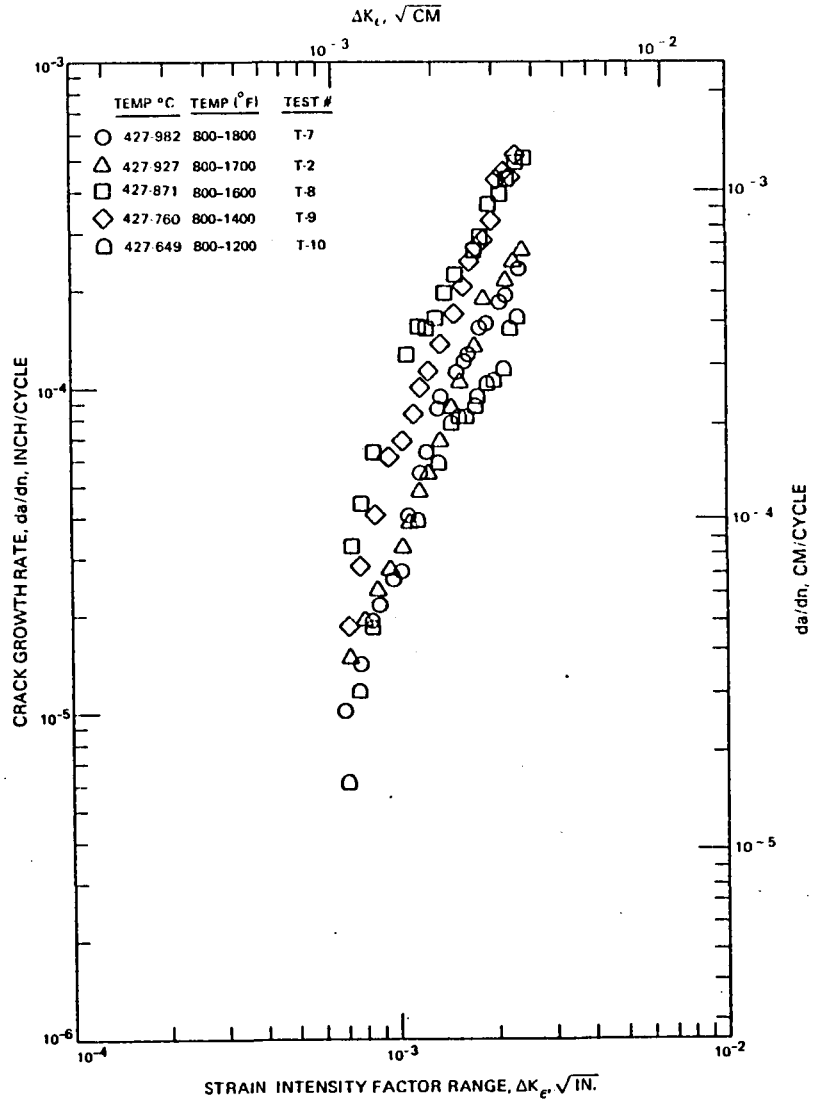

Figure A-11 Cycle I, Strain Range = 0.40%

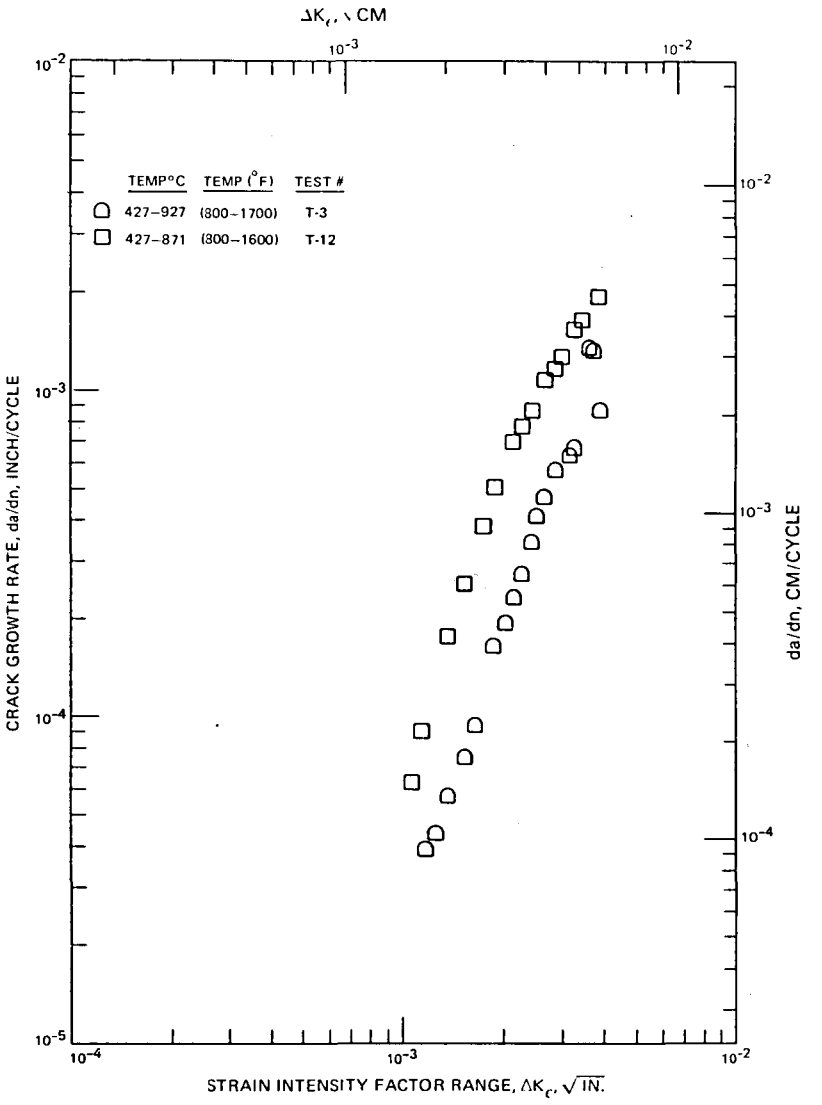

Figure A-12 Cycle I, Strain Range = 0.25%

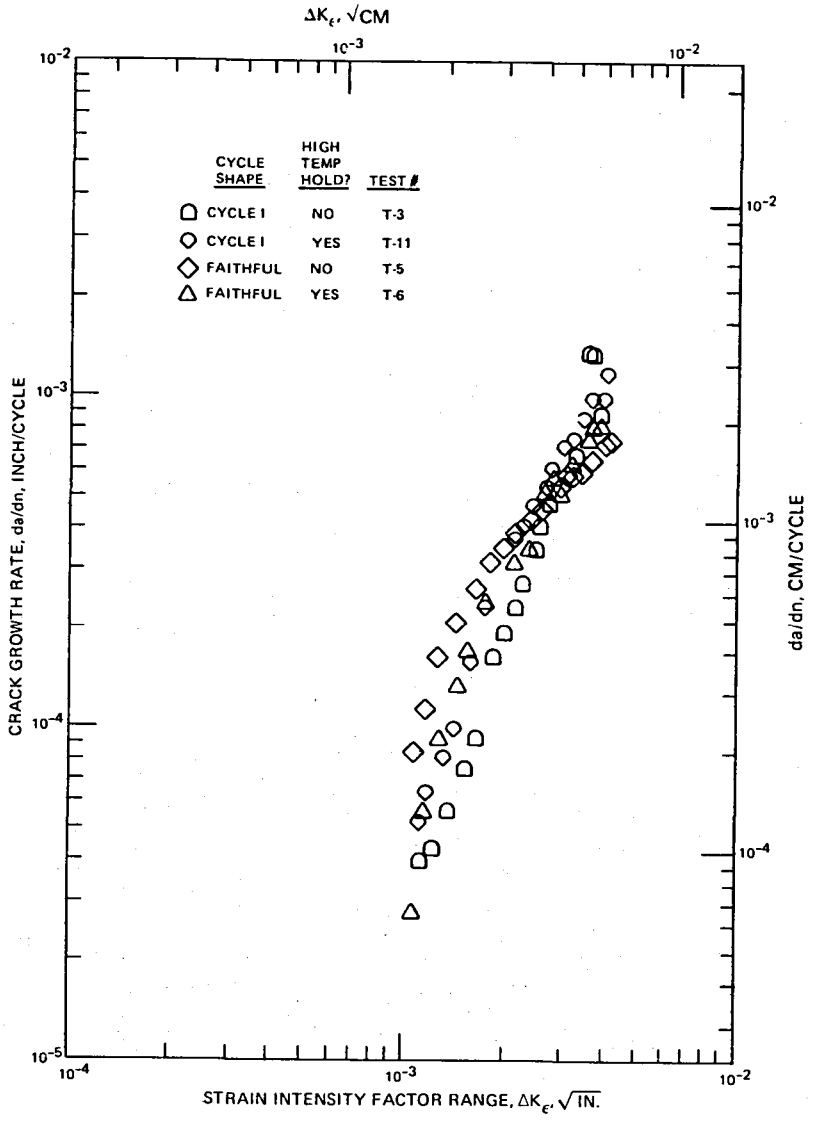

Figure A-13 427 to 927°C (800 to 1700°F), Strain Range = 0.40%

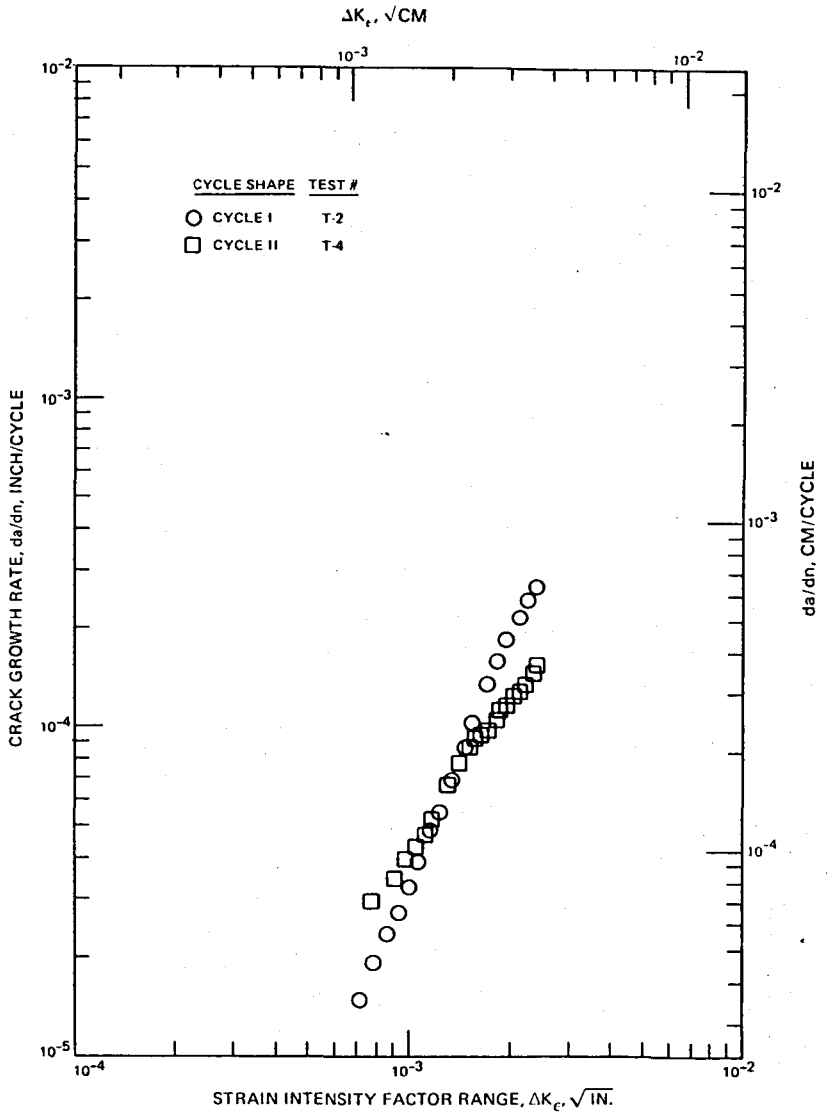

Figure A-14 427 to 927°C (800 to 1700°F), Strain Range = 0.25%

APPENDIX B STRESS INTENSITY FACTOR DATA REDUCTION

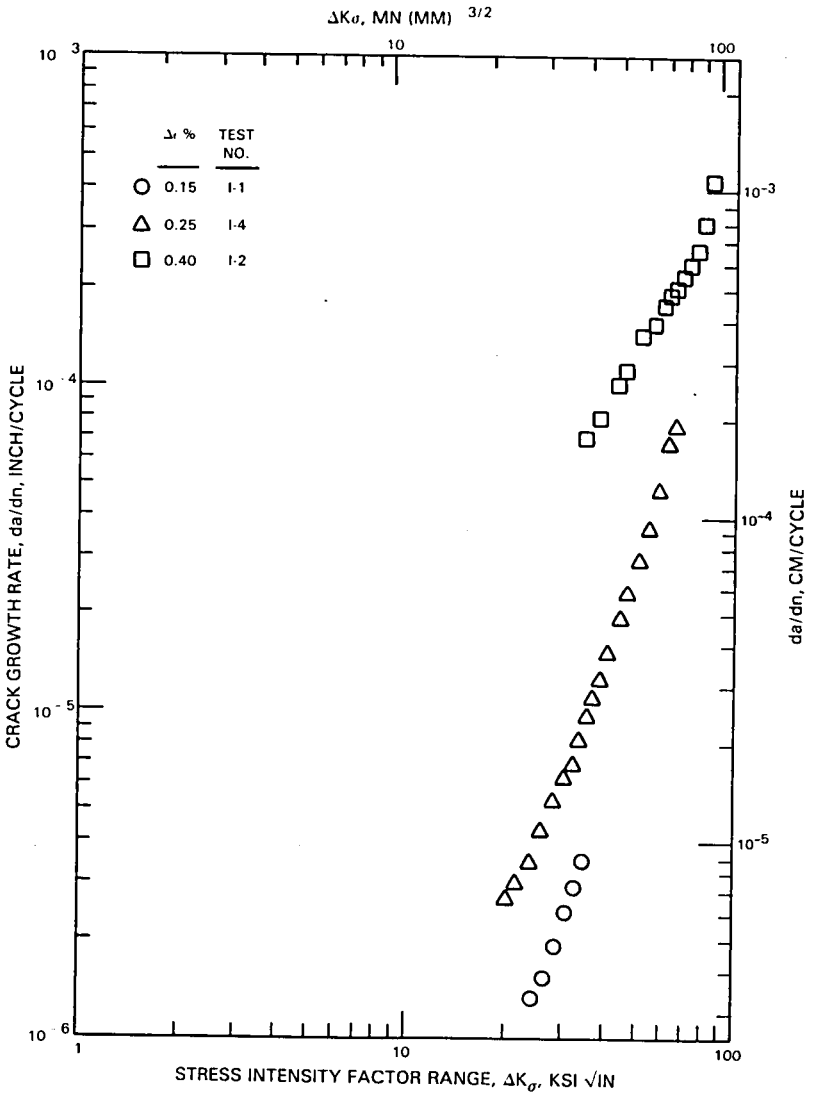

Figure B-1 427°C (800°F)

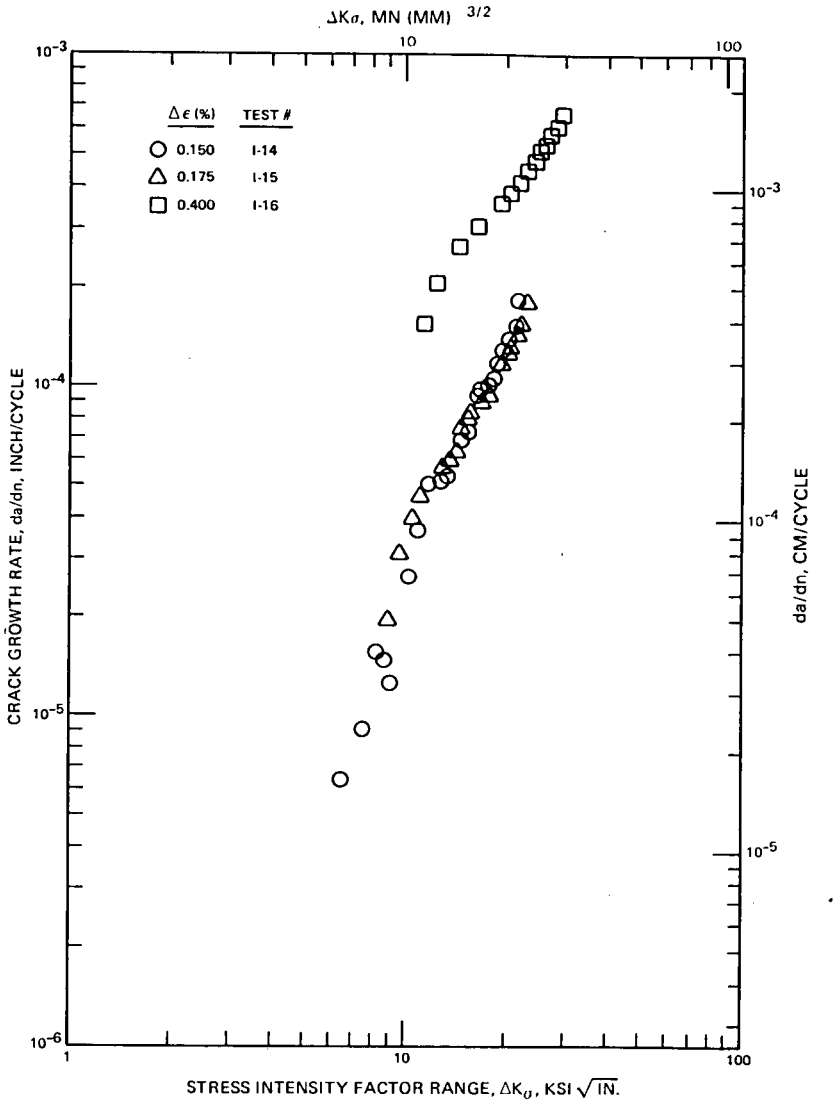

Figure B-2 871°C (1600°F)

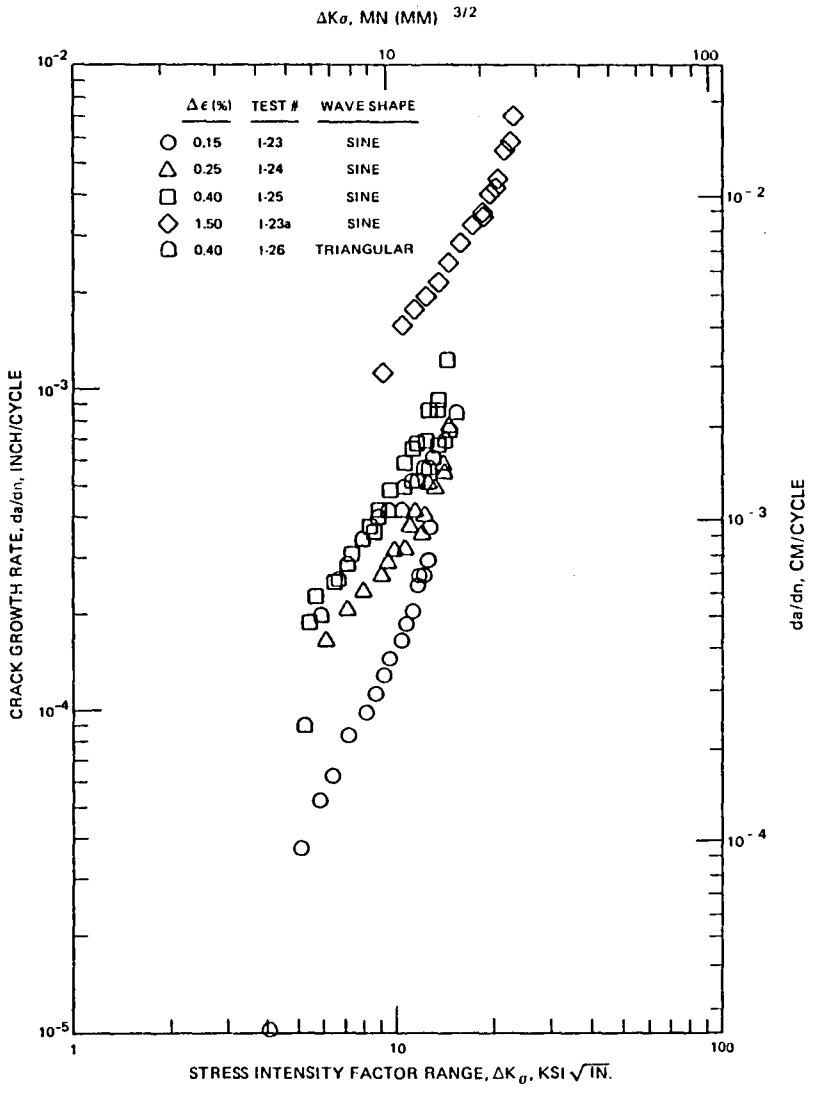

Figure B-3 982°C (1800°F)

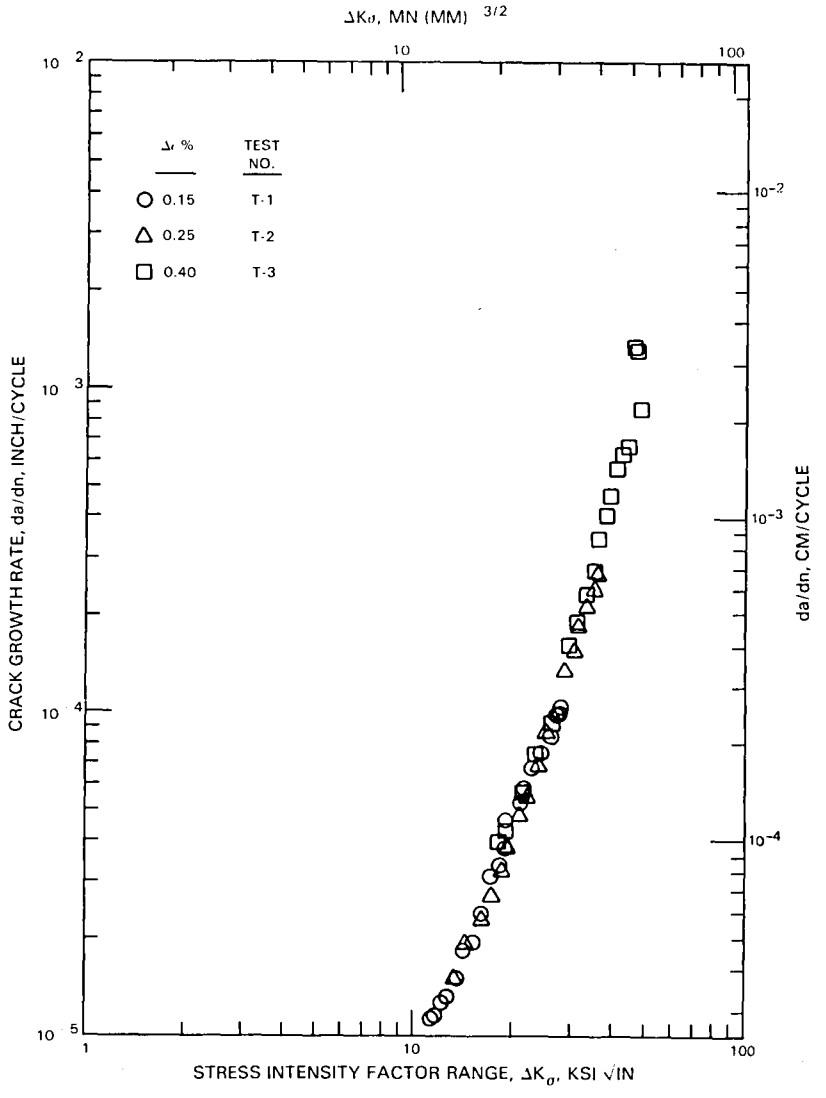

Figure B-4 427 to 927°C (800 to 1700°F) Cycle I

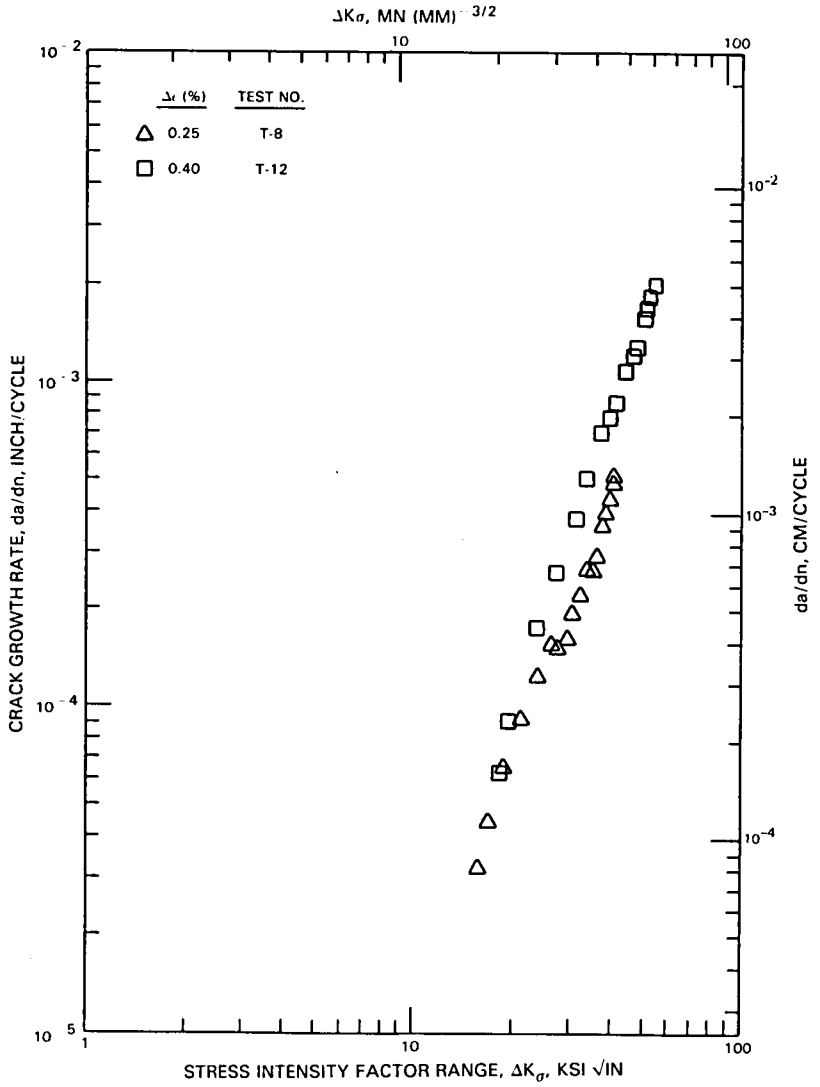

Figure B-5 427 to 871°C (800 to 1600°F) Cycle I

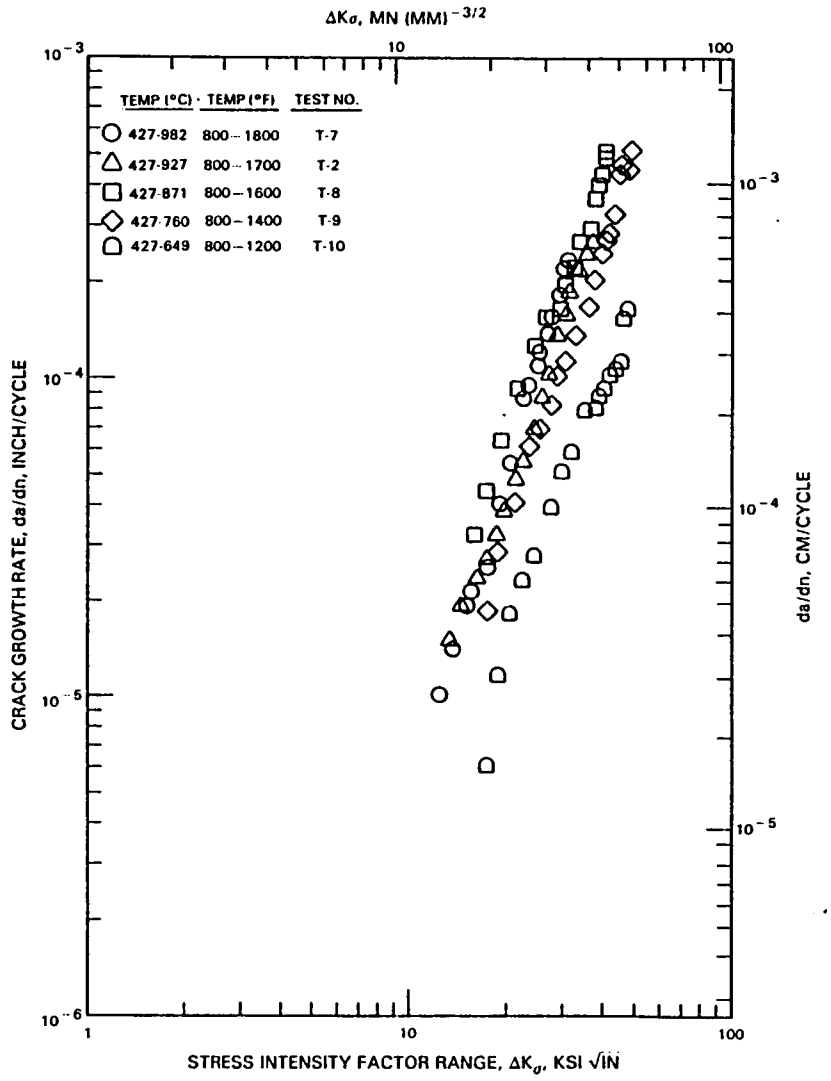

Figure B-6 Cycle I, Strain Range = 0.25%

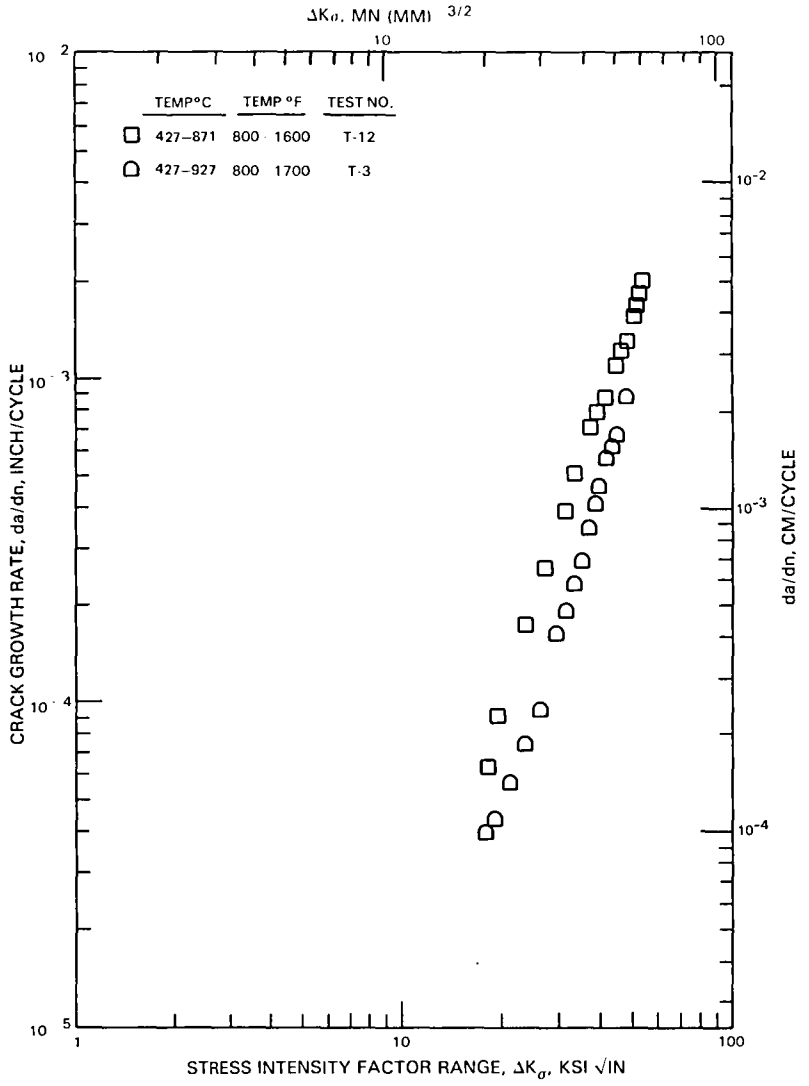

Figure B-7 Cycle I, Strain Range = 0.40%

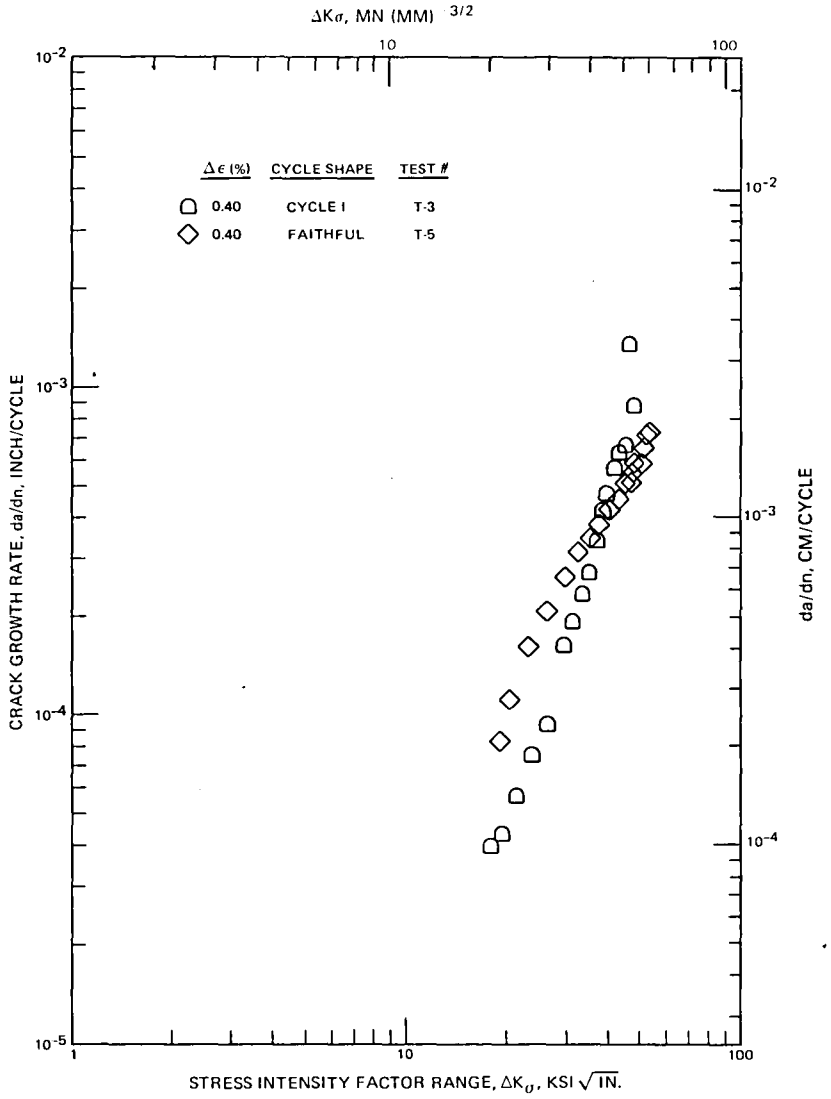

Figure B-8 427 to 927°C (800 to 1700°F), Strain Range = 0.40%

This Page Intentionally Left Blank

APPENDIX C J-INTEGRAL DATA REDUCTION

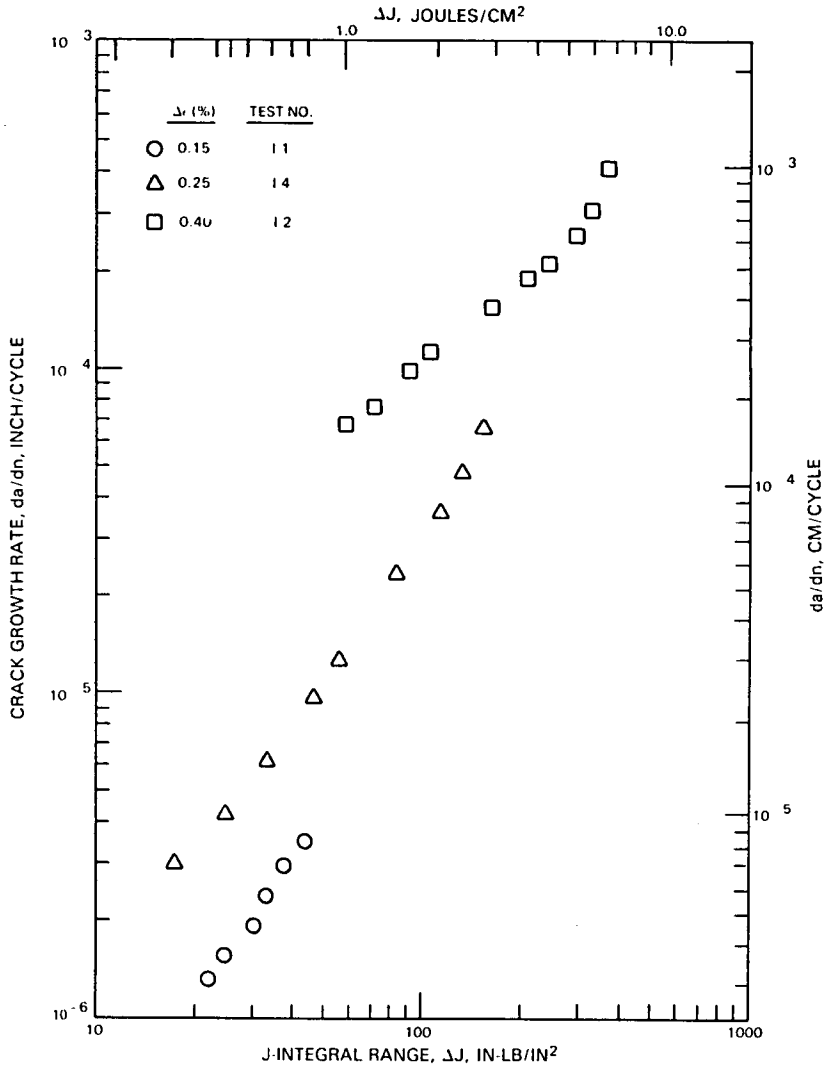

Figure C-1 427°C (800°F)

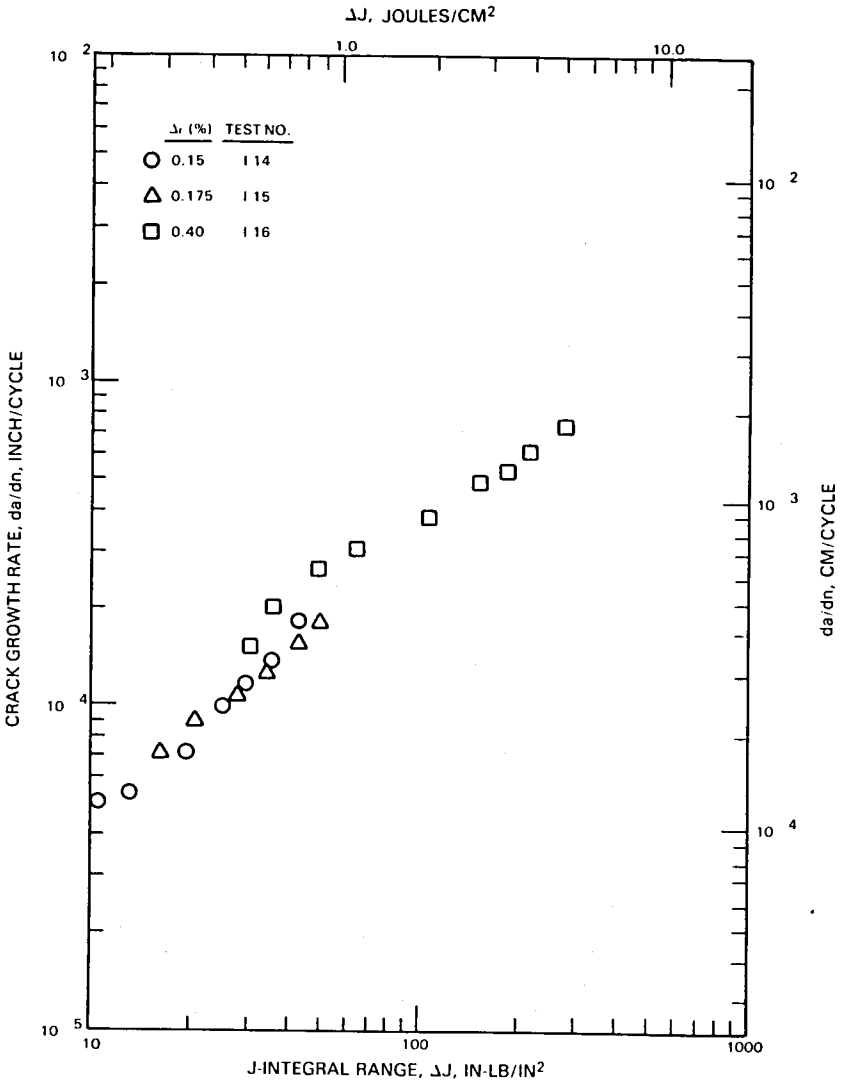

Figure C-2 871°C (1600°F)

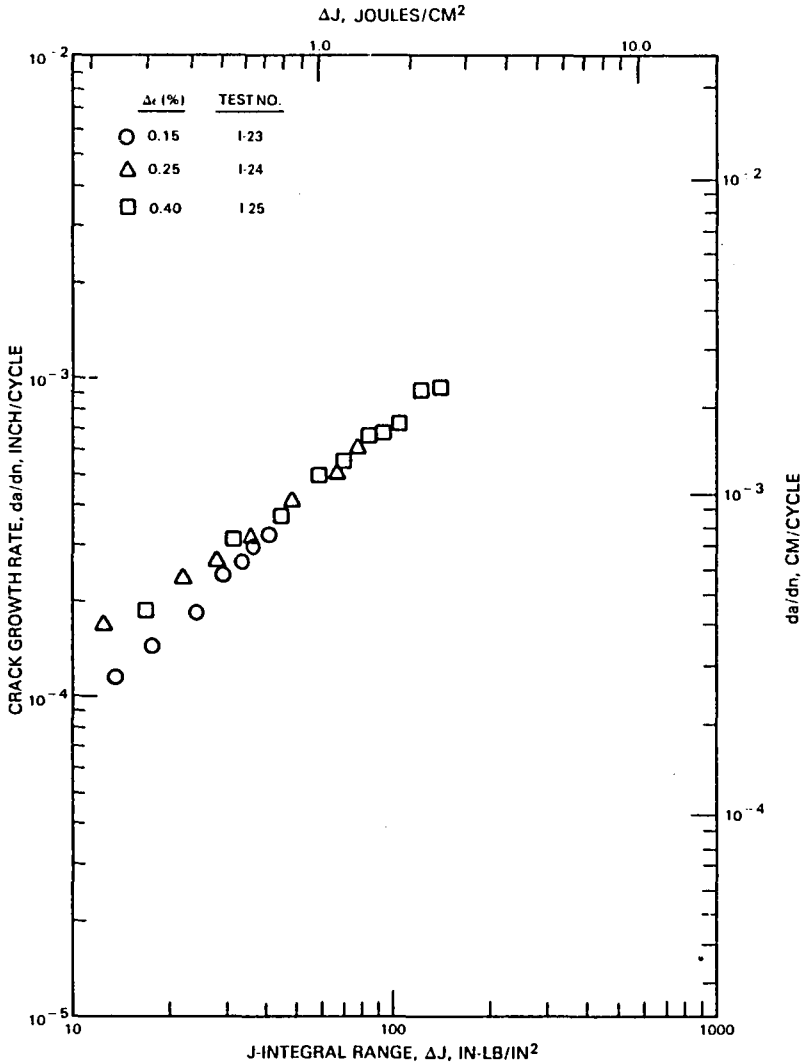

Figure C-3 982°C (1800°F)

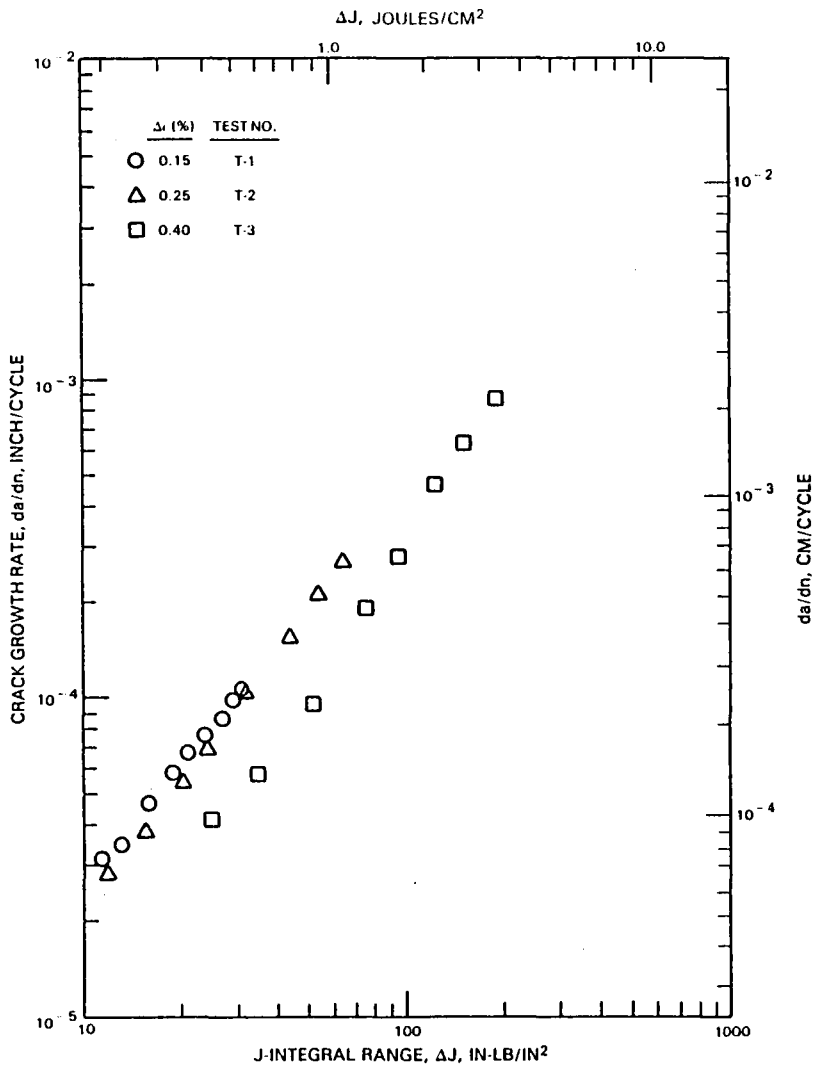

Figure C-4 427 to 927°C (800 to 1700°F) Cycle I

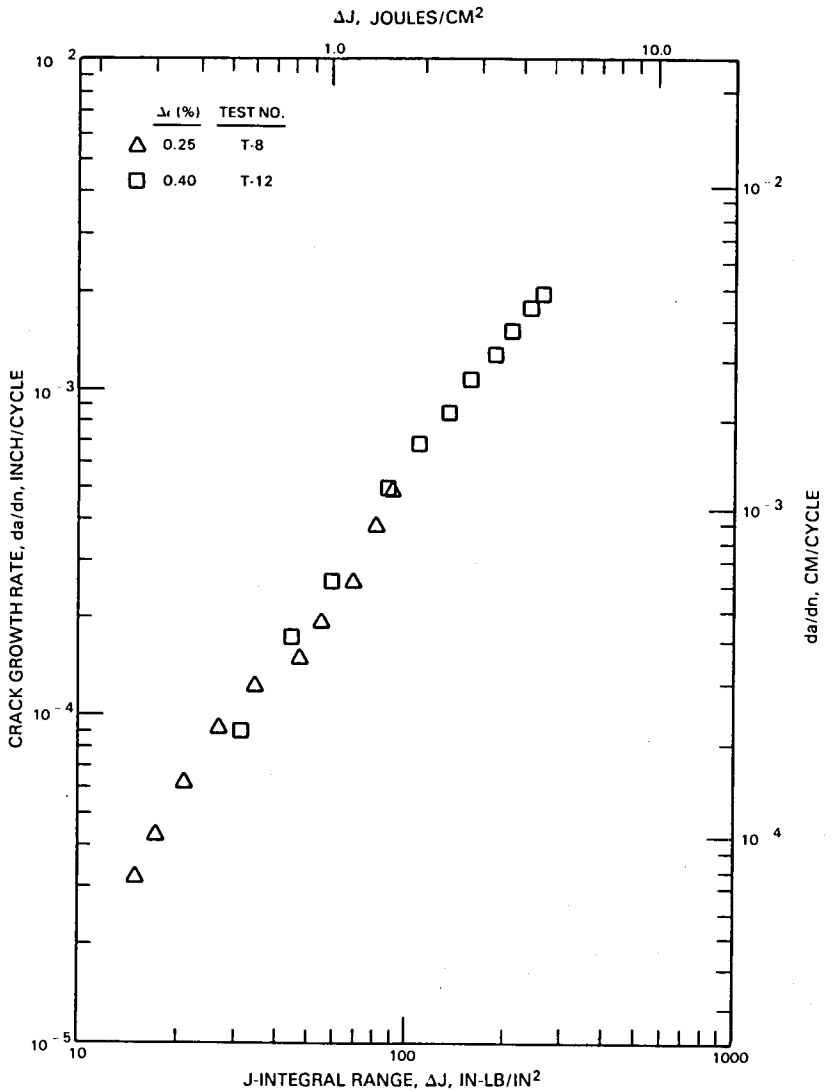

Figure C-5 427 to 871°C (800 to 1600°F) Cycle I

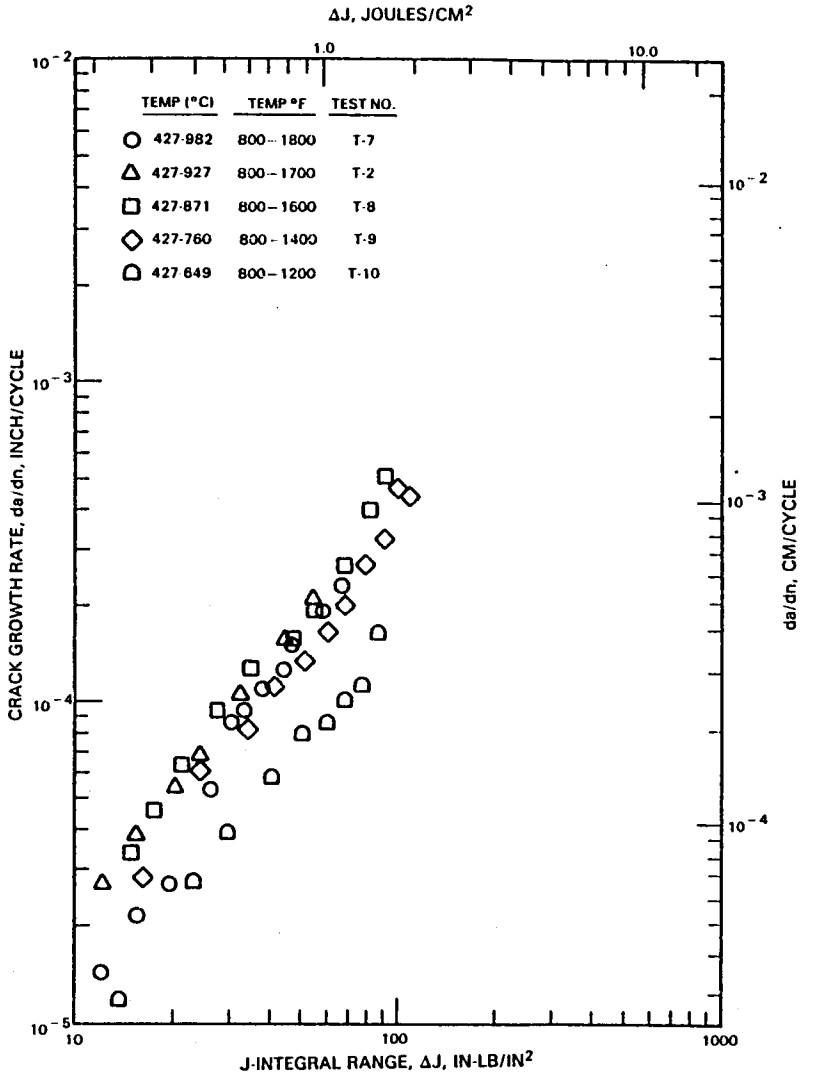

Figure C-6 Cycle I, Strain Range = 0.25%

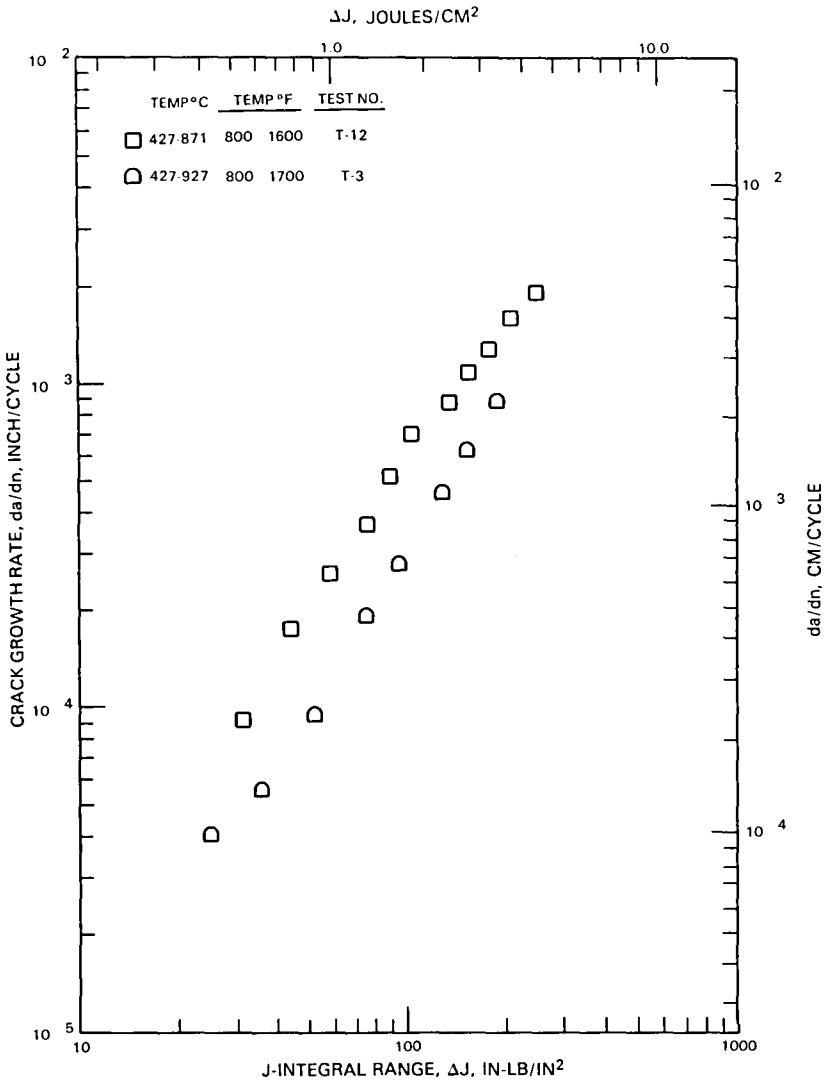

Figure C-7 Cycle I, Strain Range = 0.40%

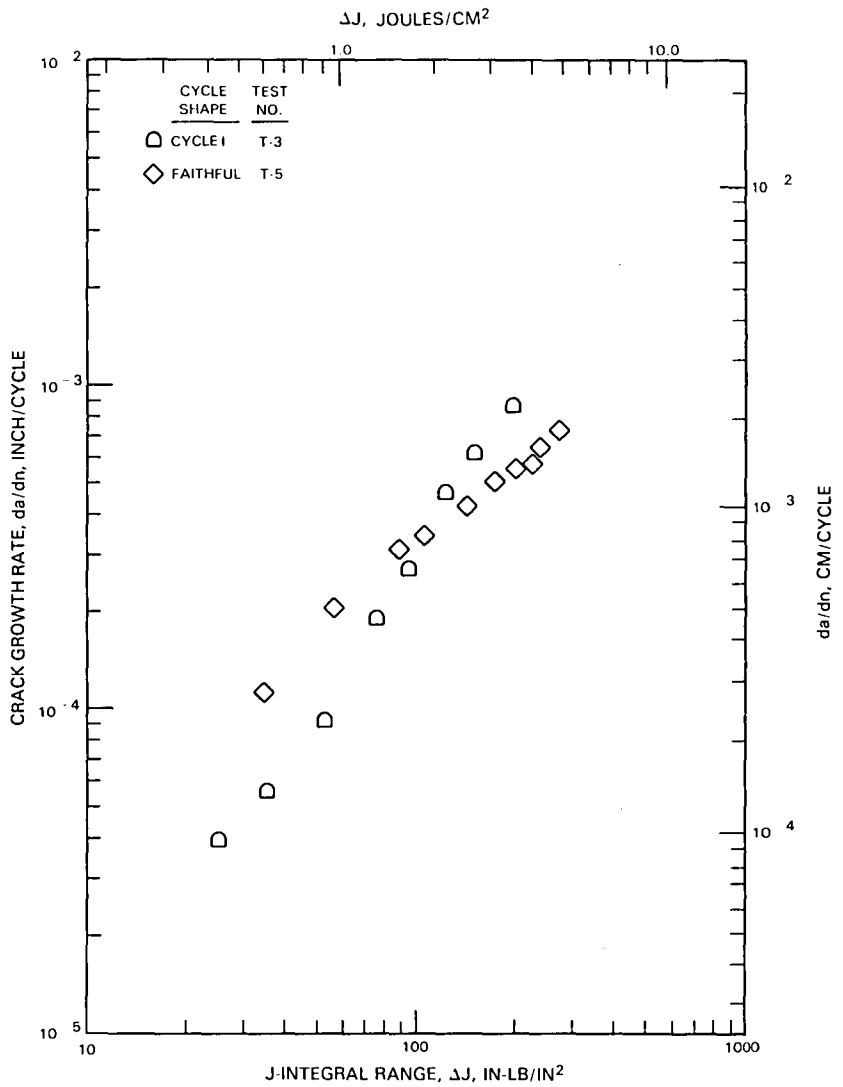

Figure C-8 427 to 927°C (800 to 1700°F), Strain Range = 0.40%

This Page Intentionally Left Blank

DISTRIBUTION LIST

NASA-Lewis Research Center
Attn: T. W. Orange MS 49-6
21000 Brookpark Road
Cleveland, OH 44135 (11 Copies)

NASA-Lewis Research Center
Attn: J. L. Shannon MS 49-6
21000 Brookpark Road
Cleveland, OH 44135

NASA-Lewis Research Center
Attn: M. H. Hirschberg MS 49-6
21000 Brookpark Road
Cleveland, OH 44135

NASA-Lewis Research Center
Attn: R. H. Johns MS 49-6
21000 Brookpark Road
Cleveland, OH 44135

NASA-Lewis Research Center
Attn: C. C. Chamis MS 49-6
21000 Brookpark Road
Cleveland, OH 44135

NASA-Lewis Research Center
Attn: R. L. Thompson MS 49-6
21000 Brookpark Road
Cleveland, OH 44135

NASA-Lewis Research Center
Attn: L. Berke MS 49-6
21000 Brookpark Road
Cleveland, OH 44135

NASA-Lewis Research Center
Attn: B. Gross MS 49-6
21000 Brookpark Road
Cleveland, OH 44135

NASA-Lewis Research Center
Attn: D. J. Gauntner MS 49-6
21000 Brookpark Road
Cleveland, OH 44135

NASA-Lewis Research Center
Attn: G. R. Halford MS 49-6
21000 Brookpark Road
Cleveland, OH 44135

NASA-Lewis Research Center
Attn: A. Kaufman MS 49-6
21000 Brookpark Road
Cleveland, OH 44135

NASA-Lewis Research Center
Attn: R. E. Jones MS 86-6
21000 Brookpark Road
Cleveland, OH 44135

NASA-Lewis Research Center
Attn: USAR-T LABORATORY 302-2
21000 Brookpark Road
Cleveland, OH 44135

NASA-Lewis Research Center
Attn: AFSC Liaison Office MS 501-3
21000 Brookpark Road
Cleveland, OH 44135

NASA-Lewis Research Center
Attn: M-S Contracts Section MS 501-11
21000 Brookpark Road
Cleveland, OH 44135

NASA-Lewis Research Center
Attn: Technology Utilization MS 7-3
21000 Brookpark Road
Cleveland, OH 44135

NASA-Lewis Research Center
Attn: Library MS 6-3
21000 Brookpark Road
Cleveland, OH 44135

NASA-Lewis Research Center
Attn: Report Control MS 5-5
21000 Brookpark Road
Cleveland, OH 44135

NASA-Lewis Research Center
Attn: Patent Counsel MS 500-318
21000 Brookpark Road
Cleveland, OH 44135

NASA-Lewis Research Center
Attn: S-MT Division MS 49-6
21000 Brookpark Road
Cleveland, OH 44135

NASA Science and Tech. Info. Fac.
Attn: Accession Dept.
Box 8757
Balt/Wash Intl. Airport, MD 21240
(10 Copies)

NASA Headquarters
Attn: RTM-6/L. Harris
Washington, DC 20546

NASA Marshall SFC
Attn: Library
MSFC, AL 35812

NASA Johnson Space Center
Attn: Library
Houston, TX 77058

NASA Ames Research Center
Attn: Library
Moffett Field, CA 94035

NASA Dryden FRC
Attn: Library
P. O. Box 273
Edwards, CA 93523

NASA Jet Propulsion Lab.
Attn: Library
4800 Oak Grove Drive
Pasadena, CA 91103

NASA Langley Research Center
Attn: Library
Hampton, VA 23665

NASA Goddard SFC
Attn: Library
Greenbelt, MD 20771

Air Force Wright Aeronautical Lab.
Attn: MLLN/J. Henderson
WPAFB, OH 45433

Air Force Wright Aeronautical Lab.
Attn: POTC/R. Hill
WPAFB, OH 45433

Air Force Wright Aeronautical Lab.
Attn: MLLN/W. Reimann
WPAFB, OH 45433

Air Force Wright Aeronautical Lab.
Attn: MLLN/T. Nicholas
WPAFB, OH 45433

Air Force Wright Aeronautical Lab.
Attn: POT/E. Bailey
WPAFB, OH 45433

Air Force Wright Aeronautical Lab.
Attn: FIBE/J. Rudd
WPAFB, OH 45433

Air Force Wright Aeronautical Lab.
Attn: MLLAM/Library
WPAFB, OH 45433

University of Alabama
Attn: A. E. Carden
Box 2908
University, AL 35486

University of Alabama
Attn: J. J. McGowan
Box 2908
University, AL 35486

Argonne National Lab.
Attn: S. Majumdar
9700 S. Cass Avenue
Argonne, IL 60439

Army Applied Technology Lab.
Attn: J. Lane/DAVDL-ATL-ATP
Fort Eustis, VA 23604

Army Applied Technology Lab.
Attn: Library
Fort Eustis, VA 23604

AVCO Lycoming Division
Attn: Louis Fiedler
550 S. Main Street
Stratford, CT 06497

AVCO Lycoming Division
Attn: Library
550 S. Main Street
Stratford, CT 06497

Babcock and Wilcox Company
Attn: Carl Schultz
1562 Beeson Street
Alliance, OH 44601

Babcock and Wilcox Company
Attn: Joseph M. Bloom
1562 Beeson Street
Alliance, OH 44601

Battelle Columbus Laboratories
Attn: Brian Leis
505 King Avenue
Columbus, OH 43201

Battelle Columbus Laboratories
Attn: MCIC
505 King Avenue
Columbus, OH 43201

Battelle Columbus Laboratories
Attn: Library
505 King Avenue
Columbus, OH 43201

Boeing Military Aircraft Company
Attn: C. F. Tiffany MS K16-36
3801 South Oliver
Witchita, KS 67210

Boeing Military Aircraft Company
Attn: Library
3801 South Oliver
Witchita, KS 67210

University of California
Attn: Prof. I. Finnie
Mechanical Engineering Dept.
Berkeley, CA 94720

Carnegie Mellon University
Attn: Prof. J. L. Swedlow
Schenely Park
Pittsburgh, PA 15213

Case Western Reserve University
Attn: Prof. S. S. Manson
10900 Euclid Avenue
Cleveland, OH 44106

Case Western Reserve University
Attn: Dr. A. Mendelson
10900 Euclid Avenue
Cleveland, OH 44106

University of Cincinnati
Attn: S. Antolovich
489 Rhodes Hall
Cincinnati, OH 45221

Colorado State University
Attn: Dr. F. W. Smith
Dept. of Mechanical Engineering
Fort Collins, CO 80523

University of Connecticut
Attn: Dr. Eric Jordan
Storrs, CT 06268

University of Connecticut
Attn: Prof. A. J. McEvily
Storrs, CT 06268

Univ. of Dayton Research Inst.
Attn: Dr. J. P. Gallagher
563 Kettering Bldg.
Dayton, OH 45469

Defense Documentation Center
Cameron Station
5010 Duke Street
Alexandria, VA 22314

Department of Energy
Attn: Tech. Info. Service
Box 62
Oak Ridge, TN 37830

Detroit Diesel Allison Div.
Attn: J. Byrd, MS U-24
P. O. Box 894
Indianapolis, IN 46206

Detroit Diesel Allison Div.
Attn: Dr. M. Doner, MS W-5
P. O. Box 894
Indianapolis, IN 46206

Detroit Diesel Allison Div.
Attn: Library
P. O. Box 894
Indianapolis, IN 46206

Ford Motor Company
Attn: Dr. Ronald Landgraf
Box 2053
Dearborn, MI 48121

AiResearch Mfg. Co.
Attn: Lee Matsch
P. O. Box 5217
Phoenix, AZ 85010

AiResearch Mfg. Co.
Attn: Library
P. O. Box 5217
Phoenix, AL 85010

General Electric Co.
Attn: M. L. Roberts, K-69
Aircraft Engine Group
Cincinnati, OH 45215

General Electric Co.
Attn: L. Beitch, K-221
Aircraft Engine Group
Cincinnati, OH 45215

General Electric Co.
Attn: A. Coles, K-221
Aircraft Engine Group
Cincinnati, OH 45215

General Electric Co.
Attn: P. Domas, K-71
Aircraft Engine Group
Cincinnati, OH 45215

General Electric Co.
Attn: H. Popp, M-87
Aircraft Engine Group
Cincinnati, OH 45215

General Electric Co.
Attn: J. H. Laflen, K-71
Aircraft Engine Group
Cincinnati, OH 45215

General Electric Co.
Attn: Library
Aircraft Engine Group
Cincinnati, OH 45215

General Electric Co.
Attn: Dr. David Woodford
Bldg K-1
Corporate R-D Center
Schenectady, NY 12301

General Electric Co.
Attn: Library
Corporate R-D Center
Schenectady, NY 12301

General Electric Co.
Attn: Warren Ostergren
1 River Road
Bldg. 53-37
Schenectady, NY 12345

General Electric Co.
Attn: Donald Mowbray
1 River Road
Bldg. 55-219
Schenectady, NY 12345

General Electric Co.
Attn: W. R. Andrews, RM 273
55 North Avenue
Schenectady, NY 12345

General Electric Co.
Attn: Library
1000 Western Avenue
Lynn, MA 01905

University of Illinois
Attn: Prof. JoDean Morrow
321A Talbot Lab
Urbana, IL 61801

Int'l. Harvestor Co. - Solar
Attn: Library
220 Pacific Highway
San Diego, CA 92101

International Nickel Co.
Attn: Library
Huntington Alloy Products Div.
Huntington, WV 25720

Louisiana State University
Attn: Dr. W. N. Sharpe, Jr.
Mechanical Engineering Dept.
Baton Rouge, LA 70803

MARC Analysis Research Corp.
Attn: Library
260 Sheridan Avenue
Suite 200
Palo Alto, CA 94306

Massachusetts Institute of Technology
Attn: Prof. R. Pelloux
77 Massachusetts Avenue
Cambridge, MA 02139

Michigan State University
Attn: Dr. John Martin
MMM Dept., 330 Engrg. Bldg.
E. Lansing, MI 48824

Naval Air Systems Command
Attn: Irving Machlin
Code AIR-52031 B
Washington, DC 20361

Naval Research Lab.
Attn: Paul Shahinian
Code 6305
Washington, DC 20375

Northwestern University
Attn: Prof. S. Nemat-Nasser
Dept. of Civil Engineering
Evanston, IL 60201

Oak Ridge National Lab.
Attn: Dr. Charles Brinkman, Box X
Oak Ridge, TN 37830

Oak Ridge National Lab.
Attn: Dr. J. M. Corum, Box Y
Oak Ridge, TN 37830

Pratt & Whitney Aircraft, GPD
Attn: D. H. Nethaway
P. O. Box 2691
West Palm Beach, FL 33402

Pratt & Whitney Aircraft, GPD
Attn: F. C. Gillette
P. O. Box 2691
West Palm Beach, FL 33402

Pratt & Whitney Aircraft, GPD
Attn: Library
P. O. Box 2691
West Palm Beach, FL 33402

Purdue University
Attn: Prof. A. F. Grandt, Jr.
School of Aeronautics and Astronautics
West Lafayette, IN 47907

Rensselaer Polytechnic Inst.
Attn: Dr. D. Duquette
Matls. Engrg. Dept.
Troy, NY 12181

Rensselaer Polytechnic Inst.
Attn: Dr. Norman Stoloff
Matls. Engrg. Dept.
Troy, NY 12181

Rocketdyne Div., NAR
Attn: G. A. Vroman
545-114-AC12
6633 Canoga Avenue
Canoga Park, CA 91304

Rocketdyne Div., NAR
Attn: Library
6633 Canoga avenue
Canoga Park, CA 91304

Sandia Laboratories
Attn: Library
Albuquerque, NM 87115

Southwest Research Inst.
Attn: Library
8500 Culebra Road
San Antonio, TX 78284

Stanford University
Attn: Dr. Henry Fuchs
Mechanical Engineering Dept.
Stanford, CA 94305

Stellite Div.
Cabot Corporation
Attn: Amer Aizaz
1020 Park Avenue
Kokomo, IN 46901

Teledyne CAE
Attn: T. Moyer
Box 6981
Toledo, OH 43612

Teledyne CAE
Attn: R. H. Gaylord
Box 6981
Toledo, OH 43612

Teledyne CAE
Attn: Library
Box 6981
Toledo, OH 43612

Texas A-M University
Attn: Dr. W. L. Bradley
Aerospace Engrg. Dept.
College Station, TX 77843

TRW, Inc.
Attn: Library
23555 Euclid Avenue
Cleveland, OH 44117

Westinghouse R-D Center
Attn: Dr. Norm Dowling
1310 Beulah Road
Pittsburgh, PA 15235

Westinghouse R-D Center
Attn: Dr. John Landes
1310 Beulah Road
Pittsburgh, PA 15235

Westinghouse-Hanford
Attn: L. K. Severud
P. O. Box 1970
Richland, WA 99352

End of Document